Roles of carbonated recycled fines and aggregates in hydration, microstructure and mechanical properties of concrete: A critical review

Tong Zhang[a], Meng Chen[a,b], Yuting Wang[a], Mingzhong Zhang[c,*]

[a] School of Resources and Civil Engineering, Northeastern University, Shenyang 110819, China

[b] Institute for Frontier Technologies of Low-Carbon Steelmaking, Northeastern University, Shenyang 110819, China

[c] Department of Civil, Environmental and Geomatic Engineering, University College London, London WC1E 6BT, UK

Abstract: CO_2 mineralisation by recycled concrete is a novel approach of carbon capture and utilisation to improve the sustainability of concrete products, which has attracted increasing attention in recent years. This paper presents a comprehensive review on carbonation mechanisms related to CO_2 mineralisation and hydration, microstructure and multiscale mechanical properties of concrete containing carbonated recycled fines and aggregates, with special focus on the chemistry-microstructure-property relationships. The carbonation kinetics of recycled fines in aqueous environment exhibit a typical particle size effect, while the high pozzolanic reactivity of carbonated recycled fines can facilitate the nucleation and stabilisation of hydration gels and contribute to the rapid hydration of cement paste. Carbonated recycled aggregates (RAs) are favourable in enhancing the micro-mechanical properties of interfacial transition zone in concrete through the synergic effects of physical interlocking and chemical bonding. Compared to concrete with plain RAs, up to 33.0%, 12.1% and 28.7% rises in compressive, splitting and flexural strengths of concrete can be achieved under 100% replacement of carbonated RAs. Due to the Stefan effect, concrete with carbonated RAs has higher dynamic peak stress but lower strain-rate sensitivity of elastic modulus than concrete with plain RAs. The global CO_2 mitigation capacity of recycled concrete varies from region to region and thus reasonable transportation network and high-efficient carbonation process are essential to ensure a balance between the environmental and economic benefits. This review summarises the recent advances in the field and discusses some future research opportunities to develop low-carbon concrete with recycled concrete as a carbon sink.

Keywords: Carbon capture and storage; Construction and demolition waste; Liquid-solid carbonation; Gas-solid carbonation; Reaction kinetics; Microstructural evolution

* Corresponding author. Email address: mingzhong.zhang@ucl.ac.uk (M. Zhang)

1. Introduction

With an annual CO_2 production of 2.2 Gt, cement and concrete production accounted for 5–8% of global greenhouse gas emissions in 2017 [1]. In order to achieve the goal of less than 0.8 Gt/year carbon footprint in the cement industry by 2050 [2], the recycling of construction and demolition (C&D) wastes can be a sustainable and cost-effective solution with a maximum potential reduction in global CO_2 emission of about 1.3 Gt/year [3]. Driven by global urbanisation, more than 3.0 Gt/year of C&D wastes were produced worldwide, which mainly consists of recycled concrete, brick, glass, asphalt, stone, metal and plastic [4]. As the major component (nearly 80%) of C&D wastes [5], recycled concrete can be divided with particle size as recycled concrete fines (RCF, finer than 0.15 mm), recycled fine aggregate (RFA, smaller than 4.75 mm) and recycled coarse aggregate (RCA, larger than 4.75 mm) [6]. In the last decade, the utilisation of recycled concrete aggregates as alternatives to natural fine and coarse aggregates is considered to be an eco-friendly recycling pathway for the disposal of C&D wastes, which can reduce CO_2 emissions and non-renewable energy consumption by 62% and 58%, respectively [7].

However, the addition of RCAs would inevitably lead to the degradation in engineering properties of concrete, suffering from the loosely packed old mortar adhered to the surface of RFAs and RCAs [8]. Therefore, modification treatments on recycled aggregates have been developed by either removing the adhered mortar (e.g., physical grinding [9], microwave heating [10], acid soaking [11]) or strengthening the adhered mortar (e.g., polymer impregnation [12], pozzolanic coating [13], bio-deposition [14]). In addition to these traditional methods, accelerated carbonation of recycled concrete has been highlighted as a sustainable modification method. Generally, CO_2 mineralisation of recycled concrete can be regarded as a type of carbon capture and utilisation approach, taking advantage of the high content of calcium and magnesium carbonates in recycled aggregates [15]. In other words, the unavoidable CO_2 source of cement and concrete even transfers to the favourable CO_2 sink, while enhancing the physical properties of RCFs, RFAs and RCAs [16].

Although the engineering properties of concrete with carbonated RCAs were discussed in Ref. [17], as a complement to the existing review, this paper aims to gain a deeper and systematic understanding of how CO_2 mineralisation affects the reaction kinetics and phase assemblage of RCFs, RFAs and RCAs as well as their contributions to the evolution of microstructure and mechanical properties. Then, recent advances in the roles of carbonated fines and aggregates on hydration, microstructure, and micro- and macro-mechanical properties of paste, mortar and

concrete were comprehensively reviewed, focusing specifically on the chemistry-microstructure-property relationships. The sustainability was assessed from local and global perspectives, aiming to address the remaining challenges for reducing the carbon footprint of recycled concrete further. The outline of this review is illustrated in Fig. 1.

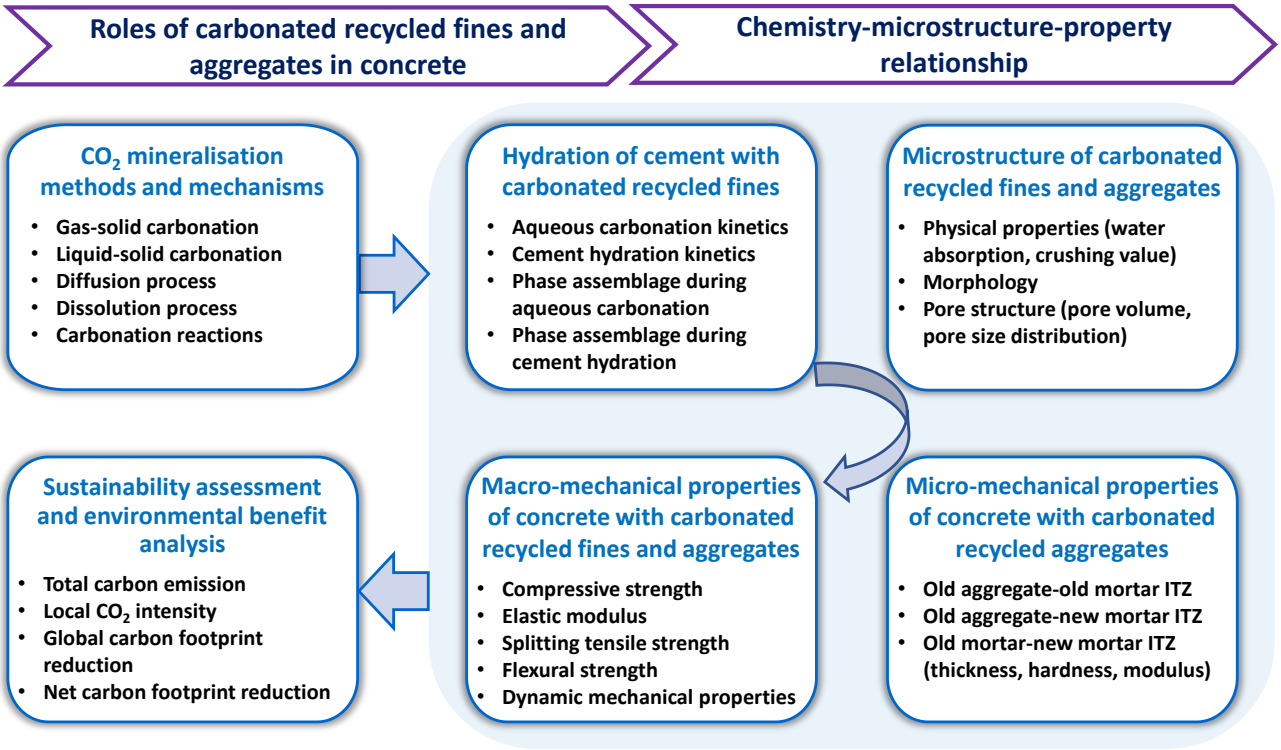

Fig. 1. Outline of this review on the roles of carbonated recycled fines and aggregates in concrete.

2. CO_2 mineralisation methods and mechanisms

2.1 Carbonation methods

As the CO_2 concentration in the atmosphere is lower than 0.06 vol%, the CO_2 diffusion coefficient of cement-based materials is approximately 10^{-10}–10^{-12} m/s [18], so the natural carbonation process of concrete would last for decades. Previous experiments suggested that the maximum carbonation depth of C25 concrete after 14-year natural carbonation only reached 16.7 mm [19]. Theoretical predictions by CO_2 emission-absorption balancing further revealed that the carbonation depth of C30 and C35 concrete after 100-year service life was about 21.8 and 12.3 mm, respectively [20]. Therefore, accelerated carbonation technologies have been adopted for CO_2 mineralisation in recycled concrete to guarantee the rapid carbonation of hydrations and clinkers within several days, which can be divided into gas-solid and liquid-solid carbonation methods. Fig. 2 displays general apparatuses utilised in the CO_2 mineralisation of recycled fines and aggregates.

2.1.1 Gas-solid carbonation methods

The gas-solid accelerated carbonation methods are developed through increased CO_2 concentration, pressure and temperature, as well as reasonable relative humidity (RH). Generally, the gas-solid methods include standard CO_2 curing, flow-through carbonation, pressurized carbonation, etc.

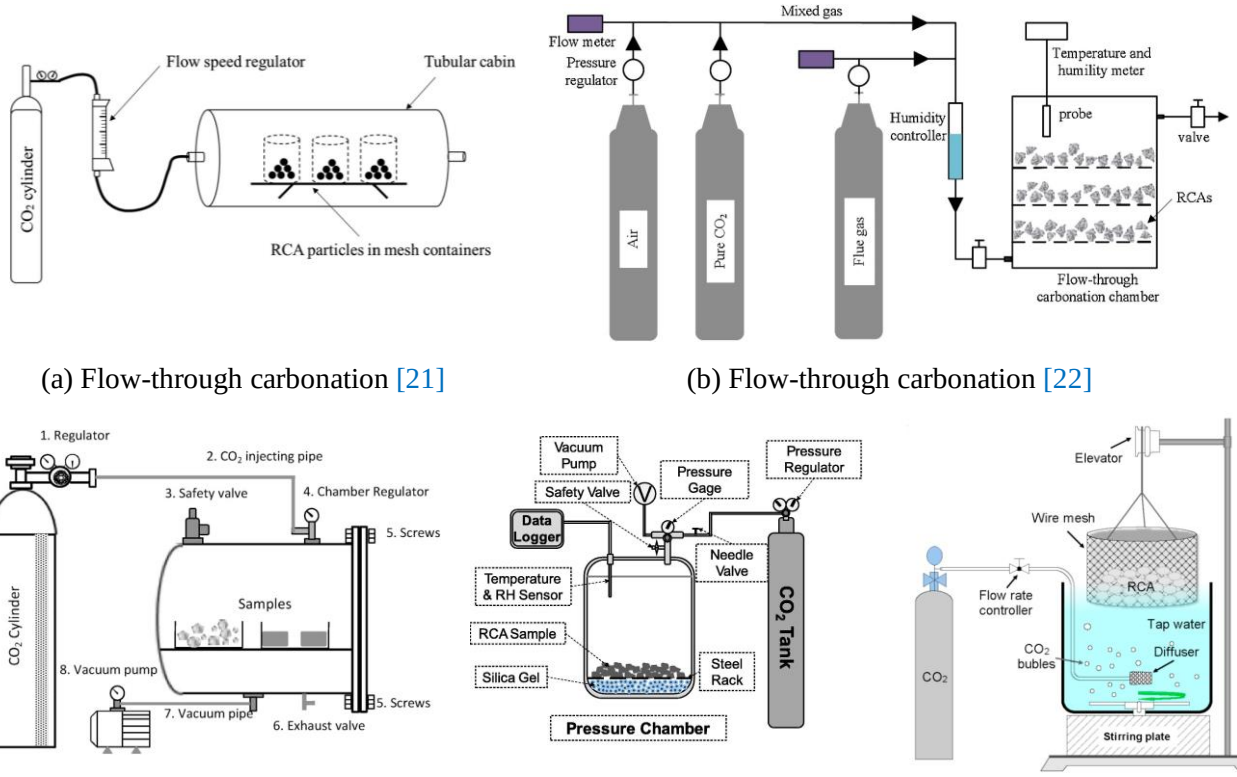

(a) Flow-through carbonation [21] (b) Flow-through carbonation [22]

(c) Pressurized carbonation [23–25] (d) Pressurized carbonation [26] (e) Aqueous carbonation [27]

Fig. 2. General apparatuses adopted for CO_2 mineralisation of recycled concrete.

Standard CO_2 curing is referred to the carbonation test of concrete, in which the CO_2 concentration, RH and temperature are maintained at 20 ± 2%, 60 ± 5% and 20 ± 2 °C, respectively [28]. But the carbonation duration should be at least 7 d due to the relatively low penetration rate of CO_2 into recycled aggregates [29]. In contrast, the flow-through carbonation method, with pure CO_2 (>99.5%) or mixed flue gas injected from one side of the chamber and discharged from the other side (Fig. 2a and b), can shorten the curing duration of recycled concrete to no more than 96 h [21,22]. Prior to the carbonation process, recycled aggregates were pre-conditioned under 50 ± 5% RH and 25 ± 2 °C for at least 24 h to ensure the moisture content approached the optimal RH of 50–70% [30]. Afterwards, recycled aggregates are suggested to be carbonated under a flow rate of 5 L/min and CO_2 concentration over 10%, while the temperature and RH remain the same as pre-condition [31]. Moreover, pressurized carbonation is more efficient to facilitate the penetration of CO_2 into the concrete matrix and reduce the carbonation duration to 24 h [23–25]. The carbonation chamber was firstly vacuumed to negative pressure lower than −0.5 bar for exclusion of air, and

then pure CO_2 was injected into the chamber until attaining target pressure levels varying from 0.1 to 5 bar [31], as displayed in Fig. 2c and d. The required RH is in accordance with the flow-through carbonation method, while saturated $Mg(NO_3)_2$ solution or silica gels can be applied to maintain the optimal RH during carbonation [26,32–34]. In addition, the increase of carbonation temperature from 25 ± 5 °C to 70 ± 5 °C considerably enhanced the CO_2 uptake of recycled aggregates by 38.6% within 24 h, in comparison with that of standard CO_2 curing [35,36].

2.1.2 Liquid-solid carbonation methods

Liquid-solid accelerated carbonation methods are more effective in promoting the carbonation efficiency of recycled concrete, as the carbonation reactions between hydrated products and water-CO_2 mixture are more complete than that in the CO_2 gas [37,38]. By continuously bubbling pure CO_2 or mixed CO_2 and N_2 gas into a solution containing recycled concrete fines (Fig. 2e), the carbonation reaction degree of cement paste was significantly improved to over 90% within only 6 h [39,40]. To ensure the uniform dispersion of recycled particles, the water-CO_2 suspension should be stirred at a speed of 200−600 rpm under the gas flow rate of 10−24 L/h [41,42]. However, the carbonation process of recycled concrete in an aqueous environment is highly dependent on the size effect [40], and accordingly the liquid-solid carbonation method is more suitable for the accelerated CO_2 curing of recycled fine aggregates or recycled concrete fines [27,43]. Additionally, several pre-treatment methods, such as spraying reclaimed wastewater [21,34], pre-conditioning in magnesium nitrate solution [44], pre-soaking in limewater or calcium nitrate water [45,46], and creating a reactive shell [33], were also proved to accelerate the carbonation process of recycled aggregates.

2.2 Carbonation mechanism

The carbonation of hardened recycled concrete includes a series of physical and chemical processes, as illustrated in Fig. 3. The carbonation kinetics can be affected by the parent materials of recycled concrete (i.e., particle size, porosity, water content, content of supplementary cementitious materials and pre-treatment methods) [17,25,47], as well as carbonation methods (i.e., gas-solid and liquid-solid carbonation) [27,48] and conditions (i.e., CO_2 concentration, gas pressure, carbonation time, RH and temperature) [31,35]. The carbonation mechanism of recycled concrete is explained in terms of the diffusion process, dissolution process and carbonation reactions.

2.2.1 Diffusion process

During accelerated carbonation, the diffusion process is denoted as the process that CO_2 diffuses into the pores from the external environment and reaches the reactive zones of recycled aggregates,

as displayed in Fig. 3a. The CO_2 diffusion process in recycled aggregates is different from that in natural aggregate due to the inhomogeneity microstructures in hardened concrete [49]. Based on Fick's law, the diffusion of CO_2 gas follows the negative gradient direction of CO_2 concentration field. Thus, the increase in CO_2 concentration can promote the carbonation efficiency. However, the promoting effect is not obvious when the CO_2 concentration exceeds 20%, as the increase of CO_2 concentration from 10% to 100% only resulted in a slight increase of CO_2 uptake from 1.0% to 1.2% within the first 24 h flow-through carbonation [31]. In a similar manner, the rise of CO_2 gas pressure is favourable in the diffusion process, while the increase of gas pressure from 0.1 bar to 5 bar only led to a minor enhancement in CO_2 uptake of 0.01% to 0.66% in recycled aggregates sizing from 10 to 20 mm [23]. Moreover, the CO_2 diffusion process is also related to the pore diameter of recycled concrete matrix, which can be affected by collisions between CO_2 molecules and pore walls as well as collisions between CO_2 molecules when the pore diameter ranged between one and ten times the mean free path of CO_2 gas [50].

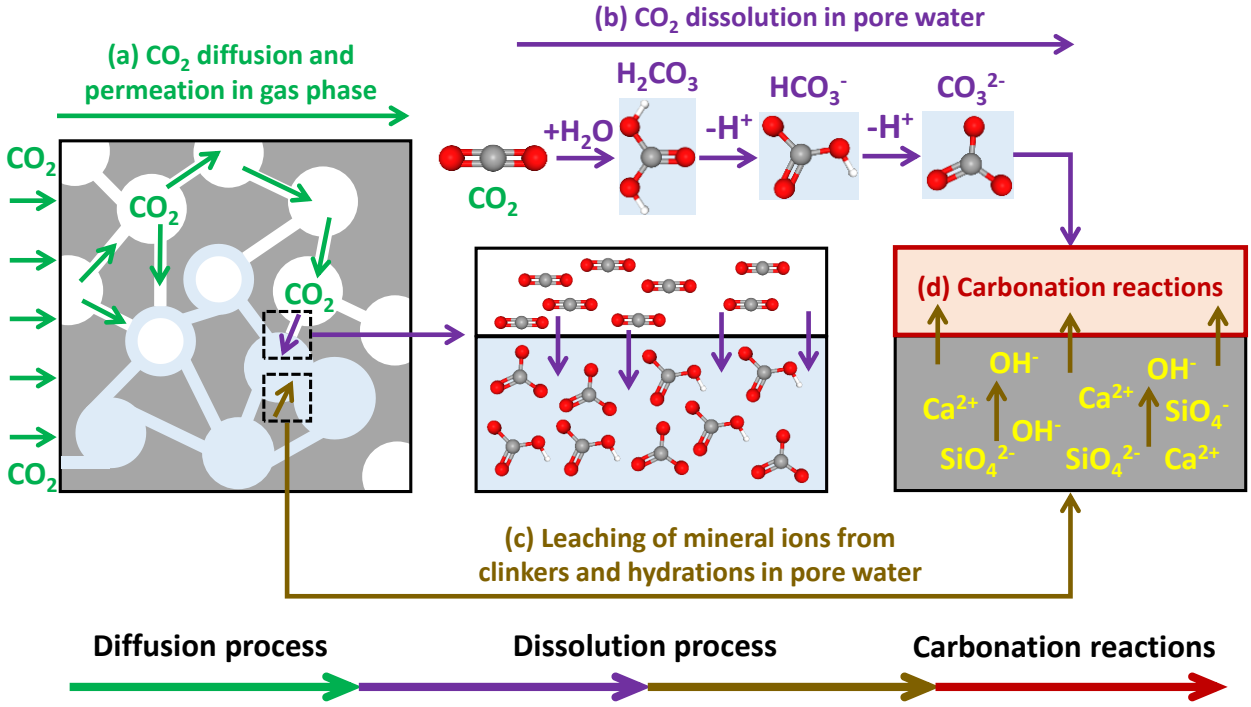

Fig. 3. Illustration of physical and chemical carbonation processes of recycled concrete.

2.2.2 Dissolution process

The dissolution of CO_2 and reactive phases in pore solution is the main dissolution process (Fig. 3b). Actually, sufficient humidity in pores is essential for CO_2 dissolution since the carbonation process requires H_2O to form the carbonate ions, as expressed in Eqs. (1) and (2).

$$CO_2 + H_2O \rightarrow H_2CO_3 \quad (1)$$

$$H_2CO_3 \rightarrow HCO_3^- + H^+,\ HCO_3^- \rightarrow CO_3^{2-} + H^+ \quad (2)$$

In general, the carbonation interface in recycled concrete is regarded as the composition of carbonation zone, carbonation front and non-carbonated zone [51]. However, scanning electron microscope (SEM) images further revealed that there exists a dissolution front between the former two zones, which is closely associated with the diffusion process and carbonation reactions [52]. The dissolution rate of CO_2 can be estimated by Henry's law [53], while CO_2 solubility should be considered for prediction at higher carbonation pressures, especially when the pressure exceeds 7 MPa [54]. In addition to the dissolution of CO_2 from gas to liquid, the leaching of mineral ions (e.g., Ca^{2+} and SiO_4^{2-}) from solid to liquid is another type of dissolution process (Fig. 3c) that is strongly affected by the calcium content, particle size and microstructure of recycled concrete [15,55].

2.2.3 Carbonation reactions

The dissolved carbonate ions in the pore solution can react with the leaching minerals from the solid matrix including calcium hydroxide (CH), calcium silicate hydrates (C-S-H) and cement clinkers [48]. The reaction between CH and CO_2 plays the dominant role as the solubility of CH is the highest among all calcium components. Consequently, the formation of insoluble calcium carbonate would lower the pH and calcium ions concentration of the pore solution as:

$$Ca^{2+} + CO_3^{2-} \rightarrow CaCO_3,\ Ca^{2+} + OH^- + HCO_3^- \rightarrow CaCO_3 + H_2O \quad (3)$$

As the reaction proceeds, calcium carbonate tends to precipitate as aragonite or vaterite under kinetics dominant conditions, while calcium carbonate can convert to more stable calcite polymorph under thermodynamic dominant conditions [56]. However, the formation of thin calcium carbonate layer on the surface of CH would hinder the permeation of CO_2 and gradually slow down the carbonation reactions [50]. Accounting for over 70% of hydrations, amorphous C-S-H gels would be carbonated on condition that most of the CH is consumed [57]. The carbonation of C-S-H forms the calcium carbonate and amorphous silica gels and reduces the Ca/Si ratio as:

$$\alpha CaO \cdot SiO_2 \cdot \beta H_2O + \alpha CO_2 \rightarrow \alpha CaCO_3 + SiO_2 \cdot \gamma H_2O + (\beta - \gamma) H_2O \quad (4)$$

Similar to the carbonation of CH, the reaction products of carbonated C-S-H gels also contain three types of calcium carbonate polymorphs, among which calcite crystals would cover the surface of C-S-H and inhibit further carbonation [58]. Moreover, residual cement clinkers (i.e., tricalcium silicate and dicalcium silicate) and aluminates (i.e., ettringite) are also potentially carbonated phases even under low CO_2 concentration [59]. The carbonation of the former one could form calcite and

silicate gels [60], while the carbonated products of aluminates include calcite, gypsum and alumina gels [61], as described in Eqs. (5)−(7). Consequently, the filling effect of produced high-density crystals can enhance the microstructures of recycled aggregates and fines.

$$3CaO \cdot SiO_2 + 3CO_2 + \alpha H_2O \rightarrow 3CaCO_3 + SiO_2 \cdot \alpha H_2O \quad (5)$$

$$2CaO \cdot SiO_2 + 2CO_2 + \alpha H_2O \rightarrow 2CaCO_3 + SiO_2 \cdot \alpha H_2O \quad (6)$$

$$3CaO \cdot Al_2O_3 \cdot 3CaSO_4 \cdot 32H_2O + 3CO_2 \rightarrow 3CaCO_3 + 3(CaSO_4 \cdot 2H_2O) + 2Al(OH)_3 + 9H_2O \quad (7)$$

3. Hydration of cement with carbonated recycled fines

3.1 Reaction kinetics

3.1.1 Kinetics during aqueous carbonation

Following the abovementioned mechanism, the aqueous carbonation kinetics of RCFs can be explained in four stages. (i) Within the first 2 min of carbonation, the dissolution rate of RCFs was higher than the dissolution rate of CO_2 gas, and thus both calcite precipitation and CO_2 dissolution could limit the carbonation reaction [39,62]. (ii) In the second stage from 2 min to 10 min, the solution was kept at high supersaturated of calcite, while a rapid drop in saturation of portlandite and C-S-H phases occurred, suggesting that the leaching of hydrations governs the carbonation rate [63]. (iii) When the carbonation duration ranged from 10 min to 20 min, the concentration of hydrates become undersaturated, during which the supersaturation of calcite dropped sharply, implying that the carbonation process was limited by the dissolution of hydrates [64]. (iv) At over 20 min, the saturation indexes of both calcite and hydrates were maintained at the minimum value, and accordingly the dense calcium carbonate layer on the surface of RCFs would no longer hinder the diffusion of CO_2 [65]. However, the concentration of amorphous silica and alumina hydroxide increased coupled with the formation of silica and alumina gels [66].

A further study reported that the carbonation kinetics of RCFs in an aqueous environment is also related to the particle size [40], as illustrated in Fig. 4. For the coarse particles (0.6–2.36 mm), there exists a synergistic effect of the initial carbonation in bulk solution and follow-up carbonation due to carbonate diffusion, which would lead to the formation a reactive shell on the particle surface and densify the internal microstructure [33]. In contrast, the finer particles smaller than 0.15 mm were completely disintegrated and converted to calcium carbonate and silica crystals after the aqueous carbonation [67]. Meanwhile, 0.15–0.6 mm can be regarded as a transition particle size range where balanced densification and disintegration of RCFs take place [40].

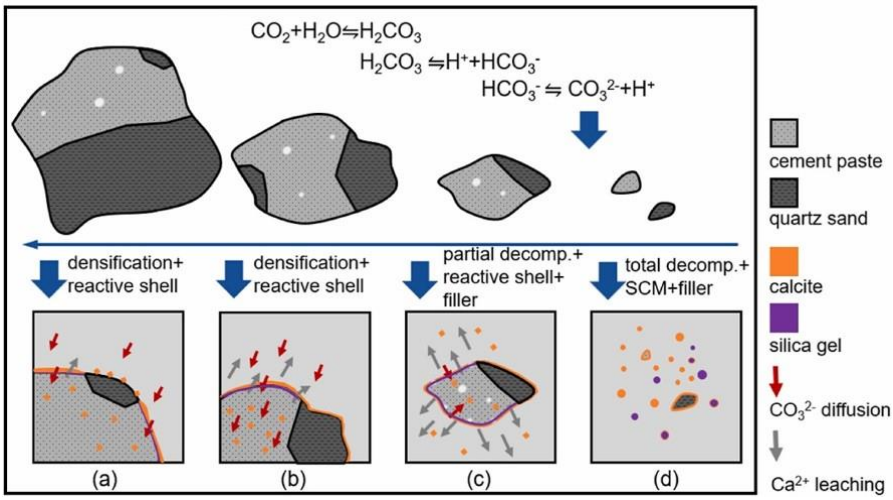

Fig. 4. Reaction process of aqueous carbonation on recycled concrete fines with a size of (a) 1.18–2.36 mm, (b) 0.6–1.18 mm, (c) 0.15–0.6 mm and (d) <0.15 mm [40].

3.1.2 Kinetics during cement hydration

Carbonated RCFs have been proved to be a pozzolanic material with high reactivity in the hydration process of composite cement. As seen in Fig. 5a, the early hydration kinetics of portlandite-RCF blends were similar to that of ternary composites consisting of portlandite, fly ash and limestone in terms of the calorimetry results [68]. The calorimetry curves were mainly affected by three aspects: (i) the first reactions related to the dissolution of anhydrous materials; (ii) the main hydration peak associated with alite hydration [69]; (iii) the inflection after the alite hydration peak due to the depletion of gypsum and the accelerated reaction of the aluminate phases [70]. It is noted that the first dissolution peak can be intensified by incorporating carbonated RCFs, while there is a minor effect on alite hydration peak as compared to the limestone-portlandite blends [71]. Moreover, the depletion of sulphate occurred earlier in the RCF blend than that in the fly ash blend, attributed to the restrained alite hydration and delayed sulphate depletion by fly ash [68].

The evolution of hydration kinetics provides more insights into the hydration degree of composite cement. The consumption rate of C_3S, C_3A and C_4AF clinkers were similar among the three blends [68], but the hydration rate of C_2S clinker was significantly lower in the carbonated RCFs blend as compared with the limestone blend (Fig. 5b). Moreover, the content of portlandite in limestone blend increased continuously due to the clinker reactions, while that in the carbonated RCFs blend was much lower and increased slowly (Fig. 5c). The latter can be explained by the rapid pozzolanic reactions of alumina-silica gels in RCFs blend [41]. In addition, the pozzolanic reaction rate of RCFs blend was higher than the fly ash blend, as indicated by the lower portlandite content and higher bound water content of the RCFs blend [68,72,73]. The zeta potential analysis

further inferred that there exists a strong acid-based chemical interaction between dissolved calcium ions and carbonated RCFs surface, in contrast with the weak electrostatic interaction of uncarbonated RCFs [74]. Therefore, the carbonated RCFs facilitated the nucleation and stabilization of C-S-H gels and contributed to the rapid hydration within a few hours [37].

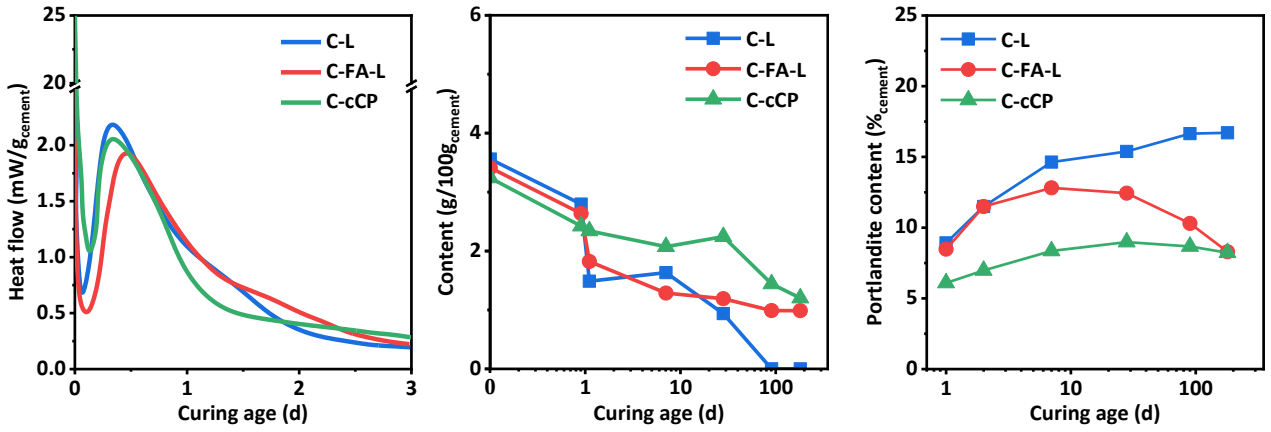

(a) (b) (c)

Fig. 5. (a) Calorimetry curves and (b) dicalcium silicate and (c) portlandite content during cement hydration (Note: L – limestone, FA – fly ash, cCP – carbonated cement paste) [68].

3.2 Phase assemblage

3.2.1 Phase assemblage during aqueous carbonation

Based on the Gibbs free energy minimization theory, the phase assemblage evolution of RCFs during aqueous carbonation was predicted through thermodynamic modelling, indicating the formation of two main carbonated products, i.e., calcium carbonate and amorphous gels [42]. As the main reaction product in carbonated RCFs, calcium carbonate can be produced by decalcification of CH, C-S-H, alite and belite clinkers. Within the first 5 min of carbonation, CH and carbonate ions dissolved from CO_2 reacts first [62], during which two types of calcium carbonates appeared, including amorphous calcium carbonate and calcite [66,75]. The carbonation of C-S-H took place when CH was completely depleted at 5–30 min, leading to the rapid development of calcite crystals on the surface of RCFs particles [76]. At over 30 min, the leaching of calcium irons under a lower Ca/Si ratio was devoted to the precipitation of calcium carbonate, and the stable calcite polymorph became the main form of calcium carbonate [77,78]. Moreover, the thermodynamic modelling results suggested that the reactions of interlayer and principal calcium occur in the meanwhile before the removal of high-Ca C-S-H [42], and only the principal calcium was left after the consumption of high-Ca C-S-H (Fig. 6a). As the carbonation duration increases from 5 min to 60 min, the pH of water-CO_2 solution significantly dropped from over 12 to nearly neutral [79], while

the Ca/Si ratio also gradually dropped from over 3.0 to around 0.66 (Fig. 6b).

Amorphous gels in the form of silica or alumina-silica gels are produced during the aqueous carbonation of RCFs. Due to the rapid carbonation of CH (Fig. 6a), the surface of RCFs would be covered by a calcite layer in the first 5 min of carbonation, which inhibits the dissolution of calcium and silicon irons. As a result, only a limited amount of silica-bearing gels can be produced through the carbonation of decalcified C-S-H gels, forming a silica-rich layer lying at the outermost surface of calcite layer with a thickness of less than 5 nm [80]. During 5–20 min, the rapid release of calcium caused the C-S-H phase transformation from a high Ca/Si ratio to a low Ca/Si ratio, as well as the formation of amorphous silica gels [65]. After carbonation of 20–60 min, the rapid carbonation of decalcified C-S-H further led to the increase of silica gels, while the RCF core would shrink and turn porous due to the continuous diffusion of calcium and silicon irons [42]. The residual RCF core disintegrated at over 60 min, but the decomposition of decalcified C-S-H phase to silica gel would last for hours [63]. Therefore, the gels with a Ca/Si ratio of 0.67 (referred to decalcified C-S-H gels) can still be observed after 6 h carbonation (Fig. 6b).

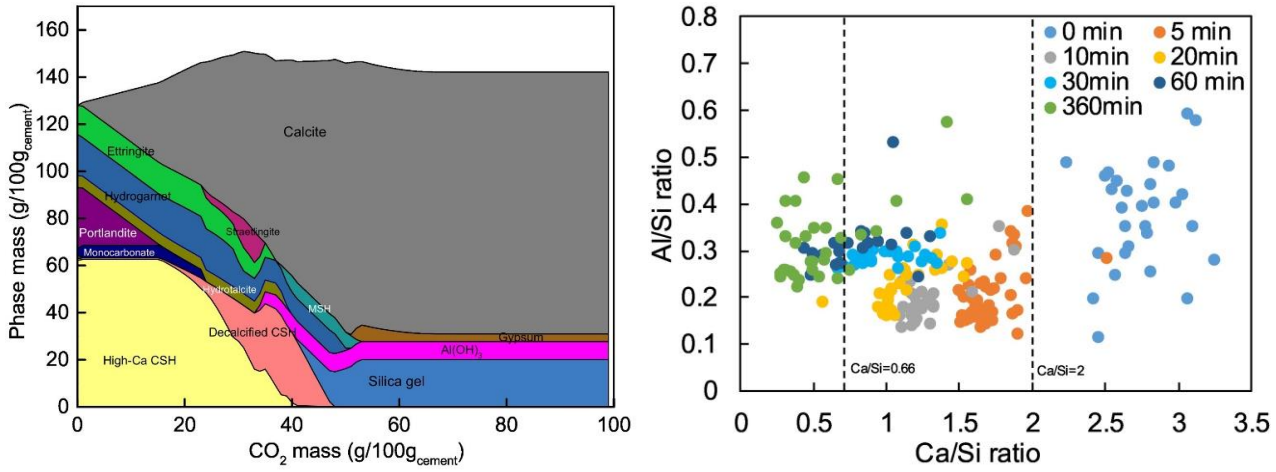

(a) (b)

Fig. 6. (a) Thermodynamic modelling of the phase assemblage and (b) chemical composition evolution of RCFs during aqueous carbonation [42].

In addition, alumina-bearing gels (i.e., alumina gels and alumina-silica gels) are also produced due to the carbonation of monosulphate (AFm), hydrated calcium aluminate and residual clinkers [81]. Meanwhile, the co-existence of alumina and silicon in the carbonated gels was proved after carbonation for 6 h [41]. However, the final structure of alumina-silica gels was independent of the cement composition and CO_2 concentration [39]. Similarly, the Al/Si ratio was nearly constant between 0.2 and 0.3 regardless of the carbonation duration, meaning that the Al/Si ratio of the inner

RCF cores or alumina-silica gels is maintained during carbonation (Fig. 6b). Apart from the silica and alumina bearing gels, a hydrotalcite-like phase was observed in the carbonated composite cement, which may decompose to magnesium and calcium carbonates [82]. It is worth noting that the contents of above-mentioned carbonated gels are sensitive to cement composition and hydration degree. To be more specific, higher content of Portland cement resulted in a higher content of calcium carbonate after carbonation, while adding more supplementary cementitious materials led to a higher amount of alumina and silica gels [39,83]. Moreover, the formation of hydrotalcite-like phase required a high hydration degree of the alkali-activated slag cement [84].

3.2.2 Phase assemblage during cement hydration

As predicted by thermodynamic modelling, the phase assemblage evolution during hydration of composite cement (i.e., portlandite and RCF blend) was similar to that of limestone and fly ash blends in terms of the hydrate types [68]. C-S-H gels, ettringite and portlandite dominated the initial hydrates, while the formation of AFm crystals appeared only after the depletion of gypsum (Fig. 7a). It is worth mentioning that the massive precipitation of C-S-H gels within the first 24 h hydration in RCFs blend was significantly different from that of limestone blend [73]. During the early hydration of 3 d, the rapid carbonation of calcium sulphate and aluminate phases can lead to the monocarbonate precipitation and ettringite stabilization, respectively [85,86]. Moreover, the higher content of ettringite and C-S-H phases in carbonated RCFs would result in a higher content of hydrates (especially the AFm phase) than that of fly ash blend [87], the phenomenon of which was maintained to 7 d. However, a similar phase assemblage of RCFs and fly ash blends was observed after 90 d hydration, suggesting that RCFs can be regarded as a pozzolanic material [39,72]. X-ray diffraction analysis further revealed a slow transformation from hemicarbonate to monocarbonate [70], which can be attributed to the slow dissolution of limestone [71].

The incorporation of carbonated RCFs also significantly affected the chemical composition of the hydrated C-S-H phase (Fig. 7b). After 28 d hydration, the Ca/Si ratio of hydrates in the case of RCFs and fly ash blends was 1.48 and 1.55, respectively, which was lower than that of the limestone blend (i.e., 1.72). However, the incorporation of fly ash or RCFs led to a rise of Al/Si ratio in hydrates to 0.07 and 0.08, respectively, in comparison with the Al/Si ratio of 0.04 in the limestone blend. The reduced Ca/Si ratio and increased Al/Si ratio in C-S-H can be ascribed to the ongoing pozzolanic reactions of carbonated RCFs or fly ash [88,89], which was similar to the phase assemblage of ternary cement containing clinker, slag and limestone [90]. From the perspective of

utilising RCFs as supplementary cementitious materials, several valorisation approaches have been developed to transform RCFs into a reactive pozzolan [91,92], including enforced carbonation through gas-liquid-solid pathway [39,72], combination of autoclaving (high-pressure steam curing) and enforced carbonation [93,94], and glass production via thermal treatment and fast quenching [95,96].

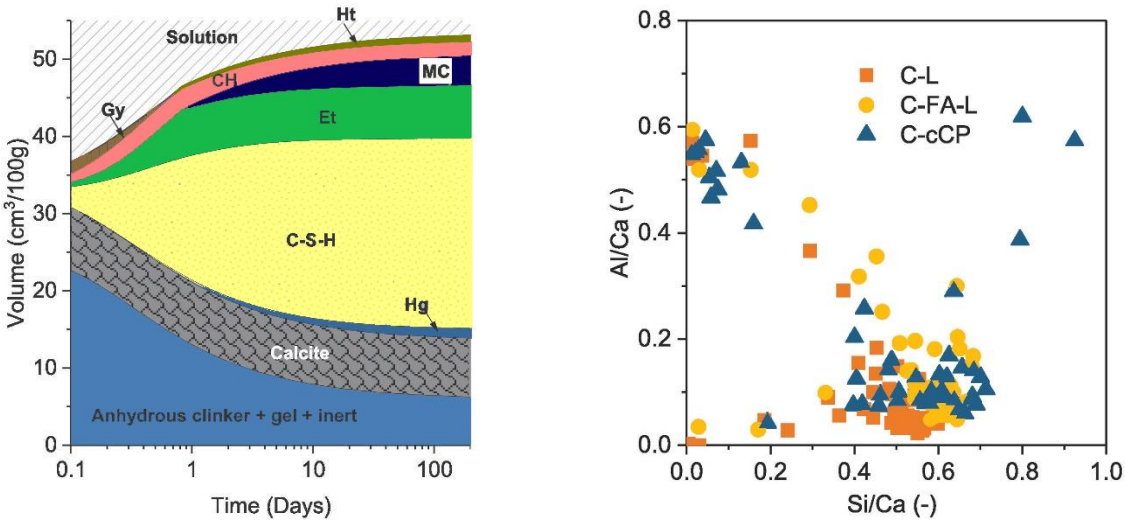

(a) (b)

Fig. 7. (a) Thermodynamic modelling of the phase assemblage evolution during cement hydration and (b) composition of C-S-H at 28 d (Note: Ht – hydrotalcite, Hg – hydrogarnet, Et – ettringite, MC – monocarbonate, Gy – gypsum) [68].

4. Microstructure of carbonated recycled fines and aggregates

4.1 Physical properties

Table 1 summarises the effect of carbonation condition on the physical properties of RCFs. After accelerated carbonation treatment, the density of RCFs increased by up to 11.79% [97], while the water absorption and porosity declined by no more than 34.80% [83] and 70.37% [36], respectively. The enhancement in physical properties of RCFs increased with prolonged carbonation time. However, the decreased rate of porosity and increased rate of CO_2 uptake slowed down after 48-h carbonation, and thereby 48 h can be regarded as an optimal duration for RCF carbonation [98]. Moreover, the carbonation temperature also affects the change of physical properties, while the most significant reduction in porosity of RCFs was observed at the chamber temperature of 100 °C [36]. In addition, a standard process for evaluating the quality of carbonated RCFs considering the particle size effect is still lacking.

Similarly, accelerated carbonation was also proved to improve the physical properties of

recycled fine and coarse aggregates, as summarised in Tables 2 and 3. In most cases, the larger partial size of recycled aggregates would lead to more obvious changes in physical properties under the same carbonation condition [99]. Moreover, carbonated RFAs and RCAs generally had lower water absorption and porosity whilst higher density and crushing value than uncarbonated recycled aggregates. Among all physical properties, the variation in water absorption was most significant, with a reduction of up to 71.72% for RFAs [30] and 56.89% for RCAs [100]. Additionally, the CO_2 concentration and pressure of 50% and 0.4 MPa respectively were found to be the optimal carbonation condition for reaching the highest CO_2 binding efficiency [30,101]. Besides, aggregate crushing value, referring to the percentage of the crushed material when subjected to a specified load, was another important indicator of recycled concrete aggregates [23]. It was found that accelerated carbonation can reduce the crushing value of RFAs and RCAs by up to 44.44% [30] and 27.34% [22], respectively. Although similar change trends of physical properties after carbonated were reported in previous studies (as listed in Tables 2 and 3), there were huge differences in terms of the absolute value of physical properties in the available literature. Thus, a standard measurement or classification of carbonated recycled aggregates is essential to evaluate the carbonation efficiency, which should consider the curing age and strength grade of the parent material of RFAs and RCAs, the method and condition of carbonation, as well as the main physical properties and indices.

4.2 Morphology

During the aqueous carbonation, poorly crystalline calcium carbonate progressively formed on the surface of RCFs within the first 5 min, which turned to be calcite grains with a layer structure with well-defined edges at 20 min [42]. Afterwards, rhombohedral calcite grains with an average size of approximately 500 nm appeared on the outer surface, followed by the disintegration of RCF particles after 60 min carbonation [37,121]. The element maps of RCFs in the final stage of carbonation (over 360 min) mainly included two density zones, i.e., darker regions with decalcified hydrates and brighter regions with the co-existence of calcite and alumina silica gels [41]. Moreover, an extensive well-crystallized calcite shell was observed as the coating of carbonated RCFs with diameters of 0.6–2.36 mm [40]. However, a loose coating with relatively small calcium carbonate clusters was formed on RCFs of 0.6 mm, in comparison with a denser coating on larger particles sizing between 1.18 mm and 2.36 mm. The former is attributed to the leaching of calcium irons and precipitation of calcium carbonate from the inner RCFs, while the latter can be explained by the delayed dissolution and leaching process due to lower contact surface area [33].

Table 1 Characteristics of RCFs under different carbonation treatments.

Particle size (μm)	Tested mixture		Carbonation parameters					Enhancement rate of physical properties (%)				Ref.
	RCF/b	w/b	CC (%)	CP (MPa)	t (h)	RH (%)	T (°C)	Density	Water absorption	Porosity	CO_2 uptake	
< 80	1	0.15	–	0.2	2	–	–	–	–	-21.85	19.80	[62]
< 75	0.20	0.40	99	0	2	60 ± 5	20 ± 1	–	–	-29.73	–	[70]
< 150	0.30	0.50	20 ± 3	0	72	70 ± 5	20 ± 2	–	-34.80	–	–	[83]
< 75	0.80/0.90	–	20	0	672	70 ± 2	20 ± 2	11.79/8.45	-16.67/-10.14	–	–	[97]
< 150	0.80/0.90	–	20	0	672	70 ± 2	20 ± 2	3.54/ 2.73	-29.32/-20.73	–	–	
< 150	0.20	0.40	20	0	0.5	5–10	20/60/ 100/140	–	–	-33.33/-52.47/ -70.37/-48.15	–	[36]
< 150	–	–	–	0.01	3/24/48/ 96/144	50 ± 5	23 ± 3	–	–	-13.64/-15.24/-18.02/ -19.28/-20.30	12.22/32.39/40.34/ 41.48/48.58	[98]

Note: RCF/b – RCF-binder ratio; w/b – water-binder ratio; CC – CO_2 concentration; CP – CO_2 pressure; t – time; RH – relative humidity; T – temperature.

Table 2 Characteristics of RFAs under different carbonation treatments.

Particle size (mm)	Parent material, f_c (MPa)	Carbonation method	Carbonation parameters					Enhancement rate of physical properties (%)			Ref.
			CC (%)	CP (MPa)	t (d)	RH (%)	T (°C)	Density	Water absorption	Crushing value	
< 4.75	30	Standard	20 ± 2	0	3	60	20	2.89	-26.42	–	[28]
0.16-2.5	30/50	Standard	20 ± 2	0	–	60 ± 5	20 ± 2	4.74/5.62	-28.29/-22.64	-9.14/-7.60	[29]
0.1-2	–	Standard	20	0	2	70	20	–	-25.70	–	[102]
< 0.5	–	Standard	20/50/70/100	0	–	60 ± 5	20 ± 2	–	-54.02/-71.72/-62.07/-54.02	-44.44/-33.33/-27.78/-12.22	[30]
0.075-2	–	Standard	4	0	7	90	50	–	-5.68	–	[103]
2-4.75	–	Standard	4	0	7	90	50	–	-33.26	–	
< 5	–	Pressurised	5	0.1	3	60 ± 5	20 ± 2	2.45	-28.99	–	[104]
0.15-5	–	Standard	20 ± 3	0	10	70 ± 5	20 ± 2	0.49/0.37/0.59	-8.65/-29.66/-33.33	–	[25]
< 5	–	Pressurised	100	0.5	1	–	–	1.02	-26.83	–	[24]
0.16-2.5	30/50	Standard	20 ± 2	0	7	60 ± 5	20 ± 2	4.74/5.62	-28.29/-22.64	-9.14/-7.60	[89]
< 5	–	Standard	20 ± 3	0	–	70 ± 5	20 ± 2	2.38	-46.15	–	[105]

Note: f_c – compressive strength.

Table 3 Characteristics of RCAs under different carbonation treatments.

Particle size (mm)	Parent material, f_c (MPa)	Carbonation method	Carbonation parameters						Enhancement rate of physical properties (%)				Ref.
			CC (%)	CP (MPa)	CFR (ml/s)	t	RH (%)	T (°C)	Density	Water absorption	Crushing value	Porosity	
5-20	–	Standard	20 ± 3	0	–	10 d	70 ± 5	20 ± 2	0.31/0.35/0.51	-15.24-/21.43/-45.32	–	–	[25]
5-10	–	Pressurised	100	0.5	–	24 h	–	–	1.37	-15.28	–	–	[24]
5-20	–	Standard	20 ± 3	0	–	–	70 ± 5	20 ± 2	0.76	-20.83	-11.84	–	[105]
20-30/30-40/> 40	–	Standard	20	0	–	3 d	70 ± 5	23 ± 2	1.59/0.91/0.50	-32.03/-25.65/-9.74	–	-42.80/-41.77/-38.04	[106]
10-20/20-30/30-40	–	Standard	20	0	–	7 d	70 ± 5	20 ± 2	0.46/0.58/0.69	-30.08/-26.95/-26.91	–	-25.88/-25.21/-24.67	[99]
10-20/20-30/30-40	–	Standard	20	0	–	14 d	70 ± 5	20 ± 2	0.81/0.97/1.01	-34.59/-34.13/-32.88	–	-30.21/-29.60/-29.72	
10-20/20-30/30-40	–	Standard	20	0	–	28 d	70 ± 5	20 ± 2	0.93/1.04/1.08	-35.49/-35.48/-34.98	–	-30.78/-30.30/-30.79	
5-20	33.33	Pressurised	99.99	0.05/0.1/0.2/0.4	–	1 h	–	–	0.76/0.57/0.95/0.76	-11.29/-17.28/-20.05/-20.51	-4.75/-8.64/-11.22/-14.13	–	[107]
5-20	33.33	Pressurised	99.99	0.1	–	3/12 h	–	–	0.95/1.15	-22.58/-26.27	-21.25/-22.44	–	
5-10	–	Pressurised	100	–	0.1	1 d	50 ± 1	25 ± 1	2.43	-23.40	–	–	[108]
5-10	40	Pressurised	> 99	0.01	–	6/12/24/48/72 h	–	25	0.17/0.47/0.81/0.89/0.98	-11.35/-28.41/-38.2/-39.43/-40.57	–	–	[100]
10-20	40	Pressurised	> 99	0.01	–	6/12/24/48/72 h	–	25	0.56/0.85/1.06/1.06/1.19	-14.38/-32.06/-38.07/-39.68/-40.86	–	–	
5-10	65	Pressurised	> 99	0.01	–	6/12/24/48/72 h	–	25	0.13/0.34/0.67/0.76/0.84	-16.84/-42.09/-54.21/-55.78/-56.89	–	–	
10-20	65	Pressurised	> 99	0.01	–	6/12/24/48/72 h	–	25	0.21/0.42/1.01/1.09/1.17	-12.69/-31.73/-47.96/-49.68/-51.18	–	–	

5-10/10-20	–	Flow	> 99	–	16.67	24 h	50	25	1.32/0.77	-8.94/-6.30	–	–	[47]
5-10/10-20	–	Pressurised	> 99	0.01	–	24 h	50	25	2.27/1.78	-14.43/-11.86	–	–	
5-10/10-20	–	Aqueous	> 99	–	33.33	6 h	–	25	0.50/0.54	-5.36/-4.15	–	–	
5-10/10-20	–	Standard	99.9	0	–	24 h	55	22	4.81/3.16	-19.41/-15.05	-31.47/-31.47	–	[109]
5-16	–	Standard	20 ± 2	0	–	24 h	70	50	0.47	-23.60	-36.18	–	[35]
5-20	20	Pressurised	> 99	0.4	–	6/12/ 24/48/ 72 h	–	–	0.34/0.23/ 0.53/0.38 /0.65	-15.38/-20.31/ -27.08/-23.38/ -28.31	-1.56/-3.28/ -4.77/-5.81/ -8.57	–	[110]
5-20	–	Pressurised	100	0.01	–	24 h	–	–	0.55	-26.28	–	–	[111]
5-20	49.3	Standard	5/10/ 20/40/ 60/80/ 100	0	–	7 d	50 ± 5	25 ± 3	0.15/0.30/ 0.76/0.84/ 0.95/1.06	-5.85/-13.88/ -21.91/-22.91/ -24.08/-25.59/ -25.92	-10.79/-17.27/ -21.58/-23.74/ -24.46/-26.62/ -27.34	–	[22]
5-25	–	Standard	20 ± 3	0	–	–	70 ± 5	20 ± 2	2.29	-13.79	-7.78	–	[112]
5-10/10-20	–	Pressurised	100	0.01	–	24 h	–	–	0.34/0.23	-11.11/-16.39	-21.22	–	[23]
5-10/10-20	–	Pressurised	100	0.5	–	24 h	–	–	1.49/0.15	-16.67/-18.03	-25.90	–	
5-10/10-20	–	Pressurised	100	0.5	–	24 h	–	–	1.10/0.39	-9.38/-5.45	-12.65	–	
5-10/10-20	–	Pressurised	100	0.1	–	7 d	–	–	0.38/0.81	-14.63/-22.29	–	–	[113]
5-20	–	Standard	20 ± 2	0.5	–	7–14 d	55 ± 5	20 ± 2	5.53	-26.58	-23.67	–	[114]
5-25	–	Pressurised	> 99.9	0.1/0.4/ 0.8	–	24 h	–	–	1.03/0.53/ 0.65	-26.15/-27.08/ -9.85	-4.99/-5.01/ -4.92	–	[101]
5-25	23.0	Standard	20	0	–	3 d	70	20	-0.26	-18.36	13.82	–	[115]
5-25	23.0	Standard	3	0	–	4/7 d	70	20	-0.33/-0.33	-9.18/-9.04	4.61/2.63	–	
5-20	–	Pressurised	100	0.08	–	24 h	–	–	1.70	17.52	-1.74	–	[116]
< 10/< 20	–	Pressurised	99.9	0.2	–	2 h	–	–	0.74/1.13	-52.74/-57.72	–	–	[117]
5-16	–	Standard	100	0	–	21 d	60	–	0.38	-21.59	–	–	[118]
5-20	30.2/48.3/ 61.6/74.0	Pressurised	–	0.01	–	1 d	30-80	23	-0.76/-0.65/ 1.91/2.27	-20.21/-21.24/ -22.52/-24.10	–	-19.03/-18.53/ -21.43/-20.95	[119]
5-10	–	Flow	> 99.9	–	83.33	24 h	–	–	6.18	-6.45	–	–	[21]
2-12.5	–	Standard	5	0	–	7 d	50	20	–	-6.47	–	-13.72	[120]

Note: CFR – CO_2 flow rate.

During the hydration of cement containing carbonated RCFs, granular C-S-H nuclei occurred on the surface of RCFs after 1 h hydration [65], while granular nuclei further grew into acicular gels at 4 h and finally presented a fine needle-like appearance in perpendicular to the RCFs surface at 7 h [74]. In contrast, there was only a bit of hydration product formed on the surface of uncarbonated RCFs particles even after 7 h hydration. This is because the outer silica gel layer of carbonated RCFs dissolves and reacts in the solution when mixed with water, and accordingly the underneath calcium carbonate layer is exposed and provides a nucleation site for C-S-H gels [122]. In addition, the strong chemical interactions between calcium carbonate and C-S-H enable the perpendicular and uniform growth of C-S-H phases on the RCFs surface [123]. After 28 d hydration, the hardened paste of the carbonated RCF blend was homogeneously filled with small calcite particles, while the residual carbonated RCF grains were re-filled with C-S-H gels [68,79].

Different from RCFs, recycled aggregates (i.e., RFAs and RCAs) would not disintegrate during carbonation, and the morphology of carbonated recycled aggregates indicated a finer and denser structure than uncarbonated aggregates regardless of the carbonation methods [32,119]. For example, the roughness of RCAs with a size larger than 4.75 mm was up to 923.55 μm, while 14 d pressurized carbonation would reduce the roughness to less than 557.38 μm due to the filling effect of pores and micro-cracks [106,124]. However, the morphology of carbonated RFAs with a size smaller than 4.75 mm was proved to be highly dependent on the accelerated carbonation method. Specifically, typical hydrated products including C-S-H, CH and AFm phases can be identified on the surface of uncarbonated RFAs (Fig. 8a). In contrast, agglomerations of calcium carbonate crystals with dense microstructure occurred on the surface of RFAs after 24-h pressurized carbonation (Fig. 8b), while RFAs were uniformly coated with the precipitated calcite granulates with a size around 1 μm after 6 h aqueous carbonation (Fig. 8c). In other words, the calcite products after the liquid-solid carbonation shows more porous and smaller particles than that of the gas-solid carbonation, which consequently promotes the carbonation reactivity of RFAs [27].

The underlying mechanism of RFA morphology is associated with the microstructure forming processes during carbonation. During gas-solid carbonation, the calcite and silica gels located inside the RFAs matrix would react with the diffused CO_2, contributing to the refined pore structure and drop of porosity [103]. The internal precipitation of RFAs can be described by the shrinking core model (Fig. 8d), which implies that the diffusion rate of CO_2 into the reactive layer dominates the carbonation process [125]. In this case, higher CO_2 pressure would result in the faster formation of

calcite precipitation and agglomerations of calcite on the RFA surface [126]. Moreover, the aqueous carbonation of RFAs is simulated using the surface coverage model (Fig. 8e). After soaking in water, calcium ions released through the dissolution of portlandite quickly reacted with the dissolved CO_2, leading to the nucleation and deposition of calcium carbonate on the surface of RFAs [127]. As the carbonation proceeded, the dissolution of ettringite and C-S-H in the outermost layer compensated the reduction in calcium ions after portlandite depletion, forming a two-layer shell on the surface of RFAs, i.e., an outer precipitated calcite layer and inner decalcified silica-rich layer [33]. When the RFAs were fully covered by calcite precipitation, both the outwards calcium ions and inwards CO_2 diffusions were inhibited, and the carbonation was progressively slowed down [128]. In addition, the reaction process of RFAs in CO_2-water solution was relatively adequate, so eventually distributed granulates were formed instead of phase agglomeration [27].

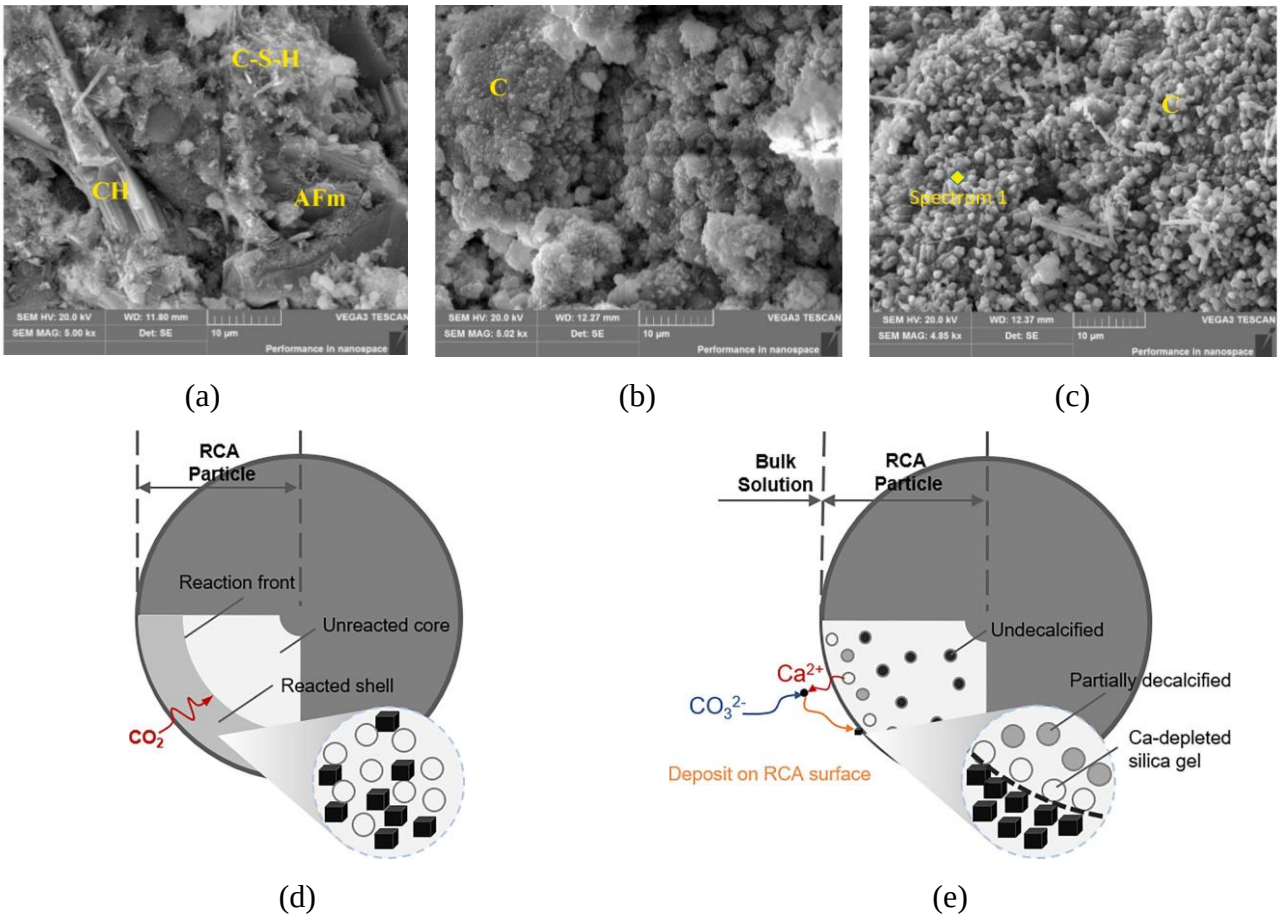

Fig. 8. SEM images of (a) uncarbonated RFAs, (b) Pressurized carbonated RFAs and (c) aqueous carbonated RFAs [27], and schematics of microstructure forming processes of RFAs during (d) pressurized carbonation and (e) aqueous carbonation [33].

4.3 Pore structure

During the aqueous carbonation of RCFs, the cumulative pore structure smaller than 200 nm firstly

increased from 0.076 m^3/g to 0.133 m^3/g within the first 30 min wet carbonation, and further considerably decreased to 0.078 m^3/g at 60 min (Fig 9a). The former increase in pore volume can be ascribed to the destroyed pore structure by decalcification of calcium-bearing hydrates [42], while the latter is because of the disintegration of RCFs particles coupled with the occurrence of capillary pores larger than 200 nm [41]. After carbonation for 6 h, the formation of amorphous silica-bearing and alumina-bearing gels led to the increase in proportion of gel pores finer than 10 nm, and thereby very fine particle sizes of carbonated RCFs can be obtained [65,129]. In addition, the pore structure of carbonated RCFs shows a strong dependency on the particle size effect. To be more specific, the extensive gel pores in silica and aluminium gels resulted in an up to 70.2% rise in the porosity of RCFs with a size smaller than 0.15 mm within 6 h carbonation [40,66,86]. In contrast, the pore volume of RCFs with a size of 1.18 mm and 2.36 mm was reduced by 31.3% and 24.8%, respectively, due to the densified structure of calcium carbonate precipitation [62]. Furthermore, both dissolution-induced pore coarsening effect and densification-induced pore refining effect can be observed in RCFs with a size of 0.6 mm, leading to the evolution of porosity with carbonation duration, as shown in Fig 9b. During the hydration of cement, the threshold pore diameter of RCF blend progressively dropped with curing age [70], due to the densification of microstructure during hydration [68]. Moreover, the hydration-dependent porosity of RCF blend was similar to that of limestone and fly ash blends within 28 d curing, regardless of the significant difference in phase assemblage (Section 3.2). After hydration of 90 d, the cumulative pore volume of RCF blends was lower than that of limestone blend but higher compared to fly ash blend, while a similar relationship was found in the evolution of pore threshold [68]. It is worth noting that the pores seemed to be finer in the RCF blend than limestone blend due to the early hydration of RCFs within first 24 h, the effect of which resembled that of the metakaolin in blended cement [130].

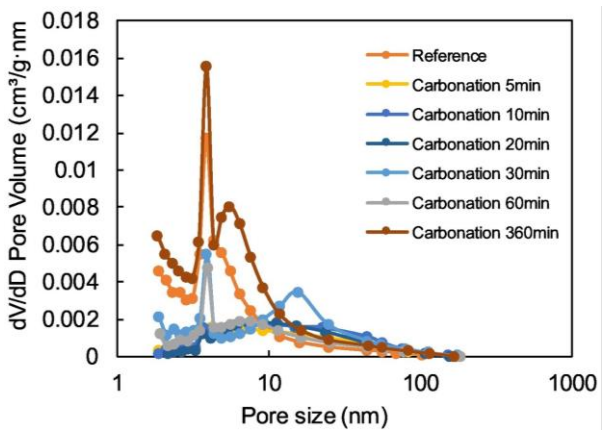

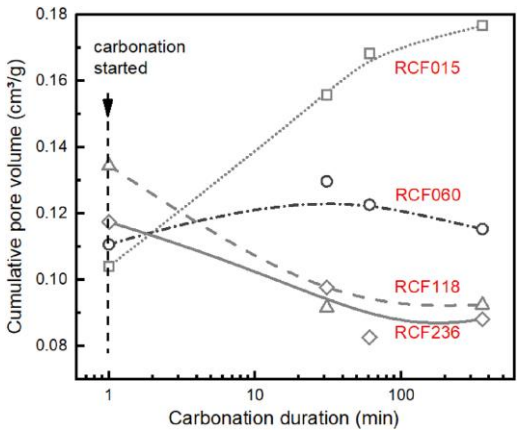

(a) (b)

Fig. 9. (a) Pore size distribution of carbonated RCFs after various carbonation durations [42] and (b) pore volume evolution of carbonated RCFs with particle size and carbonation duration [40].

For recycled aggregates, the accelerated carbonation would clog the micro-cracks and reduce the total porosity regardless of particle size and carbonation method (Tables 2 and 3). In particular, 14-d pressurized carbonation resulted in a 32.8% decrease in the cumulative pore volume of RCAs with a diameter between 4.75–9.5 mm [124]. Moreover, the medium capillary pores with size between 10–50 nm went up by 5.7% after carbonation, while the large capillary pore (i.e., 50–1000 nm) was kept as the major pore type accounting for 43.2% pore volume. Although the total pore volume of RFAs can be reduced by carbonation, the evolution of porosity is closely related to the carbonation duration [43]. For example, the cumulative pore volume of RFAs smaller than 4.75 mm dropped by 20.8% after 1 h aqueous carbonation, but an opposite trend in porosity appeared when the duration reached 6 h (i.e., 8.3% lower than uncarbonated RFAs) [27]. The former can be attributed to the filling of gel pores smaller than 10 nm by precipitation of calcium carbonate, while the latter is due to the further dissolution of calcium carbonate under excess CO_2 conditions [33,46]. In addition, pre-treatment methods can further densify the pore structure of carbonated recycled aggregates [44]. For instance, the spraying or smoking of saturated CH solution or concrete plant wastewater followed by pressurized carbonation at 0.1 MPa for 24 h was proved to significantly reduce the porosity of RCAs, as compared with conventional pressurized carbonation [34]. Moreover, the spraying of CH solution at the amount of half water absorption of RCAs showed the maximum efficiency in reducing porosity, while the pores with sizes in the range of 10–1000 nm reduced most significantly due to the pore-filling effect of carbonation products [99]. Similarly, three cycles of limewater-CO_2 treatment were proved to further reduce the total porosity of RFAs by 18.0%, relative to that after three cycles of pressurized carbonation, while the medium pores ranging from 100 nm to 1000 nm were greatly refined [46].

5. Micro-mechanical properties of concrete with carbonated recycled coarse aggregates

During the fresh stage of concrete, the wall effect and water film around aggregates would prevent the hydrated particles from covering the surface of RCAs, resulting in the formation of interfacial transition zone (ITZ) between aggregates and new mortar [131,132]. Based on the modelled recycled aggregate concrete [26,133], the multiple ITZ structures in RCA concrete can be divided into three types, i.e., old aggregate-old mortar (ITZ_1), old aggregate-new mortar (ITZ_2), and old

mortar-new mortar (ITZ_3). The complexity in micro-mechanical properties of three types of ITZs in concrete with carbonated RCAs was revealed by microhardness analysis.

5.1 Old aggregate-old mortar ITZ

Through pore segmentation of back-scattering images, the porosity of ITZ in concrete as a function of distance from high-quality (i.e., w/c = 0.25) or low-quality (i.e., w/c = 0.40) RCAs is displayed in Fig. 10a and b. For plain RCA concrete, the porosity of ITZ dropped significantly from up to 49.1% to approximately 25%, when the distance from RCAs went up from 10 μm to 60 μm, regardless of the parent materials of RCAs [118,134]. The change in porosity of carbonated RCA concrete was quite similar to that of RCA concrete in terms of both average porosity and pore gradient, except that the porosity at the innermost 10 μm of carbonated RCAs was about 6.1% lower than plain RCAs [135]. In addition, the porosity of new bulk paste fluctuated at around 25% in both RCA and carbonated RCA concrete [136]. The results indicated that although the carbonation of RCA cannot reduce the overall pore volume of ITZ and new mortar, it can to some extent densify the immediate regions of the RCA surface in concrete.

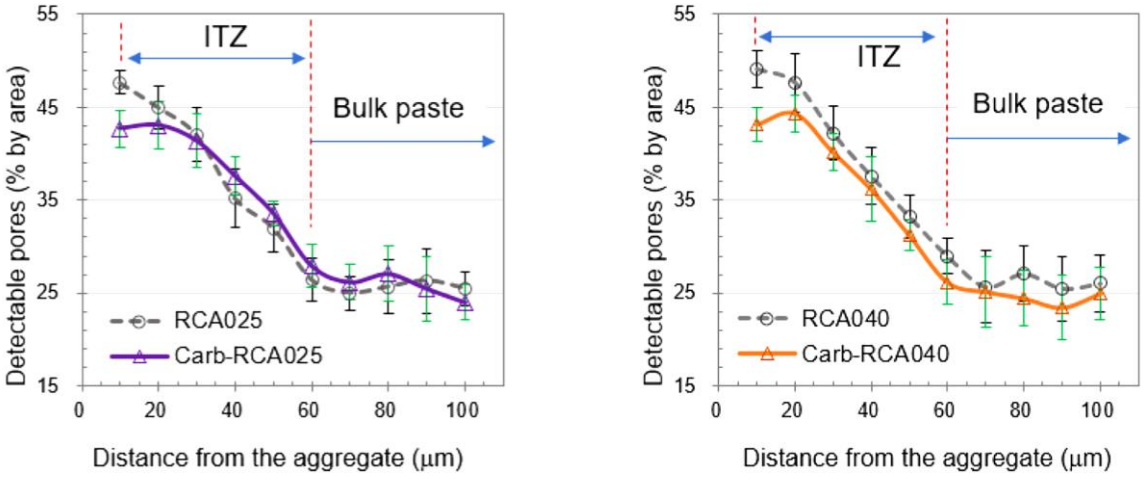

Fig. 10. Porosity of interfacial transition zone of concrete with plain RCA and carbonated RCA from parent materials with w/c ratios of (a) 0.25 and (b) 0.40 [135].

Fig. 11a and b compare the microhardness mapping and histograms of concrete with high-quality (i.e., w/c = 0.25) RCAs and carbonated RCAs. It is obvious that the microhardness of RCAs was much higher than that of the ITZ, enabling the clear identification of the starting and ending boundaries of ITZ_1. As compared with the plain RCA concrete, the microhardness of the RCA edge and ITZ_1 was improved by 10.5% and 12.5%, respectively, in the carbonated RCA concrete, while the thickness of ITZ_1 maintained at around 86 μm regardless of the aggregate type. The enhanced

property of the RCA edge can be attributed to the densification of microstructure during carbonation, while the improved ITZ_1 microhardness can be explained by reduced porosity in the innermost region of carbonated RCAs (Fig. 10). Furthermore, the micro-mechanical property of ITZ_1 was nearly independent of the RCA quality, as the average microhardness of ITZ_1 only slightly increased from 37.51 HV to 38.38 HV, when the w/c ratio of parent materials went up from 0.25 to 0.40 [135]. Statistical analysis of ITZ_1 thickness and microhardness further revealed that the elastic modulus of ITZ_1 was closely associated with the carbonation pressure, initial moisture content and carbonation duration, as illustrated in Fig. 12. The optimal carbonation condition was found to be 1 bar chamber pressure, 3 h duration and moisture content of 1.81%, under which an up to 27.4% took place in the mean elastic modulus of ITZ_1, relative to RCA concrete [107].

The microhardness analysis of ITZ also provides a quantitative method to discuss the micro-to-macro properties relationship of concrete beyond the influencing factors. For example, the pre-treatment methods on carbonated RCAs were proved to affect the ITZ properties [47], among which the pre-soaking in calcium hydroxide emulsion was proved more effective in strengthening the old aggregate-old mortar ITZ_1, as compared with the simply gas-solid carbonation [30,46,112]. However, statistical analysis suggested a strong linear correlation between compressive strength of concrete and strength of old ITZ (i.e., ITZ_1) regardless of the treatment methods (Fig. 11c). Moreover, an identical trend appeared in the relationship between dynamic elastic modulus and ITZ_1 strength (Fig. 11d), which highlights the role of old aggregate-old mortar ITZ in determining the compressive strength and dynamic elastic modulus of concrete with carbonated RCAs. Similarly, the increase of carbonation pressure from 0.5 bar to 4 bar can significantly reduce the thickness of ITZ_1 to 45 μm while improve the average elastic modulus of ITZ_1 by 11.7% (Fig. 12a and b). Nevertheless, a strong linear correlation (R^2 = 0.9592) between compressive strength of concrete and average elastic modulus of ITZ_1 can be retained, regardless of the carbonation pressure [107].

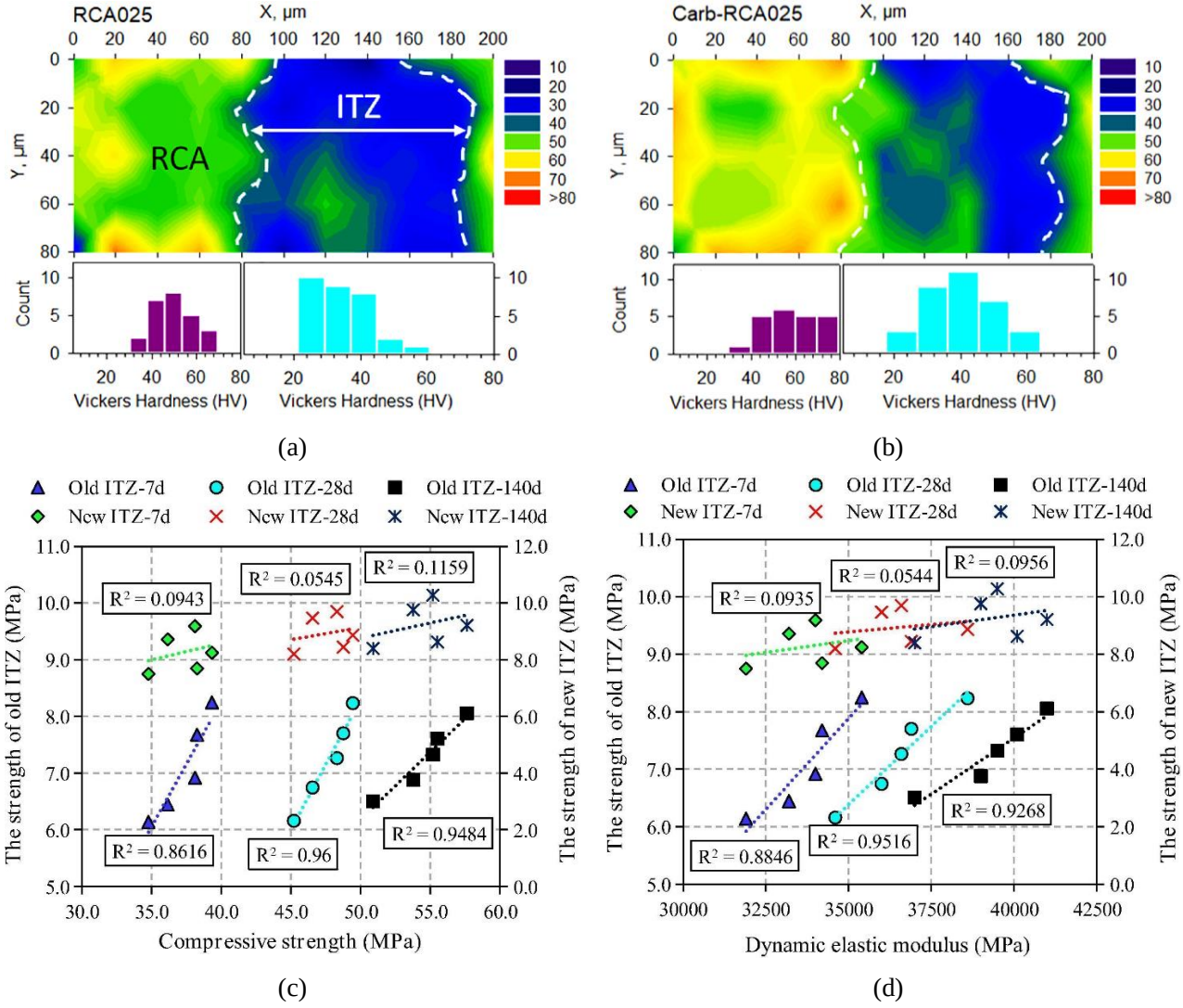

Fig. 11. Microhardness distribution of ITZ around (a) RCA and (b) CRCA in the paste with a w/c ratio of 0.25 [135], and (c) relationships between the hardness of ITZ and compressive strength of concrete and (d) relationships between the hardness of ITZ and dynamic elastic modulus [112].

5.2 Old aggregate-new mortar ITZ

Fig. 12 presents the effect of carbonation condition on thickness and average elastic modulus of ITZ_2. Similar to the evolution of ITZ_1, the increase of carbonation pressure and duration would lead to a reduction in ITZ_2 thickness and a rise in elastic modulus. In particular, the thinnest ITZ_2 of 50 μm and highest mean elastic modulus of 47.6 GPa took place after accelerated carbonation under 1 bar for 12 h, which was 28.6% lower and 78.4 higher than that of uncarbonated RCAs (Fig. 12c and d). It is worth noting that the elastic modulus of new mortar was higher than that of ITZ regardless of the carbonation condition, and thereby the decrease in ITZ thickness contributed to the overall mechanical properties of concrete [107]. Moreover, the carbonation pressure of 1 bar and duration of 3 h was regarded as a critical condition, after which the further enhancement in ITZ_2 properties

became less obvious. In contrast, the elastic properties of ITZ_2 went up with moisture content from 1.0% to 1.81%, while an opposite trend appeared with the moisture content of 3.0%. Therefore, the initial moisture content of 1.81% was an optimal condition over the measured moisture range, where a 14.3% drop in ITZ_2 thickness and 26.9% rise in average modulus occurred as compared with plain RCAs (Fig. 12e and f). The effect of three carbonation parameters on micro-mechanical properties of old aggregate-new mortar ITZ was found to be similar to that of the old aggregate-old mortar ITZ. This is because both ITZ_1 and ITZ_2 are referred to the ITZs between natural aggregates and mortar, meaning that they share similar formation processes [107]. However, the elastic modulus of ITZ_2 was lower than ITZ_1 under the same carbonation condition, which can be ascribed to the shorter hydration age and greater thickness of ITZ_2 [119]. In addition, the difference in micro-mechanical properties of ITZs was progressively narrowed with the increasing carbonation duration, as similar thickness and modulus can be observed in ITZ_1 and ITZ_2 of RCAs after 3 h carbonation (Fig. 12c and d).

5.3 Old mortar-new mortar ITZ

As demonstrated in Fig. 12, the evolution of thickness and modulus of ITZ_3 with carbonation pressure, duration and moisture content resembled that of ITZ_1 and ITZ_2, implying that the micro-mechanical properties of ITZ may be more dependent on phase assemblage rather than formation process [107]. Moreover, the properties of ITZ_3 were inferior to ITZ_1 but more sensitive to the carbonation condition than ITZ_1. This can be ascribed to manufacturing process of modelled recycled aggregate concrete: (i) the surface of RCAs was washed by running water before pouring new mortar, which would lead to the higher local moisture content and wider thickness of ITZ_3; (ii) dust and other impurities left on the surface of RCAs could cause the poorer interfacial combination of ITZ_3 [137]. Interestingly, the thickness of ITZ_3 was reduced to the lowest value of 40 μm among all types of ITZs after 12 h carbonation at 1 bar (Fig. 12c). This was because of the similar phase composition of old mortar and new mortar, resulting in better bonding performance and thereby thinner width of ITZ_3 after accelerated carbonation. Additionally, the pressure of 1 bar and duration of 3 h was the optimal combination to reach a satisfying improvement in ITZ_3 properties. The statistical analysis further revealed that the strength of new ITZ (i.e., ITZ_3) had no obvious linear relationship with compressive strength and dynamic elastic modulus of concrete (Fig. 11c and d). In other words, the mechanical properties of concrete were not directly linked to the strength of ITZ_3.

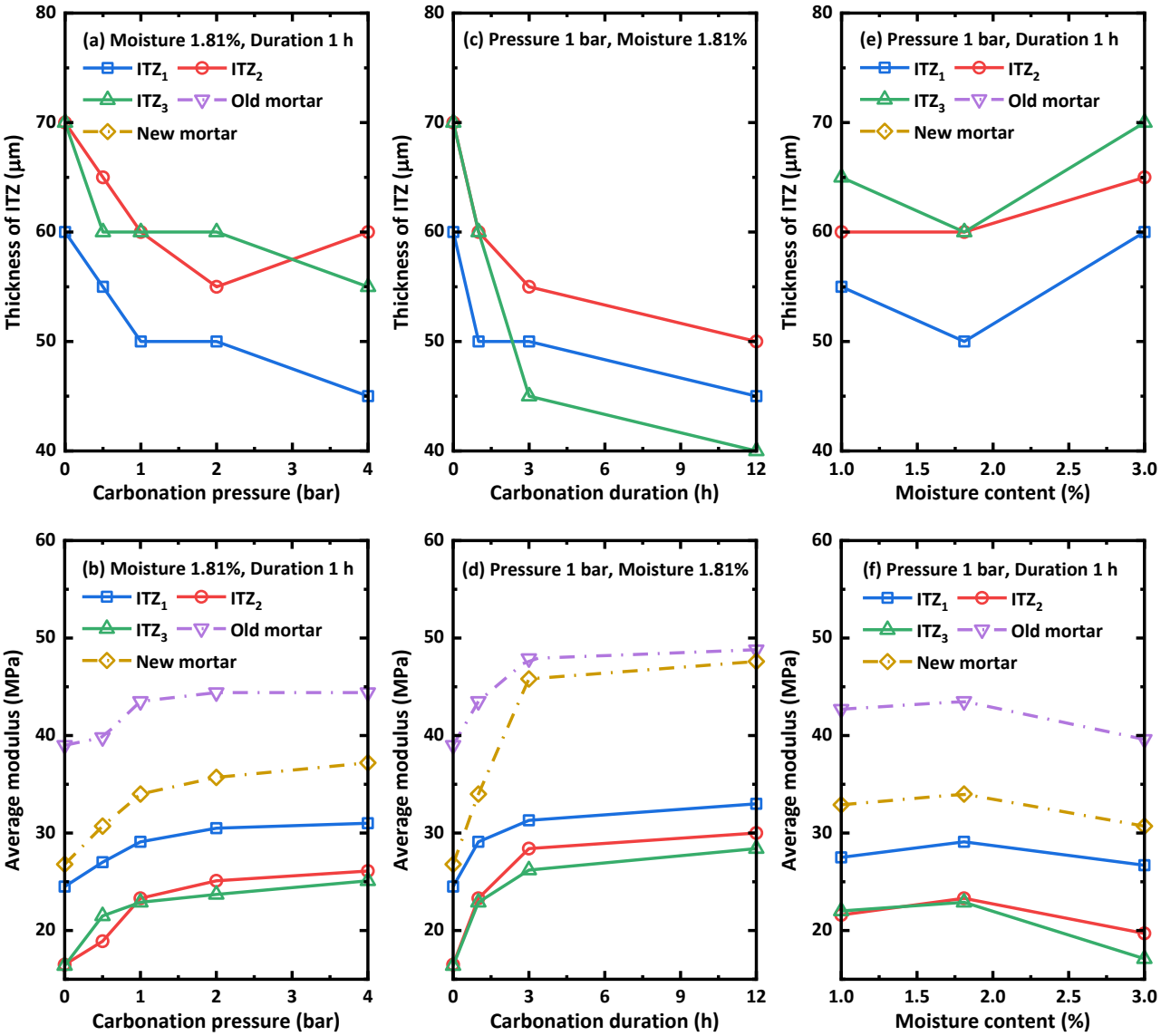

Fig. 12. Evolution of thickness and average modulus of three types of ITZs with (a) and (b) carbonation pressure, (c) and (d) carbonation duration, and (e) and (f) initial moisture content [107].

With the aid of hydration and microstructural analysis (Sections 3 and 4), the contribution of carbonated RCAs to the micro-mechanical properties of ITZs can be summarised in two aspects: (i) The physical interlocking effect. When exposed to hydrating cement, the massive calcite grains on the surface of carbonated RCAs would dissolve slowly and release carbonate ions [138]. At the same time, aluminate species from bulk paste can migrate to the RCA surface because of the wall effect [131], which further bounded with the released carbonate ions and formed monocarbonate phases [114,139,140]. Moreover, calcite grains formed on RCA surface provided nucleation sites for the precipitation of needle-like ettringite and honeycomb C-S-H gels [35,135]. In consequence, the epitaxial growth of monocarbonate and hydration crystals bridged the RCA-to-paste interface in a physical interlocking manner [141]. (ii) The chemical bonding effect. As revealed by zeta-

potential results, the calcite grains on RCA surface were favourable in capturing calcium ions from pore solution due to the chemical donor-acceptor interaction with calcium ions, leading to the formation of dense C-S-H gels on calcite surface [142]. In addition, the bound water content on the surface layer of carbonated RCAs was 2.9 times higher than that of the uncarbonated RCAs, which also facilitated the interaction with new cement paste [135]. Hence, the extensive growth of C-S-H crystals on the surface of carbonate RCAs enhanced the aggregate-to-paste interface in a chemical bonding manner. The synergic effects of physical interlocking and chemical bonding not only densify the local surface of carbonated RCAs, but also provide superior adhesion between RCAs and new paste. In contrast, poorly bonded ITZs were formed on plain RCAs as the cement particles only occurred from the new mortar side rather than from two directions [141]. As a result, the ITZ properties of carbonated RCAs were significantly higher than that of plain RCAs [23,111].

6. Macro-mechanical properties of concrete with carbonated recycled fines and aggregates

6.1 Compressive strength and elastic modulus

6.1.1 Effect of carbonation condition

Pressurized carbonation method is one of the most widely used in accelerated carbonation of RCAs. Table 4 presents the effect of two main factors of pressurized carbonation, i.e., carbonation duration and CO_2 pressure, on the compressive behaviour of RCA concrete under three replacement ratios. It can be seen that the rise in carbonation duration of RCA would promote the compressive strength of RCA concrete, while the CO_2 pressure of 75 kPa is regarded as an optimal pressure at 100% replacement. In contrast, the prolonged carbonation duration caused a drop in elastic modulus under 30% replacement while an opposite trend appeared under 100% replacement, and 75 kPa was maintained as the optimal CO_2 pressure in terms of elastic modulus. However, the replacement of carbonated RCAs did not always result in the increment of compressive strength and elastic modulus [143], and thereby it is critical to adopt reasonable carbonation conditions. For example, the pressurized carbonation of low-strength RCAs (i.e., C25) under 1 bar for 3 h was proved to be an optimal choice to increase the compressive strength of RCA concrete by up to 20.5% and 21.8%, respectively, after 7 d and 28 d of curing [107]. Under the replacement ratio of 100%, pressurized carbonation was proved more effective than flow-through carbonation in enhancing the compressive strength and elastic modulus of RCA concrete, while the synergetic effects of nano-silica spraying and pressurized carbonation on RCAs can further lead to an approximately 20% strength increase of concrete with uncarbonated RCAs [47]. However, aqueous carbonated RCAs

would result in a 1.4% drop in the elastic modulus of RCA concrete, suggesting that gas-solid carbonation is more suitable for RCAs than liquid-solid carbonation [27,47].

Table 4 Effect of carbonation condition on mechanical properties of concrete containing carbonated RCAs [117,143].

Carbonation condition		Replacement ratio of RCA (%)	Mechanical properties			
Duration (min)	Pressure (kPa)		Compressive strength (MPa)	Elastic modulus (GPa)	Splitting tensile strength (MPa)	Flexural strength (MPa)
0	0	0	32.1	39.0	3.9	4.0
	0	30	33.5 (+4.1%)	29.6 (-24.2%)	3.4 (-11.4%)	4.3 (+7.7%)
	0	100	25.7 (-20.0%)	21.9 (-45.7%)	3.0 (-23.5%)	2.5 (-37.2%)
30	75	30	34.3 (+6.7%)	34.1 (-12.6%)	4.1 (+6.2%)	4.2 (+5.2%)
	75	100	21.7 (-32.6%)	20.7 (-46.9%)	3.0 (-23.8%)	3.2 (-20.2%)
	150	30	31.5 (-2.0%)	32.3 (-17.2%)	3.6 (-7.2%)	3.8 (-4.2%)
	150	100	19.5 (-39.5%)	19.8 (-49.3%)	2.7 (-30.0%)	2.9 (-26.9%)
90	75	30	35.2 (+9.5%)	31.5 (-19.3%)	3.6 (-6.7%)	4.1 (+3.2%)
	75	100	22.2 (-30.9%)	21.9 (-44.0%)	2.6 (-31.8%)	3.0 (-25.7%)
	150	30	32.4 (+0.7%)	29.5 (-24.4%)	3.7 (-4.7%)	4.0 (+0.5%)
	150	100	27.4 (-14.8%)	21.8 (-44.1%)	2.8 (-28.9%)	3.8 (-5.2%)

6.1.2 Effect of replacement ratio

Fig. 13 shows the effect of carbonated RCFs on compressive strength of cement paste, in terms of the strength ratio between carbonated RCF paste and plain RCF paste. Obviously, the replacement of carbonated RCFs would lead to a significant increase in the compressive strength of cement paste, attributed to the densified microstructure and enhanced RCF-to-hydration interactions (Section 4.2). Moreover, the RCFs replacement ratio did not exceed 30% in the available literature, while 20% was considered as an optimal replacement ratio. The strength ratio progressively increased up to 1.46 under the replacement ratio of 20%, after which a sudden drop appeared at 30% replacement [70]. The latter can be ascribed to the adverse dilution effect of RCFs at high replacement levels, and thereby the reduction in the content of clinkers and hydrations [67].

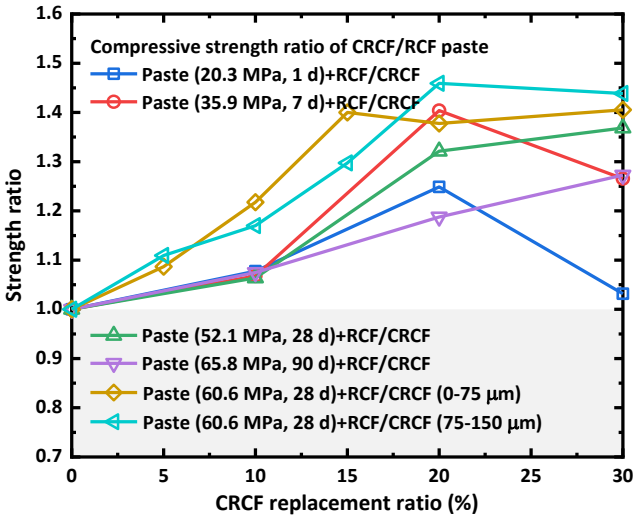

Fig. 13. Effect of carbonated RCFs (CRCFs) replacement on compressive strength of cement paste [67,70].

The strength evolution of RFA mortar with replacement ratio is shown in Fig. 14a, indicating that the replacement level of RFAs should be limited to lower than 60% to avoid significant strength loss [144]. Moreover, the replacement of RFAs by carbonated RFAs may not guarantee an improvement in strength, which is highly dependent on the strength of mortar and replacement ratio. For low-strength mortar (i.e., C25), an up to 50% replacement by carbonated RFAs would still lead to a 12.3% rise in compressive strength, relative to the plain RFA mortar [43]. For medium-strength mortar (i.e., C50), the enhancement in strength can be observed when the replacement ratio is lower than 30%, while 10% replacement was the optimal proportion where a 13.2% increase in strength took place after 28 d curing [104]. For high-strength mortar (i.e., C80), the compressive strength of carbonated RFA mortar was only 84.7–93.5% to that of plain RFA mortar with the replacement ratio varying from 0 to 50% [120]. The strength-dependent effect of carbonated RFA mortar can be explained as follows. On one hand, the carbonation process increases the density and reduces the water absorption of RFAs, which leads to the strength improvement of the produced new mortar, especially for low-strength mortar [27]. On the other hand, the carbonated RFAs would decrease the non-evaporable water content of new mortar and reduce the degree of slag-cement reactions, leading to a strength reduction of high-strength mortar [145]. Fig. 14b further plots the effect of carbonated RFAs on compressive mechanical properties of concrete with 100% RCA. It can be seen that the strength ratio between carbonated RFA concrete and plain RFA concrete fluctuated from 98.1% to 114.5%, while the elastic modulus ratio varied from 89.4% to 109.9% within the RFA replacement ratio of 0–50% [104]. This indicates that a comprehensive evaluation of replacement

ratio and matrix strength is essential to achieve an optimal compressive performance of concrete.

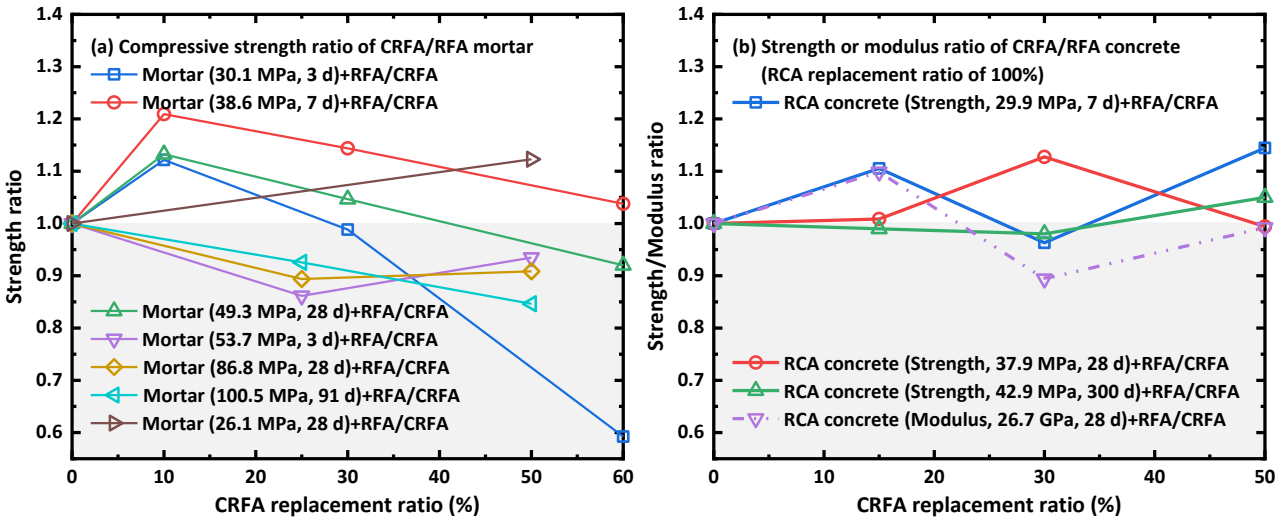

Fig. 14. Effect of carbonated RFA replacement on compressive strength and elastic modulus of (a) mortar and (b) concrete [43,104,120] (Note: CRFA – carbonated RFA).

Different from concrete with RFA, the replacement ratio of RCAs in concrete can reach up to 100% and replacing plain RCAs with carbonated RCAs has a promoting effect on compressive strength regardless of the replacement ratio and concrete strength, as presented in Fig. 15a. The strength ratio of concrete continuously went up with the rising replacement ratio of carbonated RCAs where an up to 33.0% strength rise appeared under the complete replacement condition [23,35,109,110]. Moreover, carbonated repeatedly RCAs were proved to be more efficient in enhancing the compressive strength of concrete than plain repeatedly RCAs, with a 34.2% strength increase under 80% replacement [114]. For concrete with 28 d compressive strength of 58.7 MPa, although a slight drop in strength ratio took place when the replacement ratio exceeded 50%, the strength of concrete with carbonated RCAs was still higher than that with plain RCAs (i.e., strength higher than 1.0) [24]. The improvement in compressive strength of concrete by carbonated RCAs can be ascribed to the densified microstructure of RCAs and enhanced ITZ properties between old mortar and new cement paste [107]. As seen in Fig. 15b, the evolution of elastic modulus with the replacement ratio of carbonated RCAs is similar to that of compressive strength reported in most literature [23,35,110]. However, the modulus ratio of concrete with an elastic modulus of 39.0 GPa reached the maximum value of 115.2% under the carbonated RCA replacement ratio of 30%, after which a decreasing trend occurred until 100% replacement [143]. The abnormal variation of elastic modulus might be also related to the high modulus of concrete matrix and RCA-to-matrix reactions.

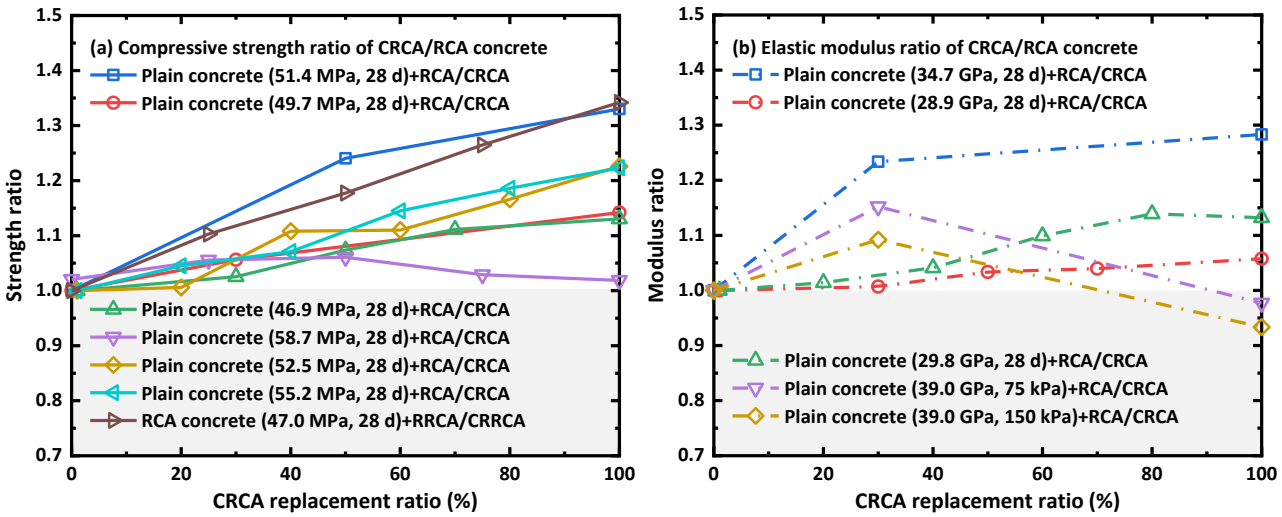

Fig. 15. Effect of carbonated RCA replacement on (a) compressive strength [22–24,35,109,110,114] and (b) elastic modulus of concrete [23,35,110,143] (Note: RRCA – repeatedly RCA).

As confirmed by a previous study [146], the uniaxial compressive stress-strain relation of RCA concrete can be described by dimensionless equations of ascending and descending curves:

$$\sigma / \sigma_c = m\left(\varepsilon / \varepsilon_c\right) + \left(3-2m\right)\left(\varepsilon / \varepsilon_c\right)^2 + \left(m-2\right)\left(\varepsilon / \varepsilon_c\right)^3,\ 0 \le \varepsilon / \varepsilon_c < 1 \tag{8}$$

$$\sigma / \sigma_c = \frac{\varepsilon / \varepsilon_c}{n\left(\varepsilon / \varepsilon_c - 1\right)^2 + \left(\varepsilon / \varepsilon_c\right)},\ \varepsilon / \varepsilon_c \ge 1 \tag{9}$$

where σ / σ_c and $\varepsilon / \varepsilon_c$ stand for the relative stress and strain to that of peak stress and strain, respectively, and *m* and *n* are referred to the fitting parameters associated with the ascending and descending regions of the stress-strain curve.

Fig. 16 presents the normalised compressive stress-strain curves of concrete under carbonated RCA replacement ratio of 30–100%, relative to concrete with natural coarse aggregates (NCAs). The ascending part of the curves is reflected by the parameter *m* in Eq. (8), which denotes the ratio between initial tangential modulus and secant modulus under the peak loading [35]. The *m* value of RCA concrete gradually increased by 2.3–23.0% as compared with NCA concrete, while the *m* value of carbonated RCA concrete was even 16.3–79.1% higher than that of RCA concrete, when the replacement ratio went up from 30% to 100% [110]. The variation of *m*-value suggested that the higher replacement ratio of carboned RCAs tends to increase the relative steepness of the ascending curve. Moreover, the descending part of the stress-strain curves is quantified using the parameter *n* in Eq. (9), the higher value of which means a steeper descending curve and thereby poorer ductility [147]. Additionally, the replacement of RCAs at 50% ratio led to no more than 45.6% decrease in *n* value, relative to that of NCA concrete, while an opposite trend of up to 108.6% increase in *n* value

appeared at 100% RCA replacement. In comparison with RCA concrete, the replacement of 30% carbonated RCAs resulted in a 48.6% rise in terms of *n* value, while the *n* value dropped by 63.6% under the complete replacement condition [110]. Thus, the result of *n* value indicated that incorporating carbonated RCAs would lead to higher ductility of RCA concrete under the replacement ratio of 30%, while an opposite trend occurred when the replacement ratio was in the range of 50–100% [116].

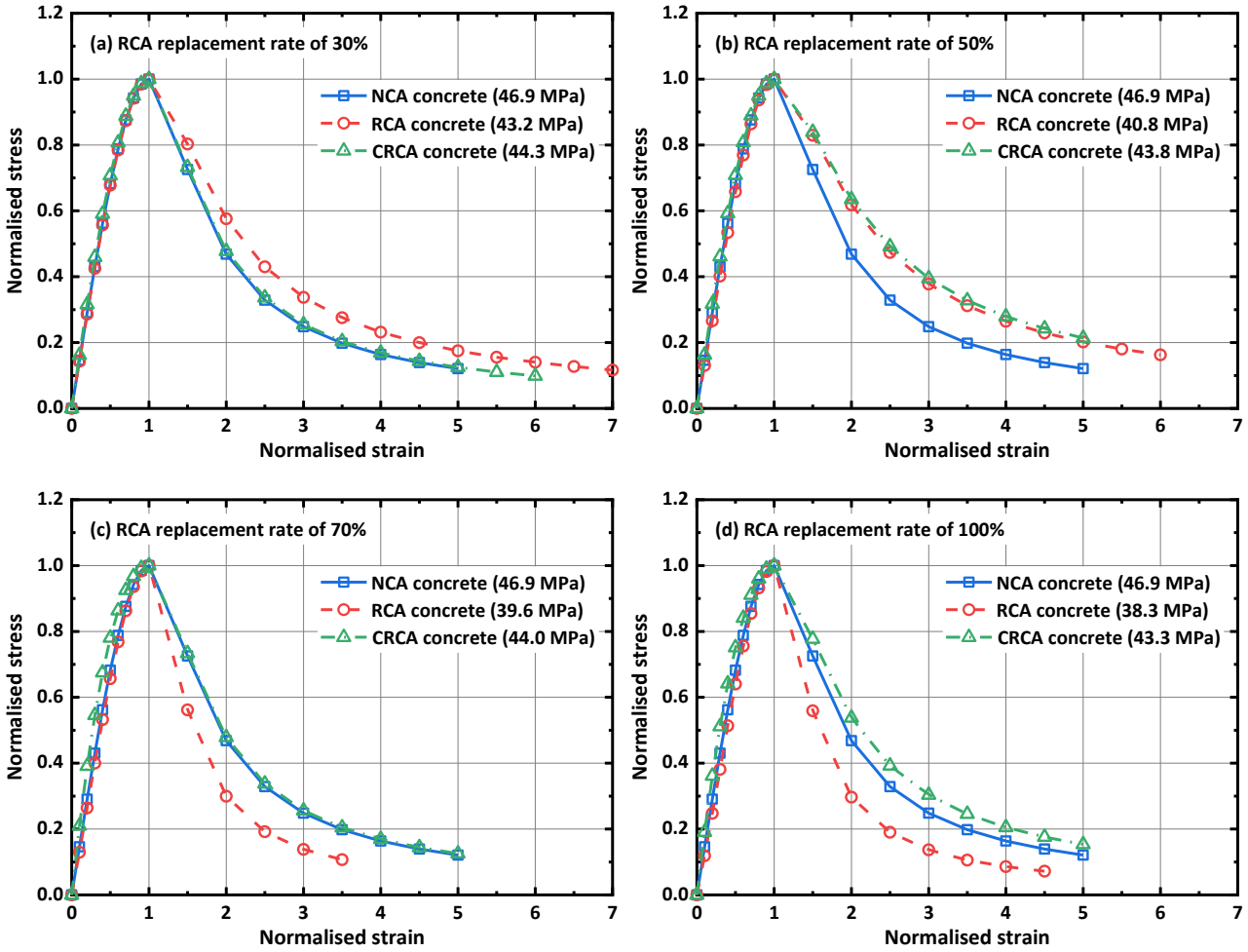

Fig. 16. Effect of carbonated RCA replacement on the stress-strain curve of concrete [110,116].

6.1.3 Effect of curing age

The compressive strength evolution of cement paste containing uncarbonated or carbonated RCFs is plotted against the strength of plain cement paste under three replacement levels of 10%, 20% and 30% (Fig. 17a). Despite the strength development during the hydration process, the strength ratio between carbonated RCF paste and plain paste went down with curing age, especially in the first 28 d [70]. However, carbonated RCFs can significantly improve the early strength of paste within 7 d, as an up to 23.6% rise in strength took place after 1 d of curing, in comparison with plain paste. Under the same replacement level, the strength ratio of carbonated RCF paste was higher than that

of plain RCF paste throughout the measured curing ages, which can be attributed to the combined effects of accelerated nucleation of C-S-H on carbonated RCFs surface [68,148], stabilization of calcium aluminates [148] and filling effect of calcite [149] (Section 3.2). Fig. 17b further displays the effect of carbonated RCFs containing 50% fly ash or ground granulated blast-furnace slag on the compressive strength of cement paste. It was observed that the improved strength (i.e., strength ratio >1.0) can be maintained at up to 28 d with 10% replacement of both types of carbonated RCFs, while slag-based RCFs were more effective in enhancing the early-age strength of paste where a 29.2% strength increase occurred at curing age of 3 d [72]. In addition, RCFs after high-temperature carbonation at 60 °C and 100 °C was also proved to promote the 3 d strength of paste by 9.7% and 12.6%, respectively, but the promoted cement hydration caused by nucleation effect of calcite in carbonated RCFs was less obvious at later ages of over 7 d [36].

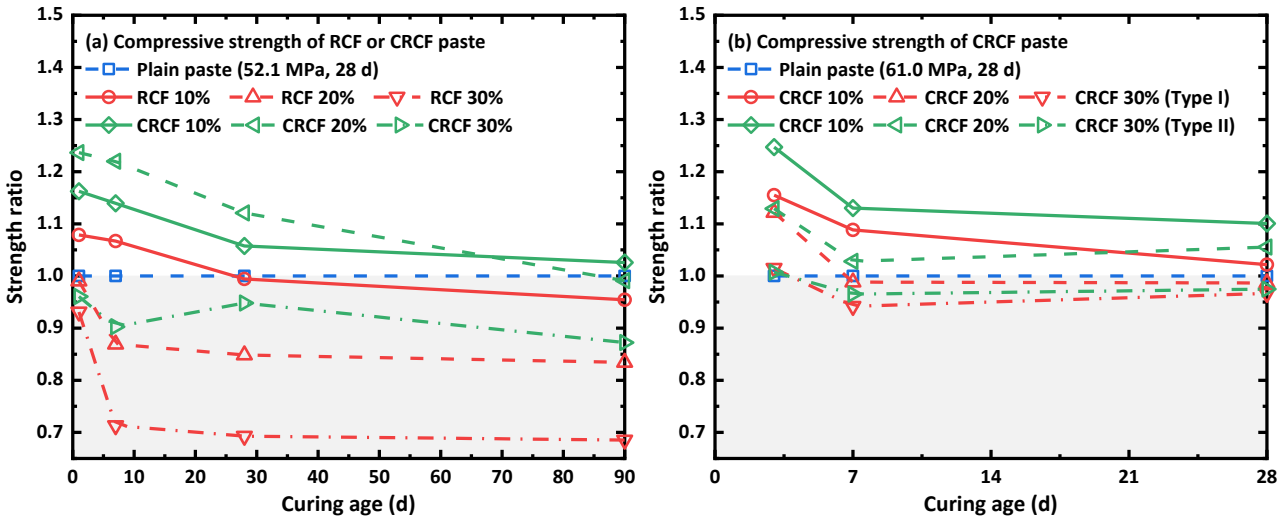

Fig. 17. Effect of curing age on compressive strength of cement paste with carbonated RCFs [70,72] (Note: Type I – recycled fly ash cement paste; Type II – recycled blast furnace slag cement paste).

Different from RCFs, the replacement of RFAs or carbonated RFAs leads to a drop in mortar strength regardless of curing age and replacement ratio, as illustrated in Fig. 18a–d. In other words, the strength ratio between carbonated RFA mortar and plain mortar was maintained at below 1.0 throughout the curing ages till 91 d [83,120]. The fluctuation in the strength ratio can only be observed within 7 d, after which the strength ratio was approximately constant under a specific replacement level [29,104]. A higher compressive strength ratio of low-strength mortar (i.e., C40) was achieved by adding more carbonated RFAs as compared with plain RFA mortar (Fig. 18a–c), while incorporating more carbonated RFAs may result in an adverse effect on strength of C80 high-strength mortar (Fig. 18d), which can be kept up to 91 d. This indicates that although the

accelerated carbonation treatment can strengthen the microstructure of RFAs (Section 4.3), the strength of attached old mortar on RFAs may be still lower than the new mortar matrix. Therefore, the increase in strength ratio occurred in low-strength mortar matrix, while an opposite trend took place in high-strength mortar matrix [44]. It is surprising to find that the 3 d strength of mortar with 100% carbonated gravel RFAs was 11.6% higher than that of mortar with natural fine aggregates (Fig. 18e), while the residual 28 d strength ratio of 99.9% was also the highest among the available literature [89], suggesting that the patent materials of RFAs also affected the strength ration of carbonated RFA mortar. In addition, the decreased porosity of RFAs during accelerated carbonation can still lead to a drop in porosity of the overall mortar, which would consequently promote the strength of mortar during hydration [45]. The 14 d strength ratio can be adopted as a critical strength index for characterising RFA mortar, as the strength ratio was nearly independent of curing age at over 14 d.

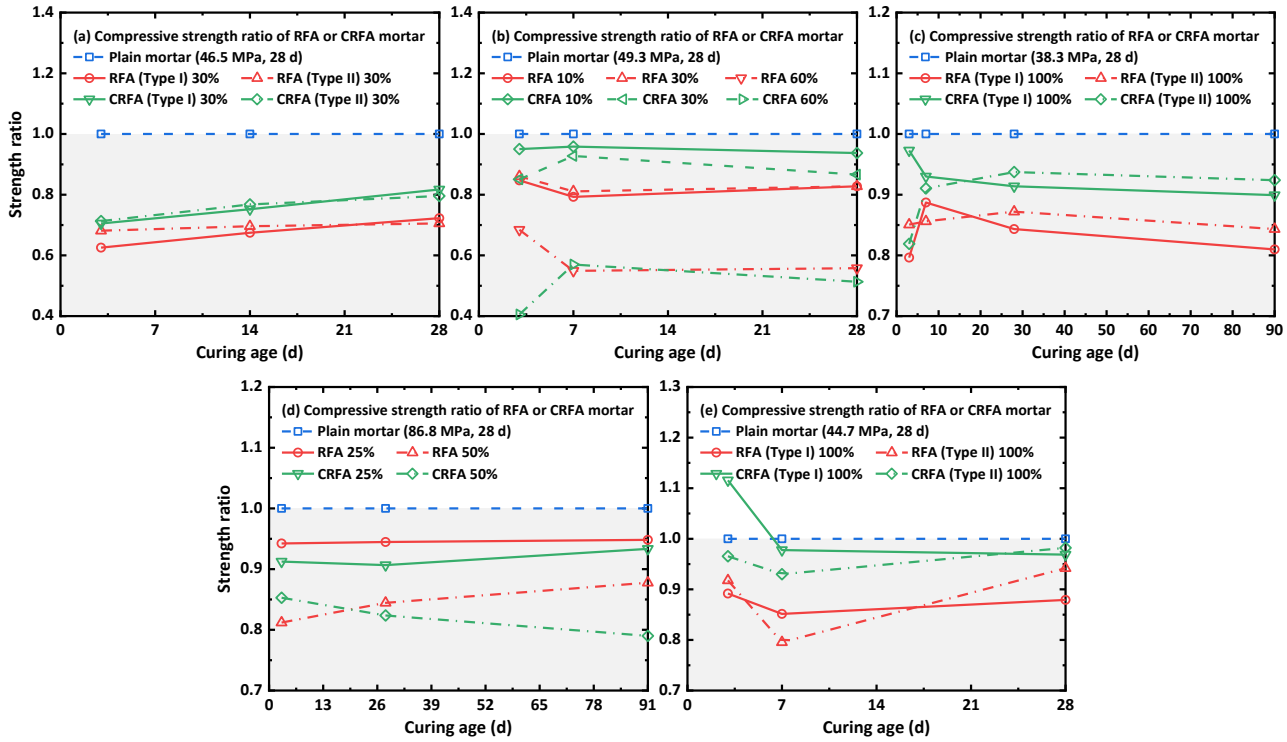

Fig. 18. Effect of curing age on compressive strength of mortar with carbonated RFAs [29,83,89,104,120].

Fig. 19 shows the development of compressive strength and elastic modulus of concrete containing plain RCAs and carbonated RCAs. In general, the compressive properties of carbonated RCA concrete are inferior to plain concrete with NCAs but better than RCA concrete regardless of curing age, which is supported by available experimental results [21,35,109,150]. In spite of the fluctuation during the first 7 d curing, the strength ratio and modulus ratio between carbonated RCA

concrete and plain concrete are nearly constant after curing of 28 d [100,112,116]. As discussed in Section 5.1, the interfacial bonding of RCA-old mortar ITZs of concrete can be improved by carbonated RCAs, which further enhanced the overall compressive strength and elastic modulus of RCA concrete. However, the overall strength of carbonated RCAs is still lower than NCAs as the strengthened microstructure by carbonation may be limited to the outer surface regions of RCAs, and thereby restricting the compressive properties of concrete [47]. Interestingly, the adverse effect of carbonated RCAs on strength of concrete is inferior to carbonated RFAs on mortar strength. The compressive strength of mortar containing 60% carbonated RFAs was only around 40% of that of plain mortar with natural fine aggregates after 3 d of curing [104], while the strength ratio between carbonated RCA concrete and plain concrete was still higher than 75% even under the complete replacement condition [100]. In addition, several pre-treatment methods such as submerging in lime-saturated water, immersing in acetic acid solution and impregnating into CH emulsion [112,116] were also proved to further improve the strength ratio of carbonated RCA concrete during hydration, as illustrated in Fig. 19f.

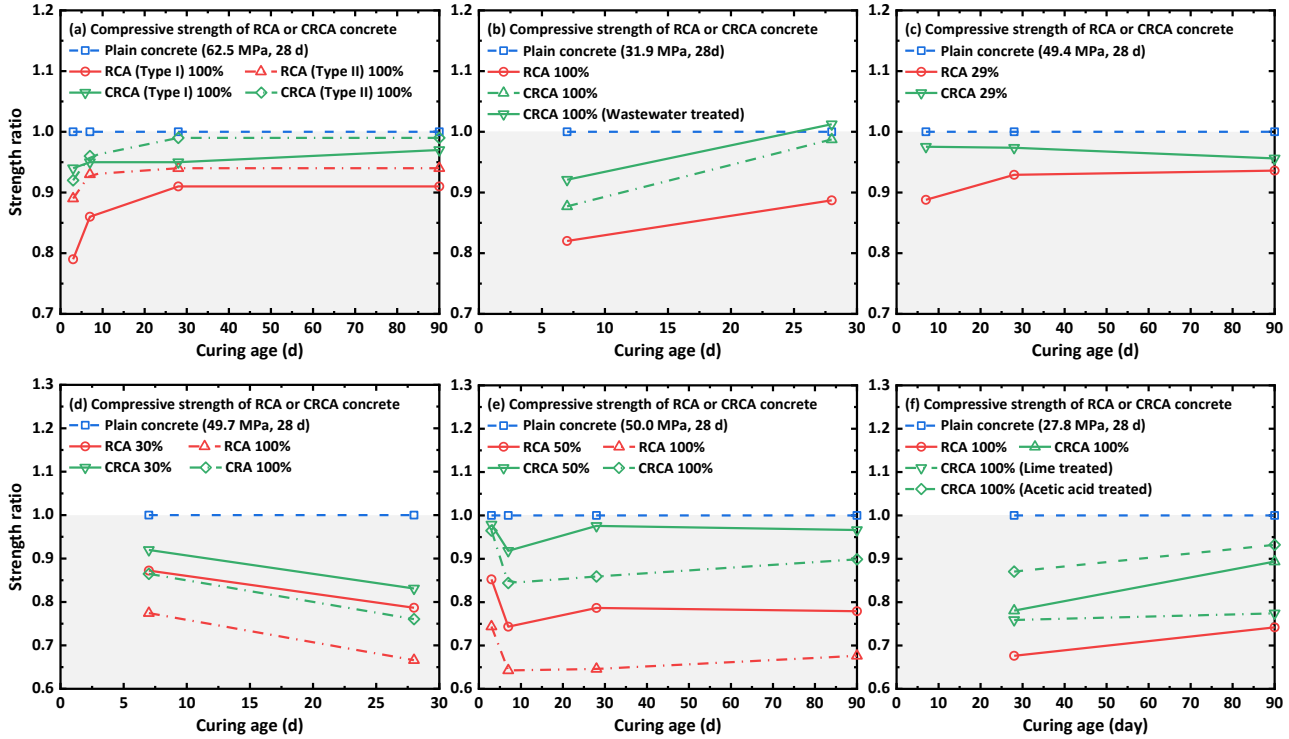

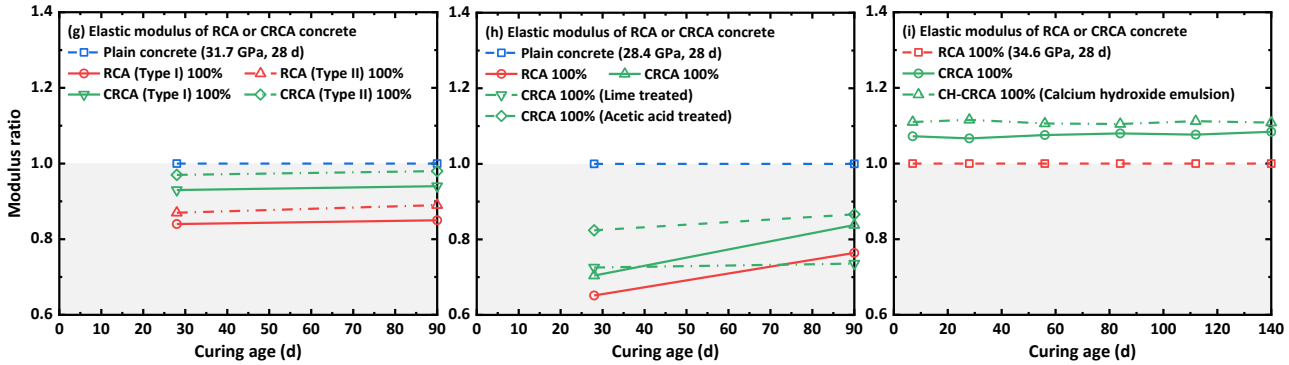

Fig. 19. Effect of curing age on (a) – (f) compressive strength [21,35,100,109,116,150] and (g) – (i) elastic modulus [100,112,116] of concrete with carbonated RCAs (CRCAs).

6.2 Splitting tensile strength

6.2.1 Effect of carbonation condition

Following a similar changing trend to compressive strength, the increase in both CO_2 pressure and carbonation duration during gas-solid carbonation of RCAs did not always lead to the enhancement in splitting tensile strength [117]. As compared with plain concrete, the replacement of 30% RCAs after carbonation at 75 kPa for 30 min would cause a 6.2% rise in splitting strength (Table 4), while a 7.2% reduction in splitting strength took place when the carbonation pressure of RCAs went up to 150 kPa [143]. The complete replacement of RCAs after carbonation under 100% CO_2 concentration for 21 d was found to enhance the splitting strength of plain concrete by up to 23.1% [118]. The enhanced splitting strength may be explained by the densified microstructure of RCAs, as carbonation at 25 kPa for 2 h was reported to increase the calcium carbonate amount by over 4 times [151]. These results indicate that the splitting tensile strength of RCA concrete can even overpass that of the concrete with natural aggregates through reasonable carbonation conditions.

6.2.2 Effect of replacement ratio

Fig. 20 presents the effect of the replacement level of carbonated RFAs or RCAs on the splitting tensile strength of concrete. As compared with plain RFA concrete, the replacement of carbonated RFAs can still enhance the splitting tensile strength at up to 50% replacement, while the maximum strength improvement of 3.7% appeared at a replacement ratio of 20% [104]. In contrast, the strength ratio between carbonated RCA concrete and plain RCA reached the peak value of 119.8% under 30% replacement, after which the strength ratio decreased to below 1.0 under the complete replacement condition [143]. Therefore, although incorporating too many carbonated RCAs may decrease the strength of concrete, carbonated RCAs were more effective in tailoring the splitting tensile strength than carbonated RFAs over a wider replacement range.

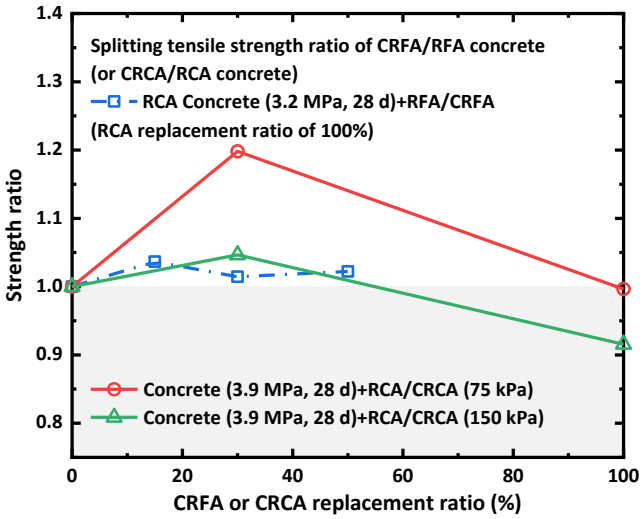

Fig. 20. Effect of carbonated RFA replacement on splitting tensile strength of concrete [104,143].

Fig. 21 further displays the evolution of splitting tensile strength of 3D printed mortar (3DPM) with carbonated RFA replacement ratio ranging from 0 to 100%. It is worth mentioning that the splitting tensile strength of 3DPM is referred to the interfacial bonding strength between mortar layers, which plays a critical role in determining the overall mechanical properties. In general, the splitting tensile strength of 3DPM with carbonated RFAs was higher than that with plain RFAs under the same replacement ratio, which was maintained throughout the measured replacement range and curing age. Compared to 3DPM with plain RFAs, the splitting tensile strength along the horizontal and vertical directions increased by up to 17.4% and 10.0%, respectively, due to the 30% replacement of carbonated RFAs [102]. The enhanced splitting tensile strength of 3DPM was ascribed to the formation of calcite precipitate in the adhered old mortar during carbonation, which not only densifies the microstructure of RFAs, but also generates more ettringite crystals in the new cement paste of 3DPM [135]. Moreover, the improved efficiency of 3DPM along the horizontal direction (Fig. 21a) was higher than that along the vertical direction (Fig. 21b), which can be ascribed to the closer contract interface along the horizontal direction as a result of the gravity, as well as the larger contact area of the horizontal interlayer than the vertical interlayer.

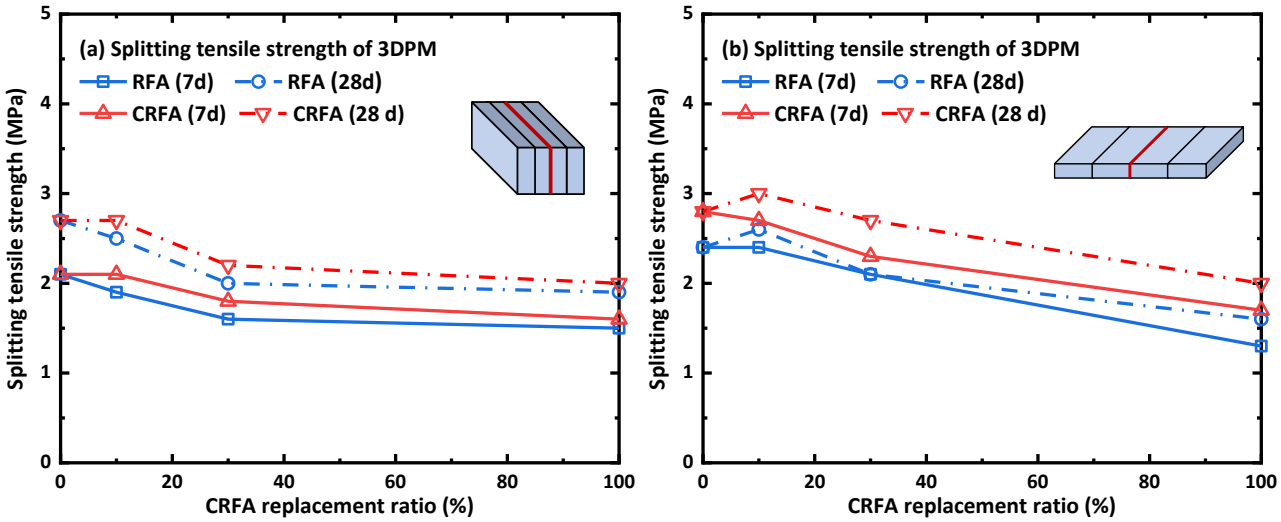

Fig. 21. Effect of carbonated RFA replacement on splitting tensile strength of 3D printed mortar [102].

6.2.3 Effect of curing age

The evolution of splitting tensile strength of carbonated RCA concrete with curing age is shown in Fig. 22a. Although the replacement of 100% carbonated RCAs would lead to a less than 3.0% reduction in splitting tensile within 28 d of curing, a significant increase by up to 11.0% took place after cured for 91 d. Moreover, the addition of RCAs from high-strength parent materials (i.e., C65) was more favourable in the strength improvement than that from C45 parent materials regardless of curing age [100]. Fig. 22b further compares the splitting tensile strength of concrete with various types of pre-treated carbonated RCAs at 28 d and 91 d, indicating that lime-treated carbonated RCAs were more effective than carbonated RCAs without pre-treatment, while acetic acid cannot improve the quality of carbonated RCAs in terms of 28-d splitting tensile strength of concrete [116]. Under the same parent material and replacement ratio, the splitting tensile strength ratio of carbonated RCA concrete was higher than that of plain RCA concrete throughout the measured curing ages, which can be attributed to the densified microstructure of RCAs through calcite precipitation [135] and strengthened ITZ properties during carbonation (Section 5.3).

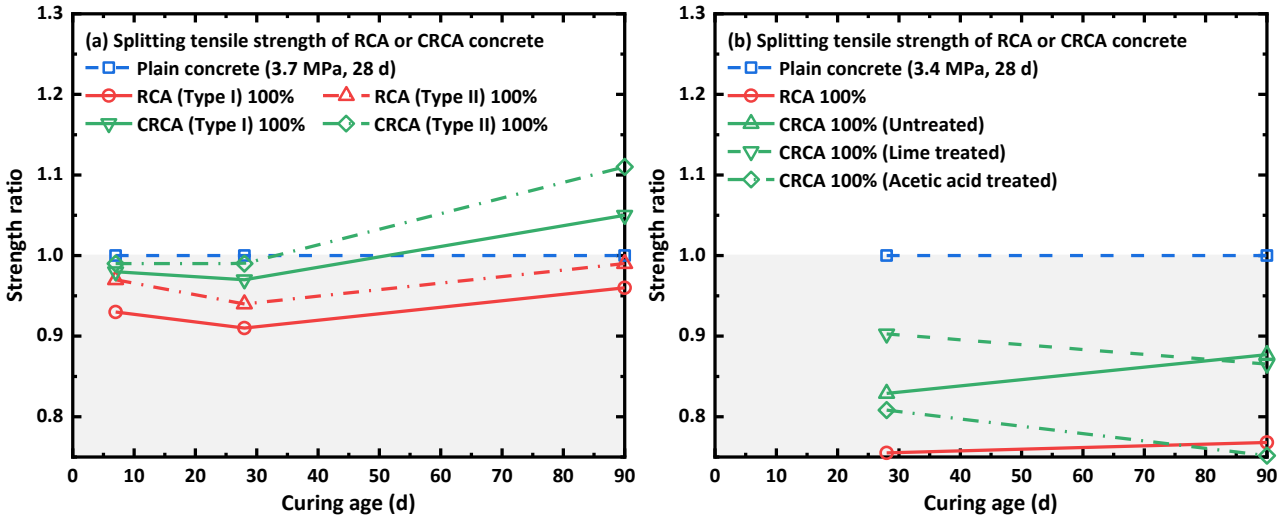

Fig. 22. Effect of curing age on splitting tensile strength of concrete with carbonated RCAs [100,116].

6.3 Flexural strength

6.3.1 Effect of carbonation condition

As listed in Table 4, the concrete with 30% RCAs presented the highest flexural strength of 4.32 MPa, while 100% replacement of RCAs produced the worst flexural strength of approximately 2.52 MPa. Similar to splitting tensile strength, RCAs after carbonated at 75 kPa for 30 min and 90 min were proved to increase the flexural strength of plain concrete by 5.5% and 3.5%, respectively, which were the only two cases with higher strength than plain concrete [143]. Moreover, the RCAs after carbonated at 150 kPa for 90 min only caused a slight decrease of 0.2 MPa in flexural strength of concrete even under complete replacement conditions [152]. The results also suggested that the low CO_2 pressure and high carbonation duration were more effective than the low CO_2 pressure and high carbonation in terms of flexural strength enhancement of carbonated RCA concrete [117]. In addition, the concrete with carbonated RCAs exhibited greater flexural performance than splitting tensile performance under the same replacement level and carbonation condition [117,143].

6.3.2 Effect of replacement ratio

The effect of carbonated RFA replacement on the flexural strength of mortar is shown in Fig. 23a, indicating a higher flexural strength of carbonated RFA mortar than mortar with uncarbonated RFAs. Within the replacement ratio range of 0–60%, the maximum improvement in flexural strength (i.e., 13.5%) took place at a replacement ratio of 30% [104], which was similar to the evolution of splitting tensile strength (Table 4). In contrast, the replacement of 30% carbonated RCAs may even lead to the lowest flexural strength ratio of concrete, as seen in Fig. 23b. Although there was no

identical regular pattern between flexural strength and replacement ratio, most experimental results confirmed that the flexural strength ratio between carbonated RCA concrete and plain RCA concrete peaked at complete replacement condition [22,23,143]. This is because the strengthening of attached old mortar during accelerated carbonation (Section 4.3) would contribute to the flexural properties of RCAs [32,34,106], and thereby the higher replacement ratio of carbonated RCAs led to the more flexural strength improvement of RCA concrete. The maximum enhancement in flexural strength (i.e., 28.7%, Fig. 23b) of RCA concrete induced by the complete replacement of carbonated RCAs was lower than that in compressive strength (i.e., 34.2%, Fig. 14a).

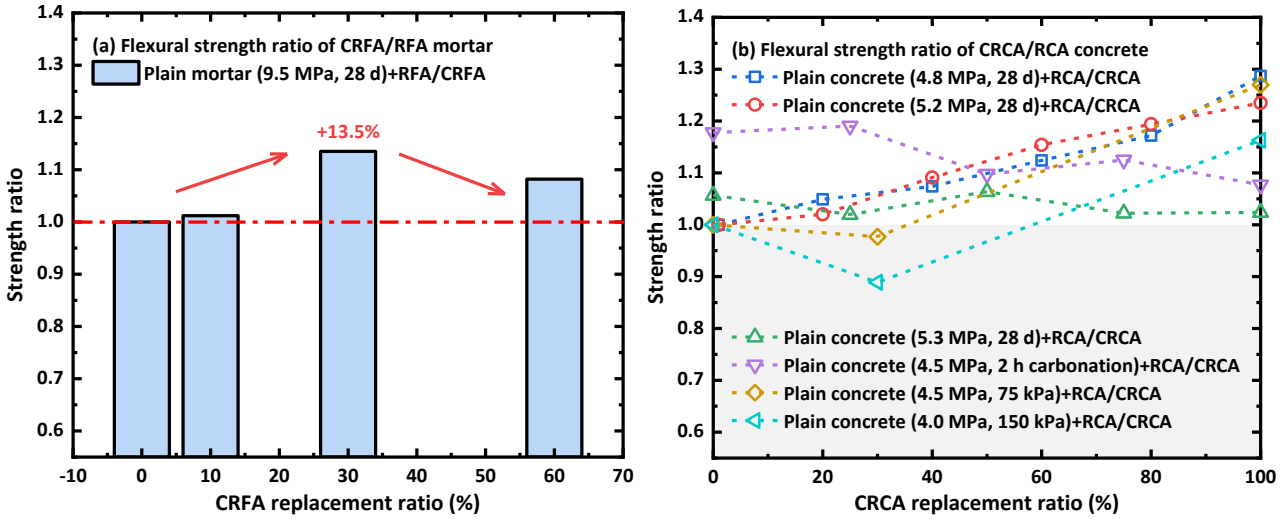

Fig. 23. Effect of carbonated RFA replacement on flexural strength of (a) mortar [104] and (b) concrete [22–24,143].

Fig. 24 displays the effect of carbonated RFAs on the flexural strength of 3D printed mortar in terms of replacement ratio, curing age and test directions. Although the flexural strength of 3DPM containing RFAs was reduced with the rising replacement ratio [153], a higher strength can be achieved by replacing plain RFAs with carbonated RFAs regardless of curing age. Moreover, the flexural strength difference between 3DPM with plain and carbonated RFAs was enlarged with replacement ratio and curing age, as an up to 21.4% increase in 28 d flexural strength appeared in 3DPM with 100% carbonated RFA replacement (Fig. 24c). Compared to the direction-dependent flexural strength, the highest and lowest strength occurred along *y*-direction and *x*-direction, respectively, while the enhancement in strength by carbonated RFAs maintained at all directions. However, the replacement of carbonated RFAs was more effective in enhancing the compressive strength of 3DPM (i.e., up to 68.5% improvement in 28 d compressive strength [102]) than that in flexural strength, which can be explained by the densified pore structure of 3DPM. As characterised

by X-ray computed tomography, the internal pore structure of 3DPM was optimised by carbonated RFAs. In particular, the volume fraction of pores smaller than 0.2 mm increased, while that of larger pores in the range of 0.2–1 mm reduced [102]. However, the denser pores induced by carbonate precipitation or hydrations crystallization of carbonated RFAs (Section 3.2) provided more resistance to axial loading, while they made less contribution to the flexural ability of 3DPM [102].

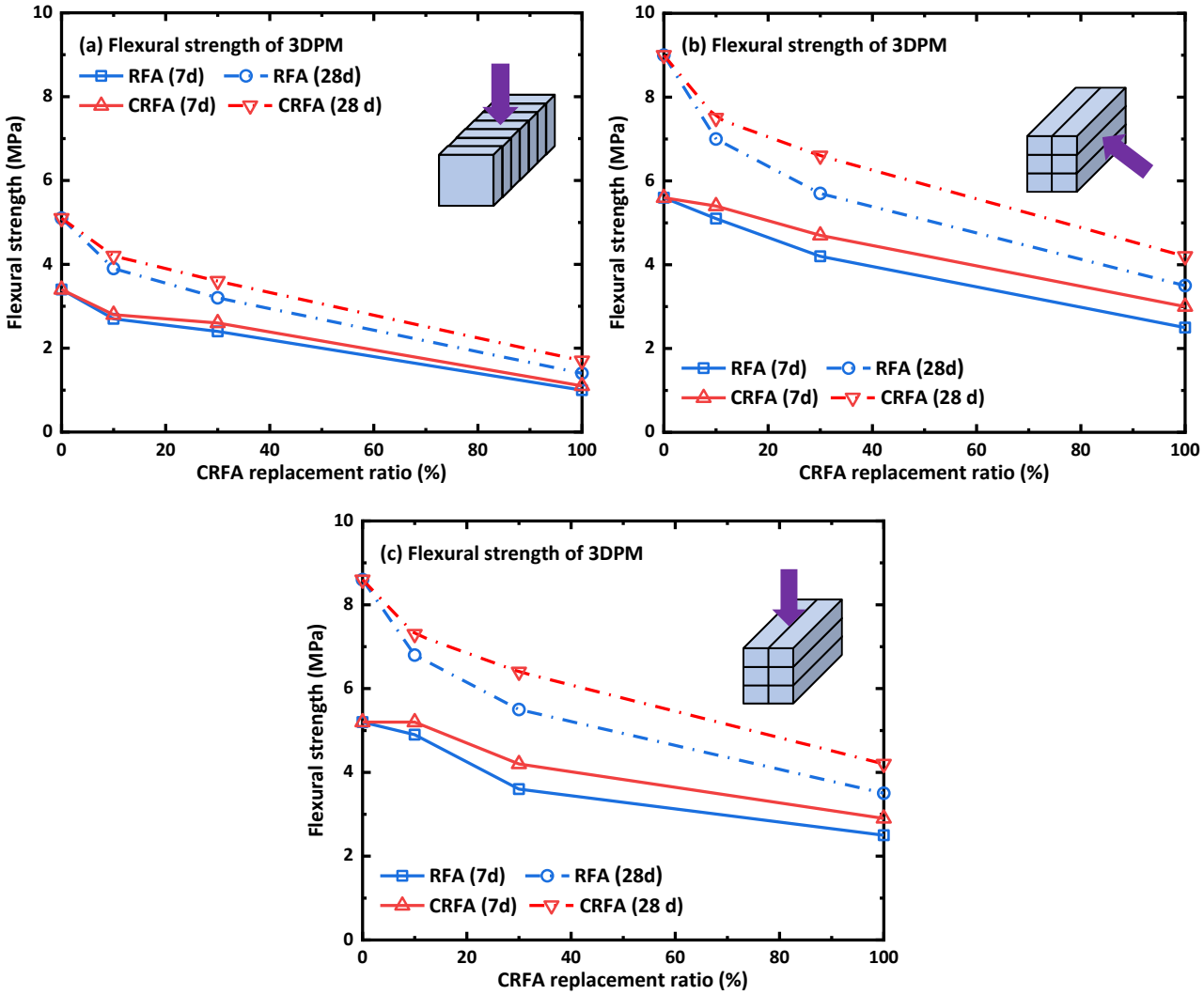

Fig. 24. Effect of carbonated RFA replacement on flexural strength of 3D printed mortar along (a) *x*-, (b) *y*- and (c) *z*-direction [102].

6.3.3 Effect of curing age

The flexural strength of carbonated RFA mortar against curing age is presented in Fig. 25. Similar to the evolution of compressive strength (Fig. 18), although the flexural strength of carbonated RFA mortar was inferior to plain mortar with natural aggregates, the strength difference was progressively narrowed during the hydration process. The maximum flexural strength ratio between carbonated RFA mortar and plain mortar after 21 d and 28 d of curing reached up to 93.2% and 95.9%, respectively. The flexural strength ratio of carbonated RFA mortar was higher than that of

plain RFA mortar throughout the measured curing ages, which can still be observed in the flexural strength of 3DPM (Fig. 24). RFAs from high-quality parent materials (i.e., P.II. 52.5 cement) were more effective in enhancing the flexural strength of mortar than those from parent materials with P.O. 42.5 cement [83]. Therefore, the early-age flexural strength of mortar suffered more due to the addition of low-strength RFAs, but the carbonation of RFAs and high-quality parent materials helped achieve a satisfying 28 d flexural strength even under complete replacement conditions.

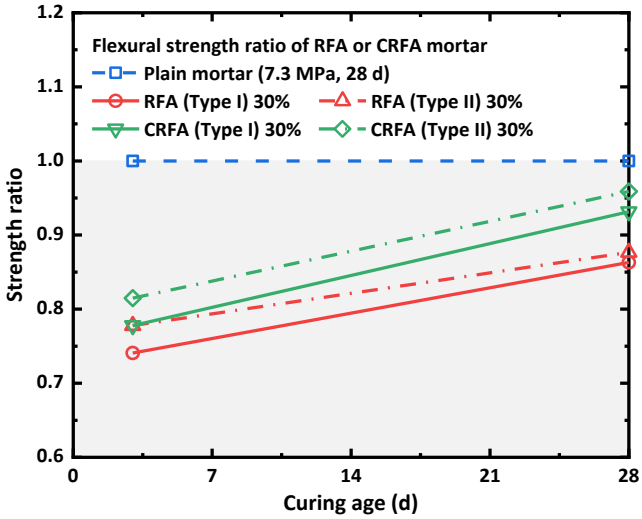

Fig. 25. Effect of curing age on flexural strength of mortar with carbonated RFAs [83].

Based on the above analysis, although most experimental results indicated similar variation trends, the effect of carbonated RCFs, RFAs and RCAs on mechanical properties of RCA concrete varied a lot from study to study, even leading to contradictory conclusions under the specific condition, as summarised in Table 5. This can be explained by the differences in the parent material of RCA and carbonation methods and conditions, which also suggests the necessity of a standard to evaluate and classify the quality of carbonated recycled fines and aggregates. In addition, the mechanical properties of carbonated RFA and RCA concrete were mainly measured at the ambient temperatures, so the temperature dependency of concrete with carbonated RFAs and RCAs still needs to be examined to gain more insights into the microstructure-property relationships [154–156].

Table 5 Effect of curing age and replacement ratio on mechanical properties of concrete containing carbonated recycled fines and aggregates.

Recycled aggregate type	Curing age (d)	Replacement ratio (%)	Relative mechanical properties (%)			
			Compressive strength	Elastic modulus	Splitting strength	Flexural strength
RCF	7	20	+40.4	–	–	–
	28	20	(+32.1, +45.9)	–	–	–
RFA	7	30	(-3.7, +14.4)	–	–	–

	7	50	+14.46	–	–	–
	28	30	(+4.7, +12.8)	-10.6	+1.5	+13.5
	28	50	(-9.2, +12.3)	-8.0	+2.2	–
RCA	28	20	(+0.6, +4.5)	+1.4	–	(+2.0, +4.9)
	28	30	(+2.5, +5.6)	(+0.7, +23.4)	(+4.7, +19.8)	(-11.1, -2.3)
	28	50	(+6.1, +24.1)	+3.4	–	(+6.4, +9.7)
	28	80	(+16.6, +18.6)	+13.9	–	(+17.2, +19.4)
	28	100	(+1.9, +34.2)	(-6.7, +28.3)	(-8.5, -0.3)	(+2.3, +28.7)

Note: (i) The experimental data were derived from Figs. 13, 14, 15, 20 and 23. (ii) The expression of (A, B) represents the variation range of data from A to B. (iii) The relative mechanical property is referred to the property ratio between concrete with carbonated recycled aggregates and plain RCA concrete.

6.4 Dynamic mechanical properties

The dynamic compressive properties of concrete with complete replacement of plain RCAs and carbonated RCAs are compared in terms of dynamic increase factors of peak stress, elastic modulus, peak strain and toughness (Fig. 26). The dynamic increase factor is defined as the ratio of mechanical properties under dynamic loading to that under static loading, which has been widely used to characterise the dynamic properties of concrete [157,158]. With the increasing strain rates from 10^{-5} /s to 10^{-2} /s, the dynamic increase factors of peak stress, elastic modulus and toughness of concrete showed increasing trends regardless of the aggregate types as a result of the strain rate effect [159]. These phenomena were closely related to the failure pattern and crack propagation resistance of concrete [160]. Under a low strain rate (i.e., 10^{-5} /s), only several main cracks passed through the RCA concrete specimen along with the micro cracks propagated from ITZs between RCAs and concrete matrix [113]. In contrast, more cracks took place under a high strain rate (i.e., 10^{-1} /s), while micro-cracks could even propagate across RCAs [161]. As a result, more fractured aggregates occurred under a higher strain rate, which consumed more energy and led to higher dynamic strength and modulus [159]. Moreover, the peak stress and elastic modulus of carbonated RCA concrete were higher than that of plain RCA concrete, but the strain-rate sensitivity of peak stress and elastic modulus was less obvious in concrete with carbonated RCAs. In other words, the slopes of fitting curves between dynamic increase factors and strain rate of RCA concrete were higher than that of carbonated RCA concrete, as shown in Fig. 26a and b. According to the Stefan theory of viscous fluid-disk composites [162], the lower porosity and fewer micro cracks in carbonated RCA concrete would reduce the micro units to resist dynamic compressive loading, and

thereby smaller increase in dynamic strength and modulus occurred at a higher strain rate [113]. In addition, more significant strain-rate sensitivity in toughness can be observed in carbonated RCA concrete (Fig. 26c), in contrast with no obvious trend in the evolution of peak strain with strain rate (Fig. 26d).

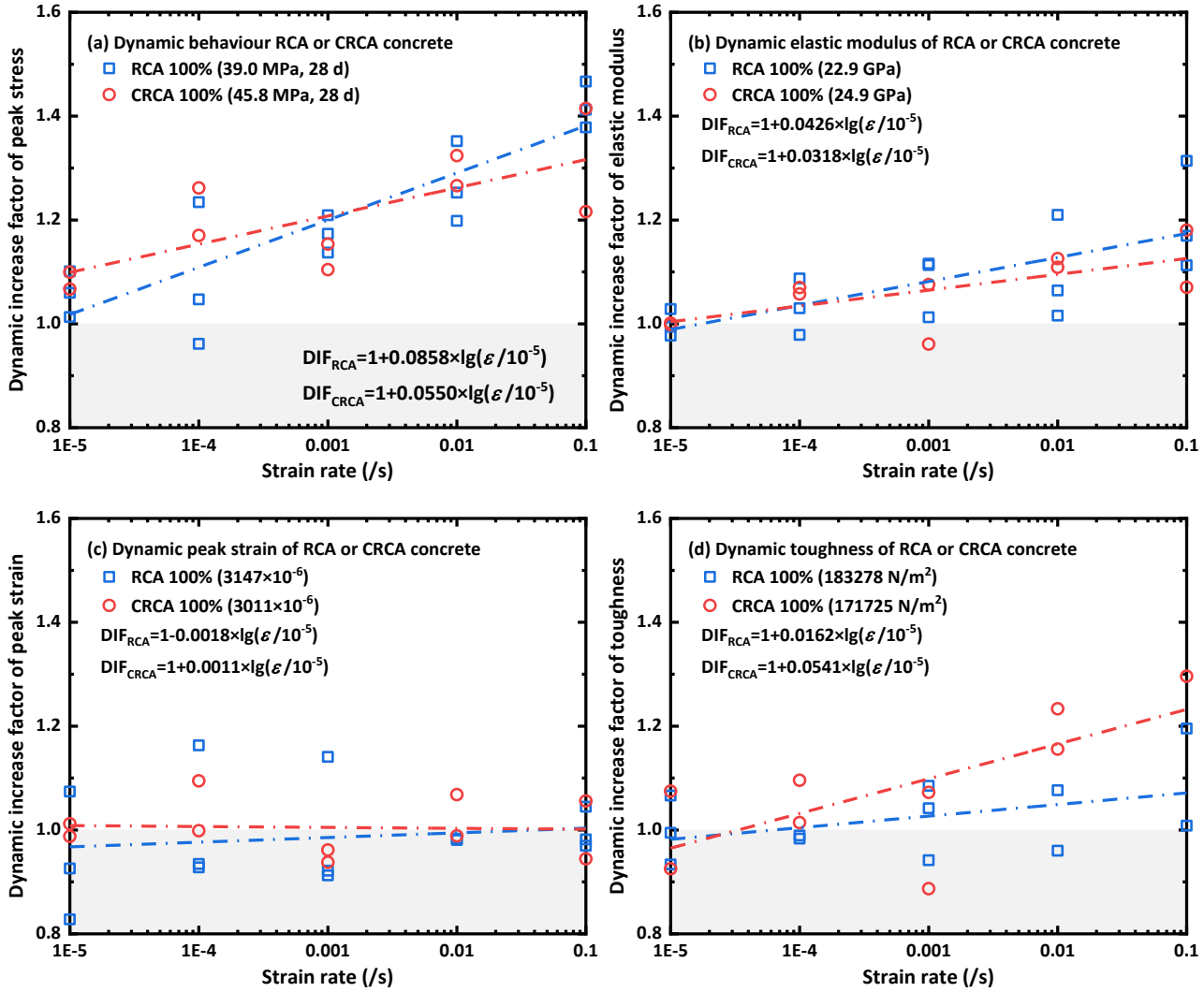

Fig. 26. Effect of carbonated RCAs on dynamic increase factor of concrete [113].

7. Sustainability assessment

In addition to the enhancements in micro- and macro-mechanical properties, the environmental benefits of utilising carbonated RCFs and RCAs are discussed at both local and global levels. From the local perspective, carbon emission analysis of carbonated recycled aggregates was conducted through a cradle-to-gate approach [163], taking into account the carbon footprint during natural resources mining, cement production, crushing and sorting of recycled aggregates as well as material transformation among plants [7]. On that basis, the parameters of total carbon emission and CO_2 intensity, referring to the ratio between carbon footprint and compressive strength of concrete, were adopted to quantify the environmental impacts [164]. The results indicated that both total

carbon emission and CO_2 intensity of concrete were reduced by 7.1–13.3% and 13.4–18.4%, respectively, through 100% replacement of NCAs or RCAs by carbonated RCAs [165]. The reduction in carbon footprint can be ascribed to the CO_2 capture of recycled aggregates during accelerated carbonation and the avoidance of waste landfill. More importantly, parameter sensitivity analysis suggested that transportation was a critical issue for reducing the carbon footprint of RCA concrete, while the carbon emission during CO_2 mineralisation of recycled aggregates was closely related to the CO_2 intensity of concrete with carbonated RCAs. In particular, the CO_2 intensity of RCA concrete was lower than that of plain concrete only when the transportation distance of natural aggregates was higher than 335.124 km, while higher environmental benefits can be achieved by carbonated RCA concrete on condition that the transportation distance was shorter than 348.15 km (Fig. 27a). In addition, the CO_2 intensity of concrete with carbonated RCAs increased linearly with the carbon emission factor (CEF) of accelerated carbonation process, while the boundary CEF was 1.95 and 2.79 to gain a lower CO_2 intensity than plain concrete and RCA concrete, respectively (Fig. 27b). Therefore, both reasonable transportation distance and high-efficient carbon capture process are essential to optimise the local environment benefits of carbonated recycled aggregates.

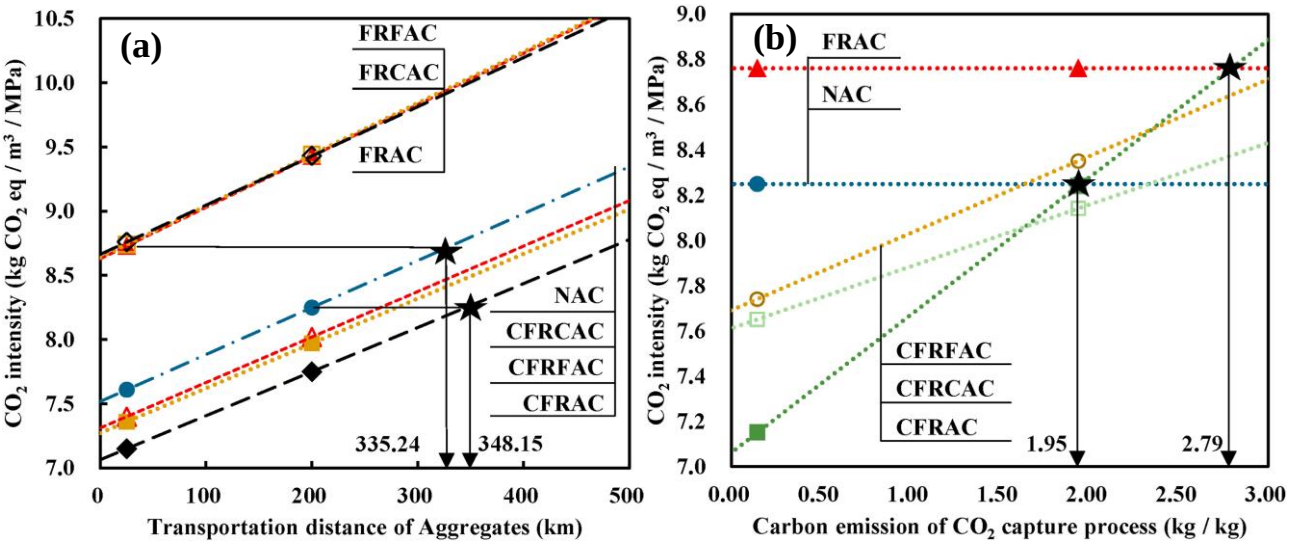

Fig. 27. Evolution of CO_2 intensity with respect to (a) transportation distance of aggregates and (b) CO_2 mineralisation process [165].

From the global perspective, no more than 50% of material CO_2 was bound during the service life of concrete structures due to the low rate of natural carbonation, and thereby there existed a considerably global potential to utilise recycled aggregates as CO_2 sink [166]. On that basis, the net CO_2 emission reduction induced by CO_2 mineralisation of RCAs in 14 global regions was estimated through life cycle assessment [167]. It was found that environmental benefits from the utilisation of

carbonated RCAs differed significantly between countries, indicating that USA and China benefited the most in terms of the annual net CO_2 emissions while the CO_2 emission per tonne CO_2 uptake varies from 0.7 in Brazil to 2.6 in Pakistan [16,167]. Moreover, the indirect global carbon footprint reduction due to the application of carbonated solid wastes in mortar and concrete was overpassed that caused by direct CO_2 reduction during the mineralisation process [168]. China and USA had potential indirect carbon reduction of 1603.7 Mt/year and 464.9 Mt/year, while the annual direct reduction potentials of these two countries were only 132.2 $MtCO_2$ and 29.4 $MtCO_2$, respectively (Fig. 28). The net negative carbon emissions and positive economic value can hardly be obtained at the same time even using CO_2 mineralisation technology, implying that the concrete recycling and CO_2 mineralisation process still need further adjustment to realise an environmental and economic balance [169,170]. Linking the local to global perspective, restructuring of transportation network and relocation of recycling plants were effective in maximising the overall CO_2 mitigation capacity regardless of spatial distribution [167].

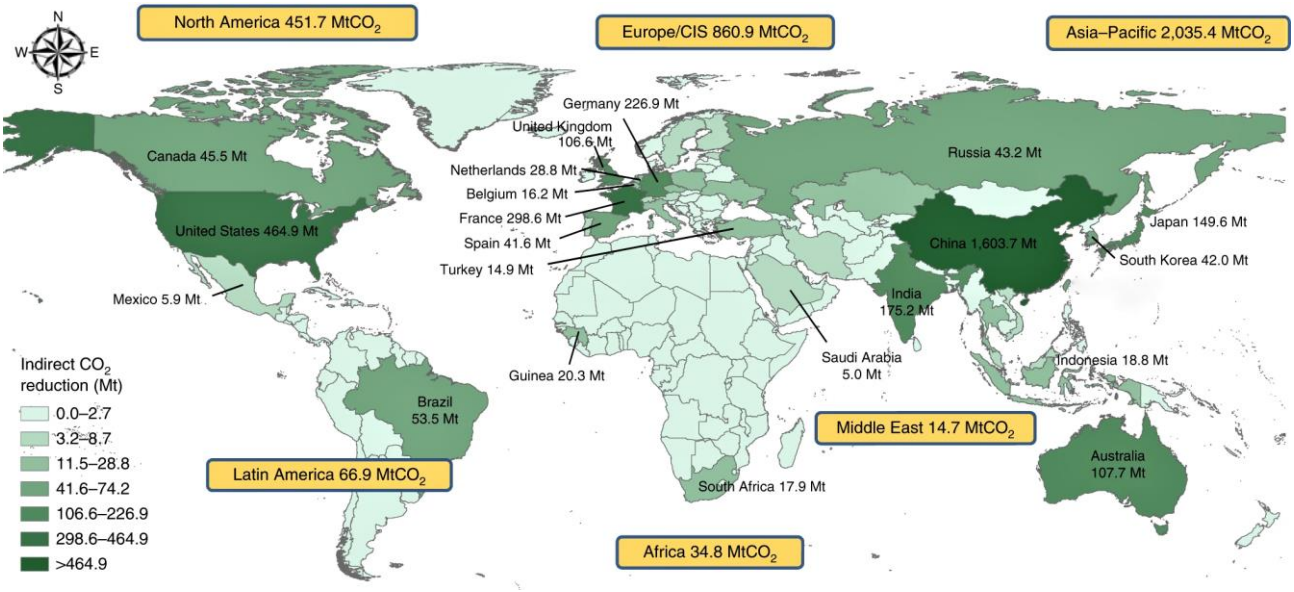

Fig. 28. Estimation of global indirect carbon footprint reduction due to utilisation of carbonated solid wastes in mortar and concrete [168].

8. Conclusions and perspectives

8.1 Conclusions

As a sustainable carbon capture approach, the CO_2 mineralisation of fines and aggregates from recycled concrete appears to be a viable alternative to reduce carbon footprint. This paper presents a critical review of concrete containing carbonated recycled fines and aggregates in terms of hydration, microstructure, mechanical properties and sustainability. The main conclusions can be

drawn as follows:

- RCFs and RCAs were more suitable for liquid-solid and gas-solid carbonation, respectively, while both types of carbonation methods can achieve a satisfactory carbonation degree in RFAs. The effectiveness of gas-solid carbonation was highly dependent on the CO_2 concentration, pressure, RH, carbonation duration and moisture content of parent materials, while liquid-solid carbonation was proved to be more efficient to finish the carbonation process within 6 h.
- The carbonation kinetics of RCFs in aqueous environment presented a typical particle size effect, as particles larger than 0.6 mm were covered with a reactive shell on the outer surface, while particles smaller than 0.15 mm were disintegrated after accelerated carbonation. During cement hydration, carbonated RCFs facilitated the nucleation and stabilization of C-S-H gels and contributed to the rapid hydration of cement due to its high pozzolanic reactivity, indicating that RCFs can be transferred to a reactive pozzolan through enforced carbonation.
- The carbonation of RFAs and RCAs resulted in the densification of microstructure, followed by the increase in density and crushing value as well as the decline in porosity and water absorption. The calcite precipitation on carbonated RCAs surface can reduce the porosity at the innermost 10 μm of ITZ, while the thickness of ITZ was not significantly affected.
- The synergic effects of physical interlocking and chemical bonding not only densify the local surface of carbonated RCAs but also provide superior adhesion between RCAs and new paste, which would consequently enhance the micro-mechanical properties of ITZ. There was a strong linear correlation between the compressive strength of concrete and the average indentation modulus of old aggregate-old mortar ITZ regardless of the carbonation condition.
- To date, the replacement ratio of RCFs in cement paste has not exceeded 30%, while the maximum replacement of RFAs and RCAs in concrete reached up to 100%. As compared with plain paste, the replacement of carbonated RCFs led to an approximately 10% increase in 28-d strength, while the higher replacement would cause a drop in strength due to the dilution effect. In contrast, the strength of concrete with carbonated RCAs is lower than the plain concrete regardless of the replacement ratio, due to the low strength of attached mortar on RCAs.
- A higher strength of concrete can be obtained by replacing uncarbonated RCAs with carbonated RCAs. Compared to concrete with plain RCAs, the elastic modulus, and compressive, splitting tensile and flexural strengths of concrete went up by up to 28.3%, 33.0%, 12.1% and 28.7%, respectively, under 100% replacement of carbonated RCAs. Due to the Stefan effect, carbonated

RCA concrete had higher dynamic peak stress but lower strain-rate sensitivity of elastic modulus than plain RCA concrete.

- Local environmental benefits in terms of an up to 13.3% and 18.4% drop in total carbon footprint and CO_2 intensity of concrete can be achieved through CO_2 mineralisation of RCAs. However, the global CO_2 mitigation capacity of recycled concrete varied from region to region, making it hard to realise a balance between environmental and economic benefits.

8.2 Perspectives

Towards better utilisation of recycled fines and aggregates through CO_2 mineralisation technology, there are still several aspects to be considered for future research.

- A standard for evaluating the quality of RFAs and RCAs after carbonation is required, accounting for the particle size, carbonation condition, duration and strength of parent materials.
- The mechanical properties of carbonated RFA and RCA concrete under cyclic loading, freeze-thaw cycles and high-temperature environments need to be examined.
- It is essential to investigate the size effect of static and dynamic mechanical properties of concrete with carbonated RCAs for large-scale applications in engineering structures.
- The relationship between the concrete properties and microstructure of carbonated recycled concrete aggregates needs to be explored to gain more insights into the overall properties.
- It is worth to study the bonding performance between carbonated RCA concrete and hybrid reinforcements such as nanomaterials, steel fibre, polymer fibre and FRP bars.
- More efforts are required to develop sustainable cementitious composites such as UHPC, ECC and 3D printed concrete using the carbonated RFAs and RCAs (Fig. 29).

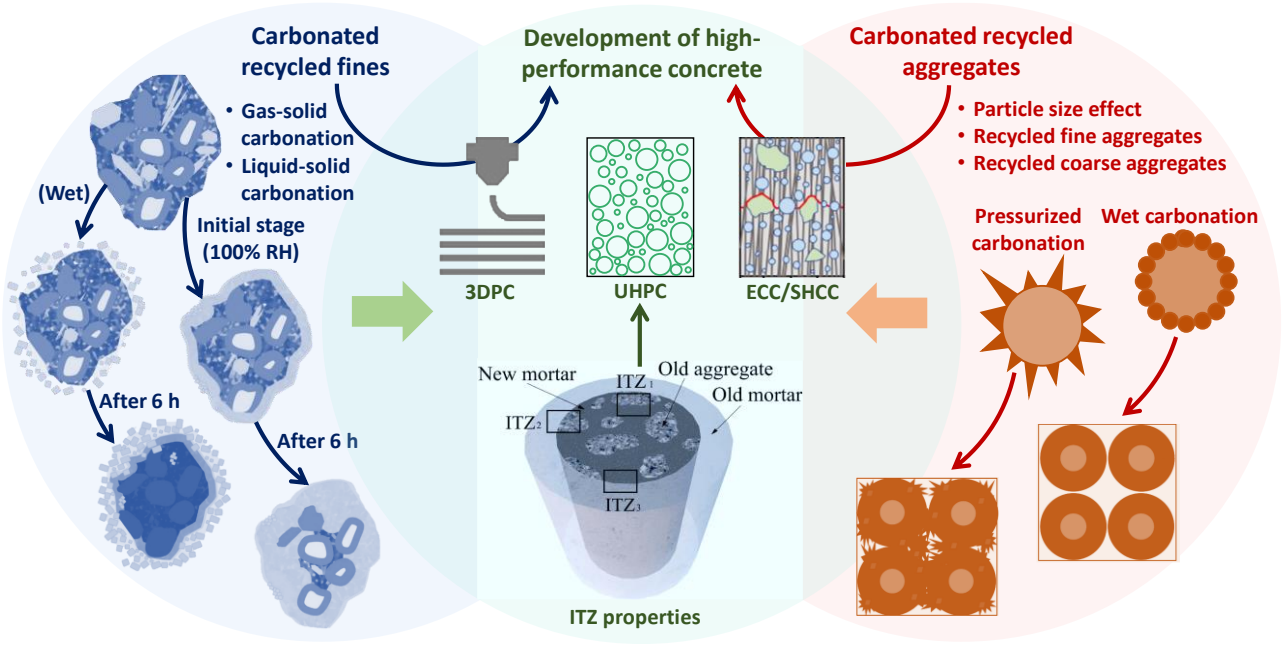

Fig. 29. Future work for CO_2 mineralisation of recycled concrete fines and aggregates.

Acknowledgements

The authors gratefully acknowledge the financial support from the National Natural Science Foundation of China (No. 52178382), the Fundamental Research Funds for the Central Universities (No. N2201023), and the Natural Science Funds of Liaoning Province (No. 2020-MS-089).

References

[1] K.L. Scrivener, V.M. John, E.M. Gartner, Eco-efficient cements: Potential economically viable solutions for a low-CO_2 cement-based materials industry, Cem. Concr. Res. 114 (2018) 2–26. https://doi.org/10.1016/J.CEMCONRES.2018.03.015.

[2] H. Ostovari, L. Müller, J. Skocek, A. Bardow, From Unavoidable CO_2 Source to CO_2 Sink? A Cement Industry Based on CO_2 Mineralization, Environ. Sci. Technol. 55 (2021) 5212–5223. https://doi.org/10.1021/acs.est.0c07599.

[3] I.H. Shah, S.A. Miller, D. Jiang, R.J. Myers, Cement substitution with secondary materials can reduce annual global CO_2 emissions by up to 1.3 gigatons, Nat. Commun. 13 (2022) 1–11. https://doi.org/10.1038/s41467-022-33289-7.

[4] A. Akhtar, A.K. Sarmah, Construction and demolition waste generation and properties of recycled aggregate concrete: A global perspective, J. Clean. Prod. 186 (2018) 262–281. https://doi.org/10.1016/J.JCLEPRO.2018.03.085.

[5] Q. Tang, Z. Ma, H. Wu, W. Wang, The utilization of eco-friendly recycled powder from concrete and brick waste in new concrete: A critical review, Cem. Concr. Compos. 114 (2020)

103807. https://doi.org/10.1016/j.cemconcomp.2020.103807.

[6] R. Infante Gomes, C. Brazão Farinha, R. Veiga, J. de Brito, P. Faria, D. Bastos, CO_2 sequestration by construction and demolition waste aggregates and effect on mortars and concrete performance - An overview, Renew. Sustain. Energy Rev. 152 (2021). https://doi.org/10.1016/j.rser.2021.111668.

[7] M.U.M.U. Hossain, C.S.C.S. Poon, I.M.C.I.M.C. Lo, J.C.P.J.C.P. Cheng, Comparative environmental evaluation of aggregate production from recycled waste materials and virgin sources by LCA, Resour. Conserv. Recycl. 109 (2016) 67–77. https://doi.org/10.1016/j.resconrec.2016.02.009.

[8] C. Shi, Y. Li, J. Zhang, W. Li, L. Chong, Z. Xie, Performance enhancement of recycled concrete aggregate - A review, J. Clean. Prod. 112 (2016) 466–472. https://doi.org/10.1016/j.jclepro.2015.08.057.

[9] W.M. Shaban, J. Yang, H. Su, K.H. Mo, L. Li, J. Xie, Quality improvement techniques for recycled concrete aggregate: A review, J. Adv. Concr. Technol. 17 (2019) 151–167. https://doi.org/10.3151/jact.17.4.151.

[10] A. Akbarnezhad, K.C.G. Ong, M.H. Zhang, C.T. Tam, T.W.J. Foo, Microwave-assisted beneficiation of recycled concrete aggregates, Constr. Build. Mater. 25 (2011) 3469–3479. https://doi.org/10.1016/j.conbuildmat.2011.03.038.

[11] V.W.Y. Tam, C.M. Tam, K.N. Le, Removal of cement mortar remains from recycled aggregate using pre-soaking approaches, Resour. Conserv. Recycl. 50 (2007) 82–101. https://doi.org/10.1016/j.resconrec.2006.05.012.

[12] S.-C. Kou, C.-S. Poon, Properties of concrete prepared with PVA-impregnated recycled concrete aggregates, Cem. Concr. Compos. 32 (2010) 649–654. https://doi.org/10.1016/j.cemconcomp.2010.05.003.

[13] D. Kong, T. Lei, J. Zheng, C. Ma, J. Jiang, J. Jiang, Effect and mechanism of surface-coating pozzalanics materials around aggregate on properties and ITZ microstructure of recycled aggregate concrete, Constr. Build. Mater. 24 (2010) 701–708. https://doi.org/10.1016/j.conbuildmat.2009.10.038.

[14] J. Wang, B. Vandevyvere, S. Vanhessche, J. Schoon, N. Boon, N. De Belie, Microbial carbonate precipitation for the improvement of quality of recycled aggregates, J. Clean. Prod. 156 (2017) 355–366. https://doi.org/10.1016/j.jclepro.2017.04.051.

[15] L. Li, M. Wu, An overview of utilizing CO_2 for accelerated carbonation treatment in the concrete industry, J. CO_2 Util. 60 (2022) 102000. https://doi.org/10.1016/j.jcou.2022.102000.

[16] S.K. Kaliyavaradhan, T.C. Ling, Potential of CO_2 sequestration through construction and demolition (C&D) waste - An overview, J. CO_2 Util. 20 (2017) 234–242. https://doi.org/10.1016/j.jcou.2017.05.014.

[17] C. Liang, B. Pan, Z. Ma, Z. He, Z. Duan, Utilization of CO_2 curing to enhance the properties of recycled aggregate and prepared concrete: A review, Cem. Concr. Compos. 105 (2020) 103446. https://doi.org/10.1016/j.cemconcomp.2019.103446.

[18] F. Georget, J.H. Prévost, B. Huet, Reactive transport modelling of cement paste leaching in brines, Cem. Concr. Res. 111 (2018) 183–196. https://doi.org/10.1016/j.cemconres.2018.05.015.

[19] O. Cascudo, P. Pires, H. Carasek, A. de Castro, A. Lopes, Evaluation of the pore solution of concretes with mineral additions subjected to 14 years of natural carbonation, Cem. Concr. Compos. 115 (2021) 103858. https://doi.org/10.1016/j.cemconcomp.2020.103858.

[20] S. Lee, W. Park, H. Lee, Life cycle CO_2 assessment method for concrete using CO_2 balance and suggestion to decrease $LCCO_2$ of concrete in South-Korean apartment, Energy Build. 58 (2013) 93–102. https://doi.org/10.1016/j.enbuild.2012.11.034.

[21] X. Fang, B. Zhan, C.S. Poon, Enhancement of recycled aggregates and concrete by combined treatment of spraying Ca2+ rich wastewater and flow-through carbonation, Constr. Build. Mater. 277 (2021) 122202. https://doi.org/10.1016/j.conbuildmat.2020.122202.

[22] Y. Pu, L. Li, Q. Wang, X. Shi, L. Fu, G. Zhang, C. Luan, A.E.F. Abomohrab, Accelerated carbonation treatment of recycled concrete aggregates using flue gas: A comparative study towards performance improvement, J. CO_2 Util. 43 (2020) 101362. https://doi.org/10.1016/j.jcou.2020.101362.

[23] D. Xuan, B. Zhan, C.S. Poon, Assessment of mechanical properties of concrete incorporating carbonated recycled concrete aggregates, Cem. Concr. Compos. 65 (2016) 67–74. https://doi.org/10.1016/j.cemconcomp.2015.10.018.

[24] D. Xuan, B. Zhan, C.S. Poon, Development of a new generation of eco-friendly concrete blocks by accelerated mineral carbonation, J. Clean. Prod. 133 (2016) 1235–1241. https://doi.org/10.1016/j.jclepro.2016.06.062.

[25] C. Liang, N. Lu, H. Ma, Z. Ma, Z. Duan, Carbonation behavior of recycled concrete with

CO_2-curing recycled aggregate under various environments, J. CO_2 Util. 39 (2020) 1–13. https://doi.org/10.1016/j.jcou.2020.101185.

[26] L. Li, J. Xiao, D. Xuan, C.S. Poon, Effect of carbonation of modeled recycled coarse aggregate on the mechanical properties of modeled recycled aggregate concrete, Cem. Concr. Compos. 89 (2018) 169–180. https://doi.org/10.1016/j.cemconcomp.2018.02.018.

[27] S. Liu, P. Shen, D. Xuan, L. Li, A. Sojobi, B. Zhan, C.S. Poon, A comparison of liquid-solid and gas-solid accelerated carbonation for enhancement of recycled concrete aggregate, Cem. Concr. Compos. 118 (2021) 103988. https://doi.org/10.1016/j.cemconcomp.2021.103988.

[28] C. Shi, Z. Wu, Z. Cao, T.C. Ling, J. Zheng, Performance of mortar prepared with recycled concrete aggregate enhanced by CO_2 and pozzolan slurry, Cem. Concr. Compos. 86 (2018) 130–138. https://doi.org/10.1016/j.cemconcomp.2017.10.013.

[29] J. Zhang, C. Shi, Y. Li, X. Pan, C.S. Poon, Z. Xie, Influence of carbonated recycled concrete aggregate on properties of cement mortar, Constr. Build. Mater. 98 (2015) 1–7. https://doi.org/10.1016/j.conbuildmat.2015.08.087.

[30] G. Pan, M. Zhan, M. Fu, Y. Wang, X. Lu, Effect of CO_2 curing on demolition recycled fine aggregates enhanced by calcium hydroxide pre-soaking, Constr. Build. Mater. 154 (2017) 810–818. https://doi.org/10.1016/j.conbuildmat.2017.07.079.

[31] X. Fang, D. Xuan, C.S. Poon, Empirical modelling of CO_2 uptake by recycled concrete aggregates under accelerated carbonation conditions, Mater. Struct. 50 (2017) 1–13. https://doi.org/10.1617/s11527-017-1066-y.

[32] A. Hosseini Zadeh, M. Mamirov, S. Kim, J. Hu, CO_2-treatment of recycled concrete aggregates to improve mechanical and environmental properties for unbound applications, Constr. Build. Mater. 275 (2021) 122180. https://doi.org/10.1016/j.conbuildmat.2020.122180.

[33] Y. Jiang, P. Shen, C.S. Poon, Improving the bonding capacity of recycled concrete aggregate by creating a reactive shell with aqueous carbonation, Constr. Build. Mater. 315 (2022) 125733. https://doi.org/10.1016/j.conbuildmat.2021.125733.

[34] X. Fang, B. Zhan, C.S. Poon, Enhancing the accelerated carbonation of recycled concrete aggregates by using reclaimed wastewater from concrete batching plants, Constr. Build. Mater. 239 (2020) 117810. https://doi.org/10.1016/j.conbuildmat.2019.117810.

[35] Z. Lu, Q. Tan, J. Lin, D. Wang, Properties investigation of recycled aggregates and concrete modified by accelerated carbonation through increased temperature, Constr. Build. Mater. 341

(2022) 127813. https://doi.org/10.1016/j.conbuildmat.2022.127813.

[36] Y. Wu, H. Mehdizadeh, K.H. Mo, T.C. Ling, High-temperature CO_2 for accelerating the carbonation of recycled concrete fines, J. Build. Eng. 52 (2022) 104526. https://doi.org/10.1016/j.jobe.2022.104526.

[37] B.J. Zhan, D.X. Xuan, C.S. Poon, C.J. Shi, B. Jian, D. Xing, C. Sun, C. Jun, B.J. Zhan, D.X. Xuan, C.S. Poon, C.J. Shi, Mechanism for rapid hardening of cement pastes under coupled CO_2-water curing regime, Cem. Concr. Compos. 97 (2019) 78–88. https://doi.org/10.1016/j.cemconcomp.2018.12.021.

[38] Y. Li, H. Wang, C. Shi, D. Zou, A. Zhou, T. Liu, Effect of post-fire lime-saturated water and water–CO_2 cyclic curing on strength recovery of thermally damaged high-performance concrete with different silica contents, Cem. Concr. Res. 164 (2023) 107050. https://doi.org/10.1016/J.CEMCONRES.2022.107050.

[39] M. Zajac, J. Skibsted, P. Durdzinski, F. Bullerjahn, J. Skocek, M. Ben Haha, Kinetics of enforced carbonation of cement paste, Cem. Concr. Res. 131 (2020) 106013. https://doi.org/10.1016/j.cemconres.2020.106013.

[40] Y. Jiang, L. Li, J.X. Lu, P. Shen, T.C. Ling, C.S. Poon, Mechanism of carbonating recycled concrete fines in aqueous environment: The particle size effect, Cem. Concr. Compos. 133 (2022) 104655. https://doi.org/10.1016/j.cemconcomp.2022.104655.

[41] M. Zajac, J. Skibsted, J. Skocek, P. Durdzinski, F. Bullerjahn, M. Ben Haha, Phase assemblage and microstructure of cement paste subjected to enforced, wet carbonation, Cem. Concr. Res. 130 (2020) 105990. https://doi.org/10.1016/j.cemconres.2020.105990.

[42] P. Shen, Y. Zhang, Y. Jiang, B. Zhan, J. Lu, S. Zhang, D. Xuan, C.S. Poon, Phase assemblance evolution during wet carbonation of recycled concrete fines, Cem. Concr. Res. 154 (2022) 106733. https://doi.org/10.1016/j.cemconres.2022.106733.

[43] X. Fang, D. Xuan, P. Shen, C.S. Poon, Fast enhancement of recycled fine aggregates properties by wet carbonation, J. Clean. Prod. 313 (2021) 127867. https://doi.org/10.1016/j.jclepro.2021.127867.

[44] Y. Jiang, L. Li, J.X. Lu, P. Shen, T.C. Ling, C.S. Poon, Enhancing the microstructure and surface texture of recycled concrete fine aggregate via magnesium-modified carbonation, Cem. Concr. Res. 162 (2022) 106967. https://doi.org/10.1016/j.cemconres.2022.106967.

[45] M. Zhan, G. Pan, Y. Wang, M. Fu, X. Lu, Effect of presoak-accelerated carbonation factors

on enhancing recycled aggregate mortars, Mag. Concr. Res. 69 (2017) 838–849. https://doi.org/10.1680/jmacr.16.00468.

[46] B.J. Zhan, D.X. Xuan, C.S. Poon, Enhancement of recycled aggregate properties by accelerated CO_2 curing coupled with limewater soaking process, Cem. Concr. Compos. 89 (2018) 230–237. https://doi.org/10.1016/j.cemconcomp.2018.03.011.

[47] L. Li, D. Xuan, A.O. Sojobi, S. Liu, C.S. Poon, Efficiencies of carbonation and nano silica treatment methods in enhancing the performance of recycled aggregate concrete, Constr. Build. Mater. 308 (2021) 125080. https://doi.org/10.1016/j.conbuildmat.2021.125080.

[48] Y. Pu, L. Li, Q. Wang, X. Shi, C. Luan, G. Zhang, L. Fu, A. El-Fatah Abomohra, Accelerated carbonation technology for enhanced treatment of recycled concrete aggregates: A state-of-the-art review, Constr. Build. Mater. 282 (2021) 122671. https://doi.org/10.1016/j.conbuildmat.2021.122671.

[49] R. Mi, K.M. Liew, G. Pan, New insights into diffusion and reaction of CO_2 gas in recycled aggregate concrete, Cem. Concr. Compos. 129 (2022) 104486. https://doi.org/10.1016/j.cemconcomp.2022.104486.

[50] X. You, X. Hu, P. He, J. Liu, C. Shi, A review on the modelling of carbonation of hardened and fresh cement-based materials, Cem. Concr. Compos. 125 (2022) 104315. https://doi.org/10.1016/j.cemconcomp.2021.104315.

[51] V.L. Ta, S. Bonnet, T. Senga Kiesse, A. Ventura, A new meta-model to calculate carbonation front depth within concrete structures, Constr. Build. Mater. 129 (2016) 172–181. https://doi.org/10.1016/j.conbuildmat.2016.10.103.

[52] G. Rimmelé, V. Barlet-Gouédard, O. Porcherie, B. Goffé, F. Brunet, Heterogeneous porosity distribution in Portland cement exposed to CO_2-rich fluids, Cem. Concr. Res. 38 (2008) 1038–1048. https://doi.org/10.1016/j.cemconres.2008.03.022.

[53] Q.T. Phung, N. Maes, D. Jacques, G. De Schutter, G. Ye, J. Perko, Modelling the carbonation of cement pastes under a CO_2 pressure gradient considering both diffusive and convective transport, Constr. Build. Mater. 114 (2016) 333–351. https://doi.org/10.1016/j.conbuildmat.2016.03.191.

[54] X. Zha, M. Yu, J. Ye, G. Feng, Numerical modeling of supercritical carbonation process in cement-based materials, Cem. Concr. Res. 72 (2015) 10–20. https://doi.org/10.1016/j.cemconres.2015.02.017.

[55] B. Gérard, C. Le Bellego, O. Bernard, Simplified modelling of calcium leaching of concrete in various environments, Mater. Struct. Constr. 35 (2002) 632–640. https://doi.org/10.1617/13937.

[56] B. Šavija, M. Luković, Carbonation of cement paste: Understanding, challenges, and opportunities, Constr. Build. Mater. 117 (2016) 285–301. https://doi.org/10.1016/j.conbuildmat.2016.04.138.

[57] A. Morandeau, M. Thiéry, P. Dangla, Investigation of the carbonation mechanism of CH and C-S-H in terms of kinetics, microstructure changes and moisture properties, Cem. Concr. Res. 56 (2014) 153–170. https://doi.org/10.1016/j.cemconres.2013.11.015.

[58] A.E. Morandeau, C.E. White, In situ X-ray pair distribution function analysis of accelerated carbonation of a synthetic calcium-silicate-hydrate gel, J. Mater. Chem. A. 3 (2015) 8597–8605. https://doi.org/10.1039/c5ta00348b.

[59] N. Hyvert, A. Sellier, F. Duprat, P. Rougeau, P. Francisco, Dependency of C-S-H carbonation rate on CO_2 pressure to explain transition from accelerated tests to natural carbonation, Cem. Concr. Res. 40 (2010) 1582–1589. https://doi.org/10.1016/j.cemconres.2010.06.010.

[60] C.J. GOODBRAKE, J.F. YOUNG, R.L. BERGER, Reaction of Hydraulic Calcium Silicates with Carbon Dioxide and Water, J. Am. Ceram. Soc. 62 (1979) 488–491. https://doi.org/10.1111/j.1151-2916.1979.tb19112.x.

[61] Q. Zhou, F.P. Glasser, Kinetics and mechanism of the carbonation of ettringite, Adv. Cem. Res. 12 (2000) 131–136. https://doi.org/10.1680/adcr.2000.12.3.131.

[62] Y. Fang, J. Chang, Microstructure changes of waste hydrated cement paste induced by accelerated carbonation, Constr. Build. Mater. 76 (2015) 360–365. https://doi.org/10.1016/j.conbuildmat.2014.12.017.

[63] T.F. Sevelsted, J. Skibsted, Carbonation of C-S-H and C-A-S-H samples studied by ^{13}C, ^{27}Al and ^{29}Si MAS NMR spectroscopy, Cem. Concr. Res. 71 (2015) 56–65. https://doi.org/10.1016/j.cemconres.2015.01.019.

[64] C. Kim, J. Kim, S. Joo, Y. Bu, M. Liu, J. Cho, G. Kim, Efficient CO_2 Utilization via a Hybrid Na-CO_2 System Based on CO_2 Dissolution, IScience. 9 (2018) 278–285. https://doi.org/10.1016/j.isci.2018.10.027.

[65] P. Shen, Y. Sun, S. Liu, Y. Jiang, H. Zheng, D. Xuan, J. Lu, C.S. Poon, Synthesis of amorphous nano-silica from recycled concrete fines by two-step wet carbonation, Cem. Concr.

Res. 147 (2021) 106526. https://doi.org/10.1016/j.cemconres.2021.106526.

[66] M. Zajac, J. Skibsted, F. Bullerjahn, J. Skocek, Semi-dry carbonation of recycled concrete paste, J. CO_2 Util. 63 (2022). https://doi.org/10.1016/j.jcou.2022.102111.

[67] H. Mehdizadeh, T.C. Ling, X. Cheng, K.H. Mo, Effect of particle size and CO_2 treatment of waste cement powder on properties of cement paste, Can. J. Civ. Eng. 48 (2021) 522–531. https://doi.org/10.1139/cjce-2019-0574.

[68] M. Zajac, J. Skocek, P. Durdzinski, F. Bullerjahn, J. Skibsted, M. Ben Haha, Effect of carbonated cement paste on composite cement hydration and performance, Cem. Concr. Res. 134 (2020) 106090. https://doi.org/10.1016/j.cemconres.2020.106090.

[69] J.W. Bullard, H.M. Jennings, R.A. Livingston, A. Nonat, G.W. Scherer, J.S. Schweitzer, K.L. Scrivener, J.J. Thomas, Mechanisms of cement hydration, Cem. Concr. Res. 41 (2011) 1208–1223. https://doi.org/10.1016/j.cemconres.2010.09.011.

[70] B. Lu, C. Shi, J. Zhang, J. Wang, Effects of carbonated hardened cement paste powder on hydration and microstructure of Portland cement, Constr. Build. Mater. 186 (2018) 699–708. https://doi.org/10.1016/j.conbuildmat.2018.07.159.

[71] M. Zajac, A. Rossberg, G. Le Saout, B. Lothenbach, Influence of limestone and anhydrite on the hydration of Portland cements, Cem. Concr. Compos. 46 (2014) 99–108. https://doi.org/10.1016/j.cemconcomp.2013.11.007.

[72] H. Mehdizadeh, X. Cheng, K.H. Mo, T.C. Ling, Upcycling of waste hydrated cement paste containing high-volume supplementary cementitious materials via CO_2 pre-treatment, J. Build. Eng. 52 (2022) 104396. https://doi.org/10.1016/j.jobe.2022.104396.

[73] J. Skocek, M. Zajac, M. Ben Haha, Carbon Capture and Utilization by mineralization of cement pastes derived from recycled concrete, Sci. Rep. 10 (2020) 1–12. https://doi.org/10.1038/s41598-020-62503-z.

[74] X. Ouyang, L. Wang, S. Xu, Y. Ma, G. Ye, Surface characterization of carbonated recycled concrete fines and its effect on the rheology, hydration and strength development of cement paste, Cem. Concr. Compos. 114 (2020) 103809. https://doi.org/10.1016/j.cemconcomp.2020.103809.

[75] C. Perdikouri, S. Piazolo, A. Kasioptas, B.C. Schmidt, A. Putnis, Hydrothermal replacement of aragonite by calcite: Interplay between replacement, fracturing and growth, Eur. J. Mineral. 25 (2013) 123–136. https://doi.org/10.1127/0935-1221/2013/0025-2261.

[76] Z. Shi, B. Lothenbach, M.R. Geiker, J. Kaufmann, A. Leemann, S. Ferreiro, J. Skibsted, Experimental studies and thermodynamic modeling of the carbonation of Portland cement, metakaolin and limestone mortars, Cem. Concr. Res. 88 (2016) 60–72. https://doi.org/10.1016/j.cemconres.2016.06.006.

[77] X. Xu, J.T. Han, D.H. Kim, K. Cho, Two modes of transformation of amorphous calcium carbonate films in air, J. Phys. Chem. B. 110 (2006) 2764–2770. https://doi.org/10.1021/jp055712w.

[78] M. Zajac, A. Lechevallier, P. Durdzinski, F. Bullerjahn, J. Skibsted, M. Ben Haha, CO_2 mineralisation of Portland cement: Towards understanding the mechanisms of enforced carbonation, J. CO_2 Util. 38 (2020) 398–415. https://doi.org/10.1016/j.jcou.2020.02.015.

[79] S.K. Kaliyavaradhan, T.C. Ling, K.H. Mo, CO_2 sequestration of fresh concrete slurry waste: Optimization of CO_2uptake and feasible use as a potential cement binder, J. CO_2 Util. 42 (2020) 101330. https://doi.org/10.1016/j.jcou.2020.101330.

[80] L. Black, K. Garbev, I. Gee, Surface carbonation of synthetic C-S-H samples: A comparison between fresh and aged C-S-H using X-ray photoelectron spectroscopy, Cem. Concr. Res. 38 (2008) 745–750. https://doi.org/10.1016/j.cemconres.2008.02.003.

[81] S. Greiser, G.J.G. Gluth, P. Sturm, C. Jäger, 29Si, 27Al and 27Al double-resonance NMR spectroscopy study of cementitious sodium aluminosilicate gels (geopolymers) and gel-zeolite composites, RSC Adv. 8 (2018) 40164–40171. https://doi.org/10.1039/c8ra09246j.

[82] K.J.D. Mackenzie, R.H. Meinhold, B.L. Sherriff, Z. Xu, ^{27}Al and^{25}Mg solid-state magic-angle spinning nuclear magnetic resonance study of hydrotalcite and its thermal decomposition sequence, J. Mater. Chem. 3 (1993) 1263–1269. https://doi.org/10.1039/JM9930301263.

[83] H. Wu, C. Liang, J. Xiao, Z. Ma, Properties and CO_2-curing enhancement of cement-based materials containing various sources of waste hardened cement paste powder, J. Build. Eng. 44 (2021) 102677. https://doi.org/10.1016/j.jobe.2021.102677.

[84] S.M. Park, J.G. Jang, H.K. Lee, Unlocking the role of MgO in the carbonation of alkali-activated slag cement, Inorg. Chem. Front. 5 (2018) 1661–1670. https://doi.org/10.1039/c7qi00754j.

[85] B. Lothenbach, G. Le Saout, E. Gallucci, K. Scrivener, Influence of limestone on the hydration of Portland cements, Cem. Concr. Res. 38 (2008) 848–860. https://doi.org/10.1016/j.cemconres.2008.01.002.

[86] A.S.S.S. Nedunuri, A.Y. Mohammed, S. Muhammad, Carbonation potential of concrete debris fines and its valorisation through mineral carbonation, Constr. Build. Mater. 310 (2021) 125162. https://doi.org/10.1016/j.conbuildmat.2021.125162.

[87] K. De Weerdt, M.B. Haha, G. Le Saout, K.O. Kjellsen, H. Justnes, B. Lothenbach, Hydration mechanisms of ternary Portland cements containing limestone powder and fly ash, Cem. Concr. Res. 41 (2011) 279–291. https://doi.org/10.1016/j.cemconres.2010.11.014.

[88] M. Zajac, M. Ben Haha, Experimental investigation and modeling of hydration and performance evolution of fly ash cement, Mater. Struct. Constr. 47 (2014) 1259–1269. https://doi.org/10.1617/s11527-013-0126-1.

[89] J. Zhang, C. Shi, Y. Li, X. Pan, C.-S. Poon, Z. Xie, Performance Enhancement of Recycled Concrete Aggregates through Carbonation, J. Mater. Civ. Eng. 27 (2015). https://doi.org/10.1061/(asce)mt.1943-5533.0001296.

[90] M. Zajac, J. Skocek, S. Adu-Amankwah, L. Black, M. Ben Haha, Impact of microstructure on the performance of composite cements: Why higher total porosity can result in higher strength, Cem. Concr. Compos. 90 (2018) 178–192. https://doi.org/10.1016/j.cemconcomp.2018.03.023.

[91] M. Zajac, J. Skocek, Ł. Gołek, J. Deja, Supplementary cementitious materials based on recycled concrete paste, J. Clean. Prod. 387 (2023). https://doi.org/10.1016/j.jclepro.2022.135743.

[92] M. Zajac, J. Skocek, J. Skibsted, M. Ben Haha, CO_2 mineralization of demolished concrete wastes into a supplementary cementitious material–a new CCU approach for the cement industry, RILEM Tech. Lett. 6 (2021) 53–60. https://doi.org/10.21809/rilemtechlett.2021.141.

[93] J. Yang, J. Zeng, X. He, Y. Su, H. Tan, H. Min, H. Hu, H. Ye, M. Ma, B. Strnadel, Utilization of submicron autoclaved aerated concrete waste to prepare eco-friendly ultra-high performance concrete by replacing silica fume, J. Clean. Prod. 376 (2022) 134252. https://doi.org/10.1016/J.JCLEPRO.2022.134252.

[94] R. Volk, J.J. Steins, P. Stemmermann, F. Schultmann, Comparison of different post-demolition autoclaved aerated concrete (AAC) recycling options, IOP Conf. Ser. Earth Environ. Sci., 2022. https://doi.org/10.1088/1755-1315/1078/1/012074.

[95] P.W. Griffin, G.P. Hammond, R.C. McKenna, Industrial energy use and decarbonisation in the glass sector: A UK perspective, Adv. Appl. Energy. 3 (2021) 100037.

https://doi.org/10.1016/j.adapen.2021.100037.

[96] M. Zajac, G. Bolte, J. Skocek, M. Ben Haha, Modelling the effect of the cement components fineness on performance and environmental impact of composite cements, Constr. Build. Mater. 276 (2021) 122108. https://doi.org/10.1016/J.CONBUILDMAT.2020.122108.

[97] M. Shi, T.C. Ling, B. Gan, M.Z. Guo, Turning concrete waste powder into carbonated artificial aggregates, Constr. Build. Mater. 199 (2019) 178–184. https://doi.org/10.1016/j.conbuildmat.2018.12.021.

[98] D. Xuan, B. Zhan, C.S. Poon, W. Zheng, Carbon dioxide sequestration of concrete slurry waste and its valorisation in construction products, Constr. Build. Mater. 113 (2016) 664–672. https://doi.org/10.1016/j.conbuildmat.2016.03.109.

[99] Y. Li, T. Fu, R. Wang, Y. Li, An assessment of microcracks in the interfacial transition zone of recycled concrete aggregates cured by CO_2, Constr. Build. Mater. 236 (2020) 117543. https://doi.org/10.1016/j.conbuildmat.2019.117543.

[100] S.C. Kou, B.J. Zhan, C.S. Poon, Use of a CO_2 curing step to improve the properties of concrete prepared with recycled aggregates, Cem. Concr. Compos. 45 (2014) 22–28. https://doi.org/10.1016/j.cemconcomp.2013.09.008.

[101] S. Luo, W. Wu, K. Wu, Effect of recycled coarse aggregates enhanced by CO_2 on the mechanical properties of recycled aggregate concrete, IOP Conf. Ser. Mater. Sci. Eng. 431 (2018) 0–8. https://doi.org/10.1088/1757-899X/431/10/102006.

[102] B. Sun, Q. Zeng, D. Wang, W. Zhao, Sustainable 3D printed mortar with CO_2 pretreated recycled fine aggregates, Cem. Concr. Compos. 134 (2022) 104800. https://doi.org/10.1016/j.cemconcomp.2022.104800.

[103] M. Sonmez, H. Ilcan, B. Dundar, G. Yildirim, Y.C. Ersan, M. Sahmaran, The effect of chemical- versus microbial-induced calcium carbonate mineralization on the enhancement of fine recycled concrete aggregate: A comparative study, J. Build. Eng. 44 (2021) 103316. https://doi.org/10.1016/j.jobe.2021.103316.

[104] G. Chinzorigt, M.K. Lim, M. Yu, H. Lee, O. Enkbold, D. Choi, Strength, shrinkage and creep and durability aspects of concrete including CO_2 treated recycled fine aggregate, Cem. Concr. Res. 136 (2020) 106062. https://doi.org/10.1016/j.cemconres.2020.106062.

[105] C. Liang, H. Ma, Y. Pan, Z. Ma, Z. Duan, Z. He, Chloride permeability and the caused steel corrosion in the concrete with carbonated recycled aggregate, Constr. Build. Mater. 218 (2019)

506–518. https://doi.org/10.1016/j.conbuildmat.2019.05.136.

[106] Y. Li, S. Zhang, R. Wang, Y. Zhao, C. Men, Effects of carbonation treatment on the crushing characteristics of recycled coarse aggregates, Constr. Build. Mater. 201 (2019) 408–420. https://doi.org/10.1016/j.conbuildmat.2018.12.158.

[107] K. Wu, S. Luo, J. Zheng, J. Yan, J. Xiao, Influence of carbonation treatment on the properties of multiple interface transition zones and recycled aggregate concrete, Cem. Concr. Compos. 127 (2022) 104402. https://doi.org/10.1016/j.cemconcomp.2021.104402.

[108] B.J. Zhan, D.X. Xuan, W. Zeng, C.S. Poon, Carbonation treatment of recycled concrete aggregate: Effect on transport properties and steel corrosion of recycled aggregate concrete, Cem. Concr. Compos. 104 (2019) 103360. https://doi.org/10.1016/j.cemconcomp.2019.103360.

[109] B. Lu, C. Shi, Z. Cao, M. Guo, J. Zheng, Effect of carbonated coarse recycled concrete aggregate on the properties and microstructure of recycled concrete, J. Clean. Prod. 233 (2019) 421–428. https://doi.org/10.1016/j.jclepro.2019.05.350.

[110] S. Luo, S. Ye, J. Xiao, J. Zheng, Y. Zhu, Carbonated recycled coarse aggregate and uniaxial compressive stress-strain relation of recycled aggregate concrete, Constr. Build. Mater. 188 (2018) 956–965. https://doi.org/10.1016/j.conbuildmat.2018.08.159.

[111] L. Peng, W. Zeng, Y. Zhao, L. Li, C. sun Poon, H. Zheng, Steel corrosion and corrosion-induced cracking in reinforced concrete with carbonated recycled aggregate, Cem. Concr. Compos. 133 (2022) 104694. https://doi.org/10.1016/j.cemconcomp.2022.104694.

[112] J. Wang, J. Zhang, D. Cao, H. Dang, B. Ding, Comparison of recycled aggregate treatment methods on the performance for recycled concrete, Constr. Build. Mater. 234 (2020) 117366. https://doi.org/10.1016/j.conbuildmat.2019.117366.

[113] L. Li, C.S. Poon, J. Xiao, D. Xuan, Effect of carbonated recycled coarse aggregate on the dynamic compressive behavior of recycled aggregate concrete, Constr. Build. Mater. 151 (2017) 52–62. https://doi.org/10.1016/j.conbuildmat.2017.06.043.

[114] H. Liu, X. Zhu, P. Zhu, C. Chen, X. Wang, W. Yang, M. Zong, Carbonation treatment to repair the damage of repeatedly recycled coarse aggregate from recycled concrete suffering from coupling action of high stress and freeze-thaw cycles, Constr. Build. Mater. 349 (2022) 128688. https://doi.org/10.1016/j.conbuildmat.2022.128688.

[115] R. Mi, G. Pan, Slowing down CO_2 effective diffusion speeds in recycled aggregate concrete

by using carbon capture technology and high-quality recycled aggregate, J. Build. Eng. 45 (2022) 103628. https://doi.org/10.1016/j.jobe.2021.103628.

[116] S.M.S. Kazmi, M.J. Munir, Y.F. Wu, I. Patnaikuni, Y. Zhou, F. Xing, Influence of different treatment methods on the mechanical behavior of recycled aggregate concrete: A comparative study, Cem. Concr. Compos. 104 (2019) 103398. https://doi.org/10.1016/j.cemconcomp.2019.103398.

[117] V.W. Tam, A. Butera, K.N. Le, Mechanical properties of CO_2 concrete utilising practical carbonation variables, J. Clean. Prod. 294 (2021) 126307. https://doi.org/10.1016/j.jclepro.2021.126307.

[118] J. Wu, Y. Zhang, P. Zhu, J. Feng, K. Hu, Mechanical Properties and ITZ Microstructure of Recycled Aggregate Concrete Using Carbonated Recycled Coarse Aggregate, J. Wuhan Univ. Technol. Mater. Sci. Ed. 33 (2018) 648–653. https://doi.org/10.1007/s11595-018-1873-1.

[119] B. Zhan, C.S. Poon, Q. Liu, S. Kou, C. Shi, Experimental study on CO_2 curing for enhancement of recycled aggregate properties, Constr. Build. Mater. 67 (2014) 3–7. https://doi.org/10.1016/j.conbuildmat.2013.09.008.

[120] S.Y. Abate, K. Il Song, J.K. Song, B.Y. Lee, H.K. Kim, Internal curing effect of raw and carbonated recycled aggregate on the properties of high-strength slag-cement mortar, Constr. Build. Mater. 165 (2018) 64–71. https://doi.org/10.1016/j.conbuildmat.2018.01.035.

[121] C. Zhu, Y. Fang, H. Wei, Carbonation-cementation of recycled hardened cement paste powder, Constr. Build. Mater. 192 (2018) 224–232. https://doi.org/10.1016/j.conbuildmat.2018.10.113.

[122] L. Li, Q. Liu, T. Huang, W. Peng, Mineralization and utilization of CO_2 in construction and demolition wastes recycling for building materials: A systematic review of recycled concrete aggregate and recycled hardened cement powder, Sep. Purif. Technol. 298 (2022) 121512. https://doi.org/10.1016/j.seppur.2022.121512.

[123] X. Ouyang, D.A. Koleva, G. Ye, K. van Breugel, Insights into the mechanisms of nucleation and growth of C–S–H on fillers, Mater. Struct. Constr. 50 (2017). https://doi.org/10.1617/s11527-017-1082-y.

[124] Y. Bian, Z. Li, J. Zhao, Y. Wang, Synergistic enhancement effect of recycled fine powder (RFP) cement paste and carbonation on recycled aggregates performances and its mechanism, J. Clean. Prod. 344 (2022) 130848. https://doi.org/10.1016/j.jclepro.2022.130848.

[125] M. Castellote, C. Andrade, Modelling the carbonation of cementitious matrixes by means of the unreacted-core model, UR-CORE, Cem. Concr. Res. 38 (2008). https://doi.org/10.1016/j.cemconres.2008.07.004.

[126] Z.F. Zhao, P.F. Jin, Q.Q. Zhao, Influence of laboratory accelerated carbonation on the properties of recycled concrete aggregates, Adv. Mater. Res. 919–921 (2014) 1817–1820. https://doi.org/10.4028/www.scientific.net/AMR.919-921.1817.

[127] S.Y. Pan, P.C. Chiang, Y.H. Chen, C.S. Tan, E.E. Chang, Kinetics of carbonation reaction of basic oxygen furnace slags in a rotating packed bed using the surface coverage model: Maximization of carbonation conversion, Appl. Energy. 113 (2014). https://doi.org/10.1016/j.apenergy.2013.07.035.

[128] M. Thiery, P. Dangla, P. Belin, G. Habert, N. Roussel, Carbonation kinetics of a bed of recycled concrete aggregates: A laboratory study on model materials, Cem. Concr. Res. 46 (2013) 50–65. https://doi.org/10.1016/j.cemconres.2013.01.005.

[129]L. Jiqiao, H. Baiyun, Particle size characterization of ultrafine tungsten powder, Int. J. Refract. Met. Hard Mater. 19 (2001) 89–99. https://doi.org/10.1016/S0263-4368(00)00051-2.

[130] M. Zajac, P. Durdzinski, C. Stabler, J. Skocek, D. Nied, M. Ben Haha, Influence of calcium and magnesium carbonates on hydration kinetics, hydrate assemblage and microstructural development of metakaolin containing composite cements, Cem. Concr. Res. 106 (2018) 91–102. https://doi.org/10.1016/j.cemconres.2018.01.008.

[131] K.L. Scrivener, A.K. Crumbie, P. Laugesen, The interfacial transition zone (ITZ) between cement paste and aggregate in concrete, Interface Sci. 12 (2004) 411–421. https://doi.org/10.1023/B:INTS.0000042339.92990.4c.

[132] C.C. Yang, Effect of the interfacial transition zone on the transport and the elastic properties of mortar, Mag. Concr. Res. 55 (2003) 305–312. https://doi.org/10.1680/macr.2003.55.4.305.

[133] Z. Lu, Q. Tan, J. Lin, D. Wang, Performance Analysis of a Recycled Concrete Interfacial Transition Zone in a Rapid Carbonization Environment, Constr. Build. Mater. 89 (2018) 104694. https://doi.org/10.1016/j.jcou.2020.101185.

[134] S. Gao, J. Guo, Y. Gong, S. Ban, A. Liu, Study on the penetration and diffusion of chloride ions in interface transition zone of recycled concrete prepared by modified recycled coarse aggregates, Case Stud. Constr. Mater. 16 (2022) e01034. https://doi.org/10.1016/j.cscm.2022.e01034.

[135] B.J. Zhan, D.X. Xuan, C.S. Poon, K.L. Scrivener, Characterization of interfacial transition zone in concrete prepared with carbonated modeled recycled concrete aggregates, Cem. Concr. Res. 136 (2020) 106175. https://doi.org/10.1016/j.cemconres.2020.106175.

[136] J. Xiao, W. Li, D.J. Corr, S.P. Shah, Effects of interfacial transition zones on the stress–strain behavior of modeled recycled aggregate concrete, Cem. Concr. Res. 52 (2013) 82–99. https://doi.org/10.1016/J.CEMCONRES.2013.05.004.

[137] A. Katz, Treatments for the improvement of recycled aggregate, J. Mater. Civ. Eng. 16 (2004) 597–603. https://doi.org/10.1061/(ASCE)0899-1561(2004)16:6(597).

[138] S. Pourchet, I. Pochard, F. Brunel, D. Perrey, Chemistry of the calcite/water interface: Influence of sulfate ions and consequences in terms of cohesion forces, Cem. Concr. Res. 52 (2013) 22–30. https://doi.org/10.1016/j.cemconres.2013.04.002.

[139] C.Z. Yuan, I. Odler, The interfacial zone between marble and tricalcium silicate paste, Cem. Concr. Res. 17 (1987) 784–792. https://doi.org/10.1016/0008-8846(87)90041-X.

[140] J.J.M. Monteiro, P.K. Mehta, Ettringite formation on the aggregate - cement paste interface, Cem. Concr. Res. 15 (1985) 378–380. https://doi.org/10.1016/0008-8846(85)90049-3.

[141] H. Ma, Z. Li, Multi-aggregate approach for modeling interfacial transition zone in concrete, ACI Mater. J. 111 (2014) 189–200. https://doi.org/10.14359/51686501.

[142] X. Ouyang, D.A. Koleva, G. Ye, K. van Breugel, Understanding the adhesion mechanisms between C-S-H and fillers, Cem. Concr. Res. 100 (2017) 275–283. https://doi.org/10.1016/j.cemconres.2017.07.006.

[143] V.W.Y. Tam, A. Butera, K.N. Le, Carbon-conditioned recycled aggregate in concrete production, J. Clean. Prod. 133 (2016) 672–680. https://doi.org/10.1016/j.jclepro.2016.06.007.

[144] J. Sim, C. Park, Compressive strength and resistance to chloride ion penetration and carbonation of recycled aggregate concrete with varying amount of fly ash and fine recycled aggregate, Waste Manag. 31 (2011) 2352–2360. https://doi.org/10.1016/j.wasman.2011.06.014.

[145] P. Lura, O.M. Jensen, S.I. Igarashi, Experimental observation of internal water curing of concrete, Mater. Struct. Constr. 40 (2007) 211–220. https://doi.org/10.1617/s11527-006-9132-x.

[146] J. Xiao, J. Li, C. Zhang, Mechanical properties of recycled aggregate concrete under uniaxial loading, Cem. Concr. Res. 35 (2005) 1187–1194.

https://doi.org/10.1016/j.cemconres.2004.09.020.

[147] J. Wu, X. Jing, Z. Wang, Uni-axial compressive stress-strain relation of recycled coarse aggregate concrete after freezing and thawing cycles, Constr. Build. Mater. 134 (2017) 210–219. https://doi.org/10.1016/j.conbuildmat.2016.12.142.

[148] D.P. Bentz, C.F. Ferraris, S.Z. Jones, D. Lootens, F. Zunino, Limestone and silica powder replacements for cement: Early-age performance, Cem. Concr. Compos. 78 (2017) 43–56. https://doi.org/10.1016/j.cemconcomp.2017.01.001.

[149] P. Lorca, R. Calabuig, J. Benlloch, L. Soriano, J. Payá, Microconcrete with partial replacement of Portland cement by fly ash and hydrated lime addition, Mater. Des. 64 (2014) 535–541. https://doi.org/10.1016/j.matdes.2014.08.022.

[150] N. Russo, F. Lollini, Effect of carbonated recycled coarse aggregates on the mechanical and durability properties of concrete, J. Build. Eng. 51 (2022) 104290. https://doi.org/10.1016/j.jobe.2022.104290.

[151] V.W.Y. Tam, A. Butera, K.N. Le, Microstructure and chemical properties for CO_2 concrete, Constr. Build. Mater. 262 (2020) 120584. https://doi.org/10.1016/j.conbuildmat.2020.120584.

[152] V.W.Y. Tam, A. Butera, K.N. Le, W. Li, Utilising CO_2 technologies for recycled aggregate concrete: A critical review, Constr. Build. Mater. 250 (2020) 118903. https://doi.org/10.1016/J.CONBUILDMAT.2020.118903.

[153] A. V. Rahul, M.K. Mohan, G. De Schutter, K. Van Tittelboom, 3D printable concrete with natural and recycled coarse aggregates: Rheological, mechanical and shrinkage behaviour, Cem. Concr. Compos. 125 (2022) 104311. https://doi.org/10.1016/J.CEMCONCOMP.2021.104311.

[154] T. Zhang, M. Zhang, Y. Shen, H. Zhu, Z. Yan, Mitigating the damage of ultra-high performance concrete at elevated temperatures using synergistic flame-retardant polymer fibres, Cem. Concr. Res. 158 (2022) 106835. https://doi.org/10.1016/J.CEMCONRES.2022.106835.

[155] T. Zhang, M. Chen, Z. Yan, S. Wang, M. Zhang, Role of micro fibres in tailoring the specific heat capacity of cementitious composites at elevated temperatures: Experimental characterisation and micromechanical modelling, Constr. Build. Mater. 369 (2023) 130550. https://doi.org/10.1016/J.CONBUILDMAT.2023.130550.

[156] Y. Zhang, S. Zhang, X. Jiang, Q. Chen, Z. Jiang, J.W. Ju, M. Bauchy, Insights into the

thermal effect on the fracture toughness of calcium silicate hydrate grains: A reactive molecular dynamics study, Cem. Concr. Compos. 134 (2022) 104824. https://doi.org/10.1016/J.CEMCONCOMP.2022.104824.

[157] Q. Yu, W. Zhuang, C. Shi, Research progress on the dynamic compressive properties of ultra-high performance concrete under high strain rates, Cem. Concr. Compos. 124 (2021) 104258. https://doi.org/10.1016/j.cemconcomp.2021.104258.

[158] H.W. Noh, V.D. Truong, J.Y. Cho, D.J. Kim, Dynamic increase factors for fiber-reinforced cement composites: A review, J. Build. Eng. 56 (2022) 104769. https://doi.org/10.1016/j.jobe.2022.104769.

[159] M. Chen, W. Chen, H. Zhong, D. Chi, Y.H. Wang, M.Z. Zhang, Experimental study on dynamic compressive behaviour of recycled tyre polymer fibre reinforced concrete, Cem. Concr. Compos. 98 (2019) 95–112. https://doi.org/10.1016/j.cemconcomp.2019.02.003.

[160] Z.X. Zhang, S.Q. Kou, J. Yu, Y. Yu, L.G. Jiang, P.A. Lindqvist, Effects of loading rate on rock fracture, Int. J. Rock Mech. Min. Sci. 36 (1999) 597–611. https://doi.org/10.1016/S0148-9062(99)00031-5.

[161] L. Li, J. Xiao, C.S. Poon, Dynamic compressive behavior of recycled aggregate concrete, Mater. Struct. Constr. 49 (2016) 4451–4462. https://doi.org/10.1617/s11527-016-0800-1.

[162] P. Rossi, F. Toutlemonde, Effect of loading rate on the tensile behaviour of concrete : Description of the physical mechanisms, Mater. Struct. Constr. 29 (1996) 116–118. https://doi.org/10.1007/bf02486201.

[163] A.E. Fenner, C.J. Kibert, J. Woo, S. Morque, M. Razkenari, H. Hakim, X. Lu, The carbon footprint of buildings: A review of methodologies and applications, Renew. Sustain. Energy Rev. 94 (2018) 1142–1152. https://doi.org/10.1016/j.rser.2018.07.012.

[164] J. Xiao, Y. Xiao, Y. Liu, T. Ding, Carbon emission analyses of concretes made with recycled materials considering CO<inf>2</inf> uptake through carbonation absorption, Struct. Concr. 22 (2021) E58–E73. https://doi.org/10.1002/suco.201900577.

[165] J. Xiao, H. Zhang, Y. Tang, Q. Deng, D. Wang, C. sun Poon, Fully utilizing carbonated recycled aggregates in concrete: Strength, drying shrinkage and carbon emissions analysis, J. Clean. Prod. 377 (2022) 134520. https://doi.org/10.1016/J.JCLEPRO.2022.134520.

[166] C. Hepburn, E. Adlen, J. Beddington, E.A. Carter, S. Fuss, N. Mac Dowell, J.C. Minx, P. Smith, C.K. Williams, The technological and economic prospects for CO_2 utilization and

removal, Nature. 575 (2019) 87–97. https://doi.org/10.1038/s41586-019-1681-6.

[167] N. Zhang, D. Zhang, J. Zuo, T.R. Miller, H. Duan, G. Schiller, Potential for CO_2 mitigation and economic benefits from accelerated carbonation of construction and demolition waste, Renew. Sustain. Energy Rev. 169 (2022) 112920. https://doi.org/10.1016/j.rser.2022.112920.

[168] S.Y. Pan, Y.H. Chen, L.S. Fan, H. Kim, X. Gao, T.C. Ling, P.C. Chiang, S.L. Pei, G. Gu, CO_2 mineralization and utilization by alkaline solid wastes for potential carbon reduction, Nat. Sustain. 3 (2020) 399–405. https://doi.org/10.1038/s41893-020-0486-9.

[169] N. Lippiatt, T.-C. Ling, S.-Y. Pan, Towards carbon-neutral construction materials: Carbonation of cement-based materials and the future perspective, J. Build. Eng. 28 (2020). https://doi.org/10.1016/j.jobe.2019.101062.

[170] T. Strunge, P. Renforth, M. Van der Spek, Towards a business case for CO_2 mineralisation in the cement industry, Commun. Earth Environ. 3 (2022) 1–14. https://doi.org/10.1038/s43247-022-00390-0.